



This is a repository copy of *Roles for globus pallidus externa revealed in a computational model of action selection in the basal ganglia*.

White Rose Research Online URL for this paper:
<http://eprints.whiterose.ac.uk/138144/>

Version: Accepted Version

Article:

Suryanarayana, S., Hellgren Kotaleski, J., Grilner, S. et al. (1 more author) (2018) Roles for globus pallidus externa revealed in a computational model of action selection in the basal ganglia. *Neural Networks*. ISSN 0893-6080

<https://doi.org/10.1016/j.neunet.2018.10.003>

Article available under the terms of the CC-BY-NC-ND licence
(<https://creativecommons.org/licenses/by-nc-nd/4.0/>).

Reuse

This article is distributed under the terms of the Creative Commons Attribution-NonCommercial-NoDerivs (CC BY-NC-ND) licence. This licence only allows you to download this work and share it with others as long as you credit the authors, but you can't change the article in any way or use it commercially. More information and the full terms of the licence here: <https://creativecommons.org/licenses/>

Takedown

If you consider content in White Rose Research Online to be in breach of UK law, please notify us by emailing eprints@whiterose.ac.uk including the URL of the record and the reason for the withdrawal request.



eprints@whiterose.ac.uk
<https://eprints.whiterose.ac.uk/>

Roles for globus pallidus externa revealed in a computational model of action selection in the basal ganglia

Shreyas M Suryanarayana^a, Jeanette Hellgren Kotaleski^{a,b}, Sten Grillner^{a,*}, Kevin N Gurney^c

^a*Department of Neuroscience, Karolinska Institutet, Stockholm, Sweden*

^b*Science for Life Laboratory, School of Electrical Engineering and Computer Science, KTH Royal Institute of Technology, Stockholm, Sweden*

^c*Department of Psychology, University of Sheffield, Sheffield, UK*

Abstract

The basal ganglia are considered vital to action selection - a hypothesis supported by several biologically plausible computational models. Of the several subnuclei of the basal ganglia, the globus pallidus externa (GPe) has been thought of largely as a relay nucleus, and its intrinsic connectivity has not been incorporated in significant detail, in any model thus far. Here, we incorporate newly revealed subgroups of neurons within the GPe into an existing computational model of the basal ganglia, and investigate their role in action selection. Three main results ensued. First, using previously used metrics for selection, the new extended connectivity improved the action selection performance of the model. Second, low frequency theta oscillations were observed in the subpopulation of the GPe (the TA or 'arkypallidal' neurons) which project exclusively to the striatum. These oscillations were suppressed by increased dopamine activity - revealing a possible link with symptoms of Parkinson's disease. Third, a new phenomenon was observed in which the usual monotonic relationship between input to the basal ganglia and its output within an action 'channel' was, under some circumstances, reversed. Thus, at high levels of input, further increase of this input to the channel could cause an *increase* of the corresponding output rather than the more usually observed decrease. Moreover, this phenomenon was associated with the prevention of multiple channel selection, thereby assisting in optimal action selection. Examination of the mechanistic origin of our results showed the so-called 'prototypical' GPe neurons to be the principal subpopulation influencing action selection. They control the striatum via the arkypallidal neurons and are also able to regulate the output nuclei directly. Taken together, our results highlight the role of the GPe as a major control hub of the basal ganglia, and provide a mechanistic account for its control function.

Keywords: Action Selection, Network models, Globus pallidus externa, Arkypallidal GPe neurons, Prototypical GPe neurons

*Corresponding Author

Email addresses: shreyas.suryanarayana@ki.se (Shreyas M Suryanarayana), jeanette@csc.kth.se (Jeanette Hellgren Kotaleski), Sten.Grillner@ki.se (Sten Grillner), k.gurney@sheffield.ac.uk (Kevin N Gurney)

Preprint submitted to Neural Networks

October 23, 2018

1 **1. Introduction**

2 The basal ganglia are an evolutionarily conserved group of subcortical nuclei,
3 which have long been implicated in action selection (Redgrave et al., 1999; Hikosaka et al.,
4 2000; Frank et al., 2004; Frank, 2005; Schroll et al., 2012; Lindahl et al., 2013; Grillner and
5 Robertson, 2016; Stephenson-Jones et al., 2011). Several computational models have been de-
6 veloped, examining their role in action selection (Mink, 1996; Hikosaka et al., 2000; Gurney
7 et al., 2001a,b; Frank et al., 2004; Schroll et al., 2012; Kamali Sarvestani et al., 2011; Berthet
8 et al., 2016). They propose the basal ganglia as a ‘selection machine’ resolving conflicts between
9 competing behaviours for common and restricted motor resources (Redgrave et al., 1999; Schroll
10 and Hamker, 2013; Frank, 2005). This notion is backed by studies showing that the stimulation
11 of the striatum, the main input nucleus, can either trigger actions or inhibit them (Kravitz et al.,
12 2010; Freeze et al., 2013). Furthermore, loss of dopamine neurons in the substantia nigra pars
13 compacta (SNc), result in a reduced ability to select motor responses (Wylie et al., 2009) in
14 pathological conditions like Parkinson’s disease. In furtherance of the selection hypothesis, the
15 basal ganglia are also implicated in learning of stimulus-response associations (Alexander et al.,
16 1986) as well as in establishing stimulus-response-outcome associations (Redgrave and Gurney,
17 2006).

18 Existing models have dealt with a variety of aspects of basal ganglia function and
19 anatomical context. Thus, many discuss the role of reinforcement learning (Brown et al., 2004;
20 Frank, 2006; Schroll et al., 2012; Redgrave and Gurney, 2006; Gurney et al., 2015) and have also
21 incorporated the thalamo-cortical loops (Humphries and Gurney, 2002; Beiser and Houk, 1998;
22 Chersi et al., 2013; Frank et al., 2004; van Albada and Robinson, 2009). These models also
23 cover a range of levels of biological description - from abstract system-level to detailed multi-
24 compartmental neuronal models, as well as simulations of ensembles of neurons. Addressing
25 computations at the level of the subnuclei of the basal ganglia, there have been several models
26 of the striatal microcircuitry (Humphries et al., 2009b,a; Damodaran et al., 2015), the subthala-
27 mic nuclei (STN, Frank 2006), as well as examinations of the oscillations associated within the
28 STN-GPe network (Blenkinsop et al., 2017; Corbit et al., 2016).

29 Most models are based on the classical architecture of connectivity of the basal
30 ganglia (Fig 1A), focusing on the direct pathway - the striatal D1 projections to the output nuclei
31 globus pallidus interna and substantia nigra pars reticulata (GPi/SNr), and the indirect pathway -
32 the striatal D2 projections to the GPe, and the GPe projections directly to GPi/SNr and the STN-
33 GPe/GPi loop. The GPe has been considered as homologous in structure and function in most of
34 these models. However, recent studies have revealed a new subpopulation of GPe neurons, the
35 *arkypallidal* cells (Mallet et al., 2012) that are active in anti-phase to their more common coun-
36 terparts, the *prototypical* GPe neurons (Mallet et al. 2012, see also Methods). These two classes
37 are also referred to as the TA and TI neurons respectively (Mallet et al., 2012). The arkypallidal
38 cells provide a major input to the striatum (Mallet et al., 2012).

39 We aimed to incorporate the arkypallidal neurons into a well-tested model archi-
40 tecture of the basal ganglia (Gurney, Prescott, Redgrave, Gurney et al. 2001a,b). The architec-
41 ture has been validated at several levels of description: at the systems level using rate coded
42 neural populations constrained by anatomical and physiological data (see Gurney et al. 2004;
43 Humphries and Gurney 2002; Blenkinsop et al. 2017); spiking neuron models challenged with
44 physiological data (Humphries et al., 2006; Stewart et al., 2012; Chersi et al., 2013); and at the
45 behavioural level in embodied (robotic) models (Prescott et al., 2006). Most recently, it has been
46 used to link a raft of neurobehavioural phenomena to neuronal mechanisms observed in vitro

47 (Gurney et al., 2015). Thus, this model architecture offers a strong platform to try to understand
48 the role and function of arky pallidal neurons and their afferent and efferent pathways in action
49 selection. Furthermore, we also included another scheme of organisation in the GPe in terms of
50 neuronal subpopulations - the *outer* and *inner* GPe neurons (Sadek et al., 2007). We built on
51 the original model and used the methodologies developed therein to assess them, on extended
52 architectures of connectivity of the GPe. The arky pallidal neurons have been accommodated
53 in a few computational models (Bahuguna et al., 2017; Lindahl and Hellgren Kotaleski, 2016;
54 Moolchand et al., 2017; Bogacz et al., 2016) and their function in supporting optimal action se-
55 lection (Bogacz et al., 2016) as well as in network dynamics underlying basal ganglia movement
56 disorders have been investigated (Bahuguna et al., 2017; Lindahl and Hellgren Kotaleski, 2016).
57 However, their role in action selection and their influence on other basal ganglia subnuclei, needs
58 additional investigation. Further, the outer and inner neuron dichotomy has not been included in
59 any model so far (to our knowledge), and their role in action selection remains unknown. Our
60 work addresses these lacunas and reveals important functions for different neuronal subpopu-
61 lations within the GPe, and unites these two prevalent schemes of organisation within the GPe
62 (GPe TI/TA and GPe outer/inner, Mallet et al. 2012 and Sadek et al. 2007) and furthermore,
63 places the GPe in perspective as an important control center of the basal ganglia.

64 2. Materials and methods

65 2.1. Anatomy of the basal ganglia

66 The classical anatomy of the basal ganglia (Redgrave et al., 1999; Bolam et al.,
67 2000; Calabresi et al., 2014) is shown in Fig 1A. It consists of the following principal nuclei:
68 the striatum, the globus pallidus ((GPe) and internal (GPi) divisions in primates), the STN and
69 the substantia nigra (SNr and SNc). The primary input nuclei are the striatum and the STN.
70 The output nuclei are the GPi and the SNr. The input nuclei receive afferent signals from most
71 of the cerebral cortex and the thalamus. The output nuclei project back to the thalamus, the
72 superior colliculus and other mid-brain regions. The striatum projects to GPi/SNr as well as
73 to the GPe. STN provides diffuse excitatory connections to the GPe and GPi/SNr. All other
74 connections of the basal ganglia nuclei are inhibitory. The SNc provides dopaminergic input to
75 the striatum, but is known to also project to other subnuclei of the basal ganglia (Bolam et al.,
76 2000; Calabresi et al., 2014). There are two types of dopamine receptors associated with two
77 subpopulations of the principal GABAergic projection neurons (>90%) in the striatum - the spiny
78 projection neurons (SPNs) or medium spiny neurons. One population, contains substance P and
79 dynorphin, and preferentially expresses the D1-type of receptor, which facilitates cortico-striatal
80 transmission. The other population contains enkephalin and preferentially expresses D2-type
81 receptors, which attenuates cortico-striatal transmission (Akkal et al., 1996; Jr and Zigmond,
82 1997). The SPNs provide phasic inhibitory output through their efferents to the GPe and GPi/SNr.

83 **Fig 1. Basal ganglia connectivity.** (A) Functional architecture of the GPR model, showing the
84 *selection* and *control* pathways. One component of the architecture - 'selection pathway' has its
85 output as the GPi/SNr and the other component - 'control pathway' has its output as the GPe.
86 (B) Architecture of connectivity within the basal ganglia, based on the intrinsic connectivity of
87 the GPe, showing GPe TI and GPe TA neurons. The prototypical TI neurons project to the TA
88 neurons and the GPi/SNr. They also project back to STN and have local collaterals amongst
89 their own subpopulation. The TA neurons project exclusively to the striatum. The numbers
90 (1-4) represent connections tested in step-wise models based on this scheme of connectivity. (C)

91 Architecture of connectivity within the basal ganglia, based on the intrinsic connectivity of the
92 GPe, showing outer and inner neurons. The outer neurons project to the inner neurons and both
93 populations project to the STN and GPi/SNr. Both populations have projections to the striatum
94 and finally, local collaterals amongst their own populations. The numbers (5-8) represent
95 connections tested in step-wise models based on this scheme of connectivity. (D) The extended
96 architecture of connectivity modelled in this study detailing the subpopulations within the GPe
97 and unifying the GPe TA/TI and outer/inner schemes, is shown here.

98 2.1.1. Anatomy of the GPe

99 Almost all of the GPe neurons are GABAergic except for a small subpopulation
100 ($\sim 5\%$) of cholinergic neurons which are sometimes regarded as an extension of basal fore-
101 brain cholinergic neurons (Mastro et al., 2014; Abdi et al., 2015; Hernández et al., 2015). The
102 GABAergic GPe neurons were largely considered a homogeneous population until two schemes
103 of population classifications emerged from the studies of (Mallet et al., 2012) and (Sadek et al.,
104 2007). These two schemes form the basis for our modelling the GPe. New data from several
105 studies have also subsequently contributed to the classification of GPe neuronal subtypes which
106 we detail below.

107 *TI and TA Neurons.* A hitherto unknown subpopulation of atypical GABAergic GPe neurons
108 were first described by (Mallet et al., 2012). The study dichotomises GPe neural population in
109 Parkinsonian rats based on physiological behaviour. A major portion of GPe neurons (75%),
110 discharge during the surface-negative component of cortical slow wave activity and are called
111 GPe TI, Type I or ‘prototypical’ neurons. The other major portion (20%) of neurons, discharge
112 during the surface-positive component of cortical slow wave activity, and are called GPe TA ,
113 Type A or ‘arkypallidal’ neurons. The GPe TI neurons give rise to projections which innervate
114 the STN and GPi/SNr. Some of them also have modest projections to the striatum, which target
115 the fast-spiking interneurons (FSNs, see also Glajch et al. 2016; Saunders et al. 2016). They also
116 have extensive local axonal collaterals, targeting other TI neurons as well as GPe TA neurons.
117 These neurons are parvalbumin positive and express the transcription factor Nkx2.1 (Abdi et al.,
118 2015; Dodson et al., 2015). There is also a subset of these neurons which express Lhx6 (Abdi
119 et al., 2015; Hernández et al., 2015; Hegeman et al., 2016). The firing pattern of the prototypical
120 GPe cells is regular spiking (Abdi et al., 2015; Hernández et al., 2015). The GPe TA neurons
121 on the other hand, are devoid of parvalbumin (Abdi et al., 2015; Hernández et al., 2015) and do
122 not conform to this extrinsic axonal projection and do not have descending projections to either
123 the STN or the GPi/SNr, but have long range axonal projections which provide a massive and
124 dense innervation of the striatum (see also Glajch et al. 2016), along with local axonal collaterals.
125 These cells express the transcription factors Npas1 and FoxP2 (Mallet et al., 2012; Hernández
126 et al., 2015; Hegeman et al., 2016). The GPe TA neurons are thus described as a novel atypical
127 neural population which do not conform to the premise that all GPe neurons invariably project
128 back to the STN. The architecture incorporating the GPe TA/TI dichotomy is shown in Fig 1B.

129 *Outer and Inner GPe Neurons.* The other core aspect of our new modelling connectivity archi-
130 tecture is from the study of (Sadek et al., 2007). Two neural subpopulations in the GPe have been
131 described, based on their relative distance from the striato-pallidal border, and on the number of
132 varicosities on their local axonal arborisations as the inner and outer neurons. The outer neurons
133 are located closer to the striato-pallidal border ($< 96\mu\text{m}$), and the inner neurons are located away
134 from the striato-pallidal border ($\geq 96\mu\text{m}$). There is significant asymmetry in the connections of

135 the two subpopulations. Inner neurons have more extensive local axonal collaterals, with neigh-
136 bouring GPe neurons, and thus receive more input. The outer neurons substantially innervate the
137 inner neurons, through axons traversing through the inner neuron regions on their way to the out-
138 put nuclei. While a reverse *inner to outer* neuron connection exists, it is reportedly weak. Both
139 the neural populations receive afferents from the striatum and STN and have efferents back to the
140 STN, as well as to the output nuclei GPi/SNr. This dichotomous clustering of the GPe outer and
141 inner neurons, can be matched to the dual representation of the striatum in the GPe (Chang et al.,
142 1981). There is also mention of projections from both outer and inner neurons to the striatum.
143 As a whole, about a third of the GPe neurons have projections to striatum. On cross-referencing
144 with other studies, which reported projections of prototypical parvalbumin positive GPe neurons
145 innervating the FSNs in the striatum (Bevan et al., 1998; Mastro et al., 2014; Glajch et al., 2016;
146 Saunders et al., 2016), we concluded that both the outer and inner neurons project to the striatal
147 FSNs. The end effect of these projections being mediated via FSNs, would be reduction of FSN
148 GABAergic inhibition of the SPNs (Szydłowski et al., 2013). The connectivity of the GPe with
149 respect to other basal ganglia nuclei along with the dual representation of outer and inner neurons
150 is shown in Fig 1C.

151 While the authors report that they have not correlated data across the two levels of
152 organisation - the GPe prototypical, TI/arkypallidal, TA from (Mallet et al., 2012) and - the GPe
153 outer/inner from (Sadek et al., 2007), following careful comparisons of the various studies de-
154 scribed here, we concluded that the prototypical GPe TI neurons could be assumed to consist of
155 both outer and inner GPe neurons. For instance, the axons of GPe TI neurons are quantitatively
156 similar to the individual GPe neurons in dopamine-intact rats. Furthermore, the number of bou-
157 tons on axonal projections in the striatum and STN of GPe TI neurons are well within the ranges
158 of axonal boutons accounted for in single GPe prototypical neurons in dopamine-intact rats. The
159 firing patterns of outer and inner neurons during cortical slow wave activity, which is said to be a
160 highly regular single-spike pattern, matched with that of the GPe TI neurons. Striatal projections
161 reported in the outer neurons (4 out of every 8 neurons), and in inner neurons (2 out of every 9
162 neurons), were also reported as modest striatal projections from GPe TI neurons. The GPe TA
163 arkypallidal cells on the other hand, form a separate subpopulation.

164 Taking the anatomical considerations together, we propose the extended architec-
165 ture shown in Fig 1D. We expand the connectivity of the GPe, by including the GPe TA neural
166 subpopulation and its afferent and efferent connections, while the prototypical GPe TI neurons
167 were accommodated in the modelling of outer and inner neurons.

168 2.2. *Quantitative model development*

169 2.2.1. *Existing Model*

170 We used the model by Gurney Prescott and Redgrave (Gurney et al., 2001a,b)
171 - henceforth referred to as the GPR model - as the basis for the extended architecture of
172 connectivity modelled in this study. The architecture for the GPR model was based on the
173 connectivity shown in Fig 1A. It included all the major pathways known at the time of its
174 construction (for related review see Prescott et al. 2002, see also Humphries and Gurney 2002;
175 Gurney et al. 2004; Humphries et al. 2006; Stewart et al. 2012; Chersi et al. 2013; Blenkinsop
176 et al. 2017) and provides a firm base for our model building. The assumption in the GPR model
177 was that the brain processes a large number of sensory and cognitive streams or *channels* acting
178 in parallel, each of them representing and requiring an action to be performed. To resolve the
179 conflicts arising due to the processing in parallel of representations of different channels, it was

180 proposed that the vertebrate brain has developed a ‘central arbitrating mechanism’ in which
 181 the ‘urgency’ or *saliency* of the representations are supplied to a ‘centralised arbitrator’, which
 182 in turn selects the representation with the greatest saliency, and to which motor (and possibly
 183 cognitive) resources are then allocated. The basal ganglia were hypothesised as this centralised
 184 arbitrator (Redgrave et al., 1999). A *functional architecture* with two components - ‘selection
 185 pathway’ and ‘control pathway’ (see Fig 1A) was proposed, which demonstrated that the basal
 186 ganglia could perform action selection (Gurney et al., 2001a,b). The role of the GPe in the
 187 GPR model was that of a ‘regulator’ of the selection pathway; the exact nature of the role was,
 188 however, not clear. By modelling the GPe, we have attempted to define that role more precisely,
 189 and tried to identify how various subpopulations within the GPe might contribute to that role.

190 The underlying assumption in the functional architecture was that an active
 191 representation of a putative action or *action request* (in cortex or subcortex) excites a population
 192 of neurons in striatum. This in turn, inhibits a corresponding population in GPi/SNr. This
 193 selective suppression of the tonic inhibitory control GPi/SNr normally exerts on its efferent
 194 targets, allows the action to be expressed. The combination of neural populations in various
 195 basal ganglia nuclei mediating an action request are said to comprise a processing *channel*.
 196 In addition, the STN also receives all action requests and supplies a diffuse excitation to
 197 GPi/SNr. In this way, striatum and STN comprise an off-centre, on-surround network that
 198 enables competitive processing between action channels. Each population in a channel, within
 199 a nucleus, was modelled by a single leaky integrator unit. Saliency was represented as a scalar
 200 value at the input with one saliency per channel. Selection in the model was defined with
 201 respect to a *selection threshold* in GPi/SNr such that, an output below this level was deemed
 202 to be associated with selection on the corresponding channel. In addition, a second, somewhat
 203 higher threshold - *distortion threshold*, allowed a subclassification of non-selected actions into
 204 those that are clearly playing no role in the current competition, and those which are just above
 205 the selection threshold, and which may *interfere* with selected actions, given small changes in
 206 saliency. Further details are found in ‘assessment and evaluation of selectivity’ below. We now
 207 describe the model developed in this study.

209 2.3. Model formalisation

210 2.3.1. Neuron Model

211 All the models we describe make use of the leaky-integrator artificial neurons,
 212 which were used in the GPR model (Gurney et al., 2001b). We give a brief description of the
 213 same. The model will be made available on ModelDB. In each nucleus, the i^{th} channel is repre-
 214 sented by a single artificial neuron. The level of abstraction of the semilinear neuron means that
 215 it represents the population activity associated with the entire channel. If u be the total afferent
 216 input to the artificial neuron, and if k is a constant which determines the rate of activation decay,
 217 the total activation \dot{a} of the leaky-integrator is given by:

$$\dot{a} = -k(a_i - u_i) \quad (1)$$

218 If \tilde{a} is the activation at equilibrium, which is what we use in all our models, $\tilde{a} = u$. The output of
 219 the leaky-integrator denoted by y , is defined as a piecewise linear compression function, which
 220 ensures its value is bounded below by 0 and above by 1. The relation is given by:

$$y = m(a - \epsilon)H(a - \epsilon) \quad (2)$$

221 where m is the slope of the output function, which is set to 1 in all our simulations.
 222 $H()$ is the Heaviside function, and ϵ is an activation threshold, below which, the output is zero.

223 2.3.2. Synaptic weights

224 The synaptic weights associated with the different modelled pathways are listed
 225 in Table 1. The synaptic weight symbols have been named using a general mnemonic
 $W_{source-destination}^{excitatory/inhibitory}$.

Table 1: Synaptic weight symbols

Weight	Pathway
w_i^{str}	Cortico-striatal weight for the i^{th} channel
w_{d2-ot}^-	Striatum D2 to GPe outer
w_{d2-in}^-	Striatum D2 to GPe inner
w_{d2-ta}^-	Striatum D2 to GPe TA
w_{d1-snr}^-	Striatum D1 to GPi/SNr
w_i^{stn}	Cortico-STN weight for the i^{th} channel
w_{stn-ot}^+	STN to GPe outer
w_{stn-in}^+	STN to GPe inner
w_{stn-ta}^+	STN to GPe TA
$w_{stn-snr}^+$	STN to GPi/SNr
w_{ot-d2}^-	GPe outer to striatum D2
w_{ot-d1}^-	GPe outer to striatum D1
w_{in-d2}^-	GPe inner to striatum D2
w_{in-d1}^-	GPe inner to striatum D1
w_{ot-stn}^-	GPe outer to STN
w_{ot-snr}^-	GPe outer to GPi/SNr
w_{in-stn}^-	GPe inner to STN
w_{in-snr}^-	GPe inner to GPi/SNr
w_{ta-d2}^-	GPe TA to striatum D2
w_{ta-d1}^-	GPe TA to striatum D1
w_{ta-ta}^-	GPe TA to GPe TA
w_{ot-ot}^-	GPe outer to GPe outer
w_{in-in}^-	GPe inner to GPe inner
w_{ot-in}^-	GPe outer to GPe inner
w_{ot-ta}^-	GPe outer to GPe TA
w_{in-ta}^-	GPe inner to GPe TA

Symbols used for synaptic weights of the different pathways modelled.

226

227 2.3.3. Striatum

228 In the GPR model, the SPNs of the striatum have been modelled whereas the in-
 229 terneurons have been omitted. We limit to the modelling of SPNs here as well. The SPNs are
 230 divided into two populations, distinguished by the neurochemistry and response to dopamine

231 which they receive from the SNc. This in turn divides the striatal model into two striatal sub-
 232 systems. The ‘up/down’-state behaviour of SPNs, shifting between the more depolarised mem-
 233 brane potential -‘up’ state, and the resting -‘down’ state has been modelled by using a positive
 234 threshold in the output equation described in (2). Coming to the input to the striatum, we use a
 235 cortico-striatal weight w_i^{str} for the i^{th} channel. We now describe the dopamine input to striatum.

236 2.3.4. Dopaminergic influence on selectivity

237 The role of dopamine in basal ganglia function was a pivotal aspect of this inves-
 238 tigation. We have included dopaminergic influence through the innervations of the striatum by
 239 the SNc. While this influence is not modelled as a ‘pathway’ explicitly, we included dopamine
 240 influence with modulation of striatal weights. Dopaminergic influence has been reported in two
 241 instantiations, a short phasic burst (~ 100 ms) and tonic activity (upto 8 Hz, Grace et al. 2007;
 242 Schultz 1998). We have modelled only the tonic level variations. We captured the difference in
 243 dopamine modulation on the D1 and D2 SPNs with dopaminergic transmission being facilitatory
 244 on D1 SPNs and cortico-striatal transmission being attenuated on D2 SPNs (Akkal et al., 1996;
 245 Jr and Zigmond, 1997; Planert et al., 2013). We replaced w_i^{str} with $(1 \pm \lambda)w_i^{str}$, where λ is the
 246 value of the tonic dopamine (see also Gurney et al. 2001b, 1998). To define the dopamine level,
 247 it was more instructive to consider a ratio of facilitation and attenuation - the *Dopamine ratio*,
 248 R_w given by,

$$R_w = \frac{1 + \lambda}{1 - \lambda} \quad (3)$$

249 where, $0 \leq \lambda \leq 1$

250 2.3.5. Modelled inputs

251 We summarise the modelled synaptic inputs for each subpopulation of neurons in
 252 various subnuclei of the basal ganglia. The activation function and the output relation as well as
 253 more details for each modelled subpopulation in all the nuclei can be found in the Appendix S1.

254 *Striatum D1.* The SPN D1 subpopulation in the striatum receives excitatory input from the cor-
 255 tex, diffuse inhibitory input from the GPe TA neurons, and the projections from the GPe outer
 256 and GPe inner neurons to striatum, as well as dopamine input from the SNc.

257 *Striatum D2.* The SPN D2 subpopulation in the striatum receives excitatory input from the cor-
 258 tex, diffuse inhibitory input from the GPe TA neurons, and the projections from the GPe outer
 259 and GPe inner neurons to striatum, as well as dopamine input from the SNc.

260 *STN.* The STN receives excitatory input from the cortex and inhibitory inputs from the GPe
 261 outer and GPe inner subpopulations.

262 *GPe outer (part of GPe TI).* GPe outer neurons receive diffuse excitatory input from the STN,
 263 inhibitory input from the striatum SPN D2 and inhibitory local collaterals from other GPe outer
 264 neurons.

265 *GPe inner (part of GPe TI).* GPe inner neurons receive diffuse excitatory input from the STN,
 266 input from the striatum SPN D2 and local inhibitory collaterals from other GPe inner neurons.
 267 Additionally, they also receive processed input from the GPe outer neurons.

268 *GPe TA*. GPe TA neurons receive diffuse excitatory input from the STN, input from striatum
 269 SPN D2 neurons, local inhibitory collaterals from GPe outer and GPe inner neurons along with
 270 local inhibitory collaterals from other GPe TA neurons.

271 *GPi/SNr*. The output nuclei receive inhibitory input from the striatum SPN D1 neurons, diffuse
 272 excitatory input from the STN along with inhibitory inputs from the GPe outer and GPe inner
 273 neuron subpopulations.

274 2.4. Parameter Values

275 The fixed parameter values included the thresholds for different neuronal subpopulations and some synaptic weights. They were chosen based on the criteria set out in the GPR model (Gurney et al., 2001b, 2004). Most of the synaptic weights and thresholds associated with the GPR model nuclei were simply extended to new neural populations. The rate constant k in Eq (1) was set at 25 (equivalent to a neural membrane time constant of 50ms), and the slope for each nuclei m , was set to 1 (see Gurney et al. 2001b). The thresholds associated with different subnuclei are given in Table 2. All the synaptic weights which were fixed, are shown in Table 3. The simulations also required varying a number of synaptic weights and combinations of synaptic weights from different pathways for trying to understand functions of different pathways. The weights were varied in steps of 0.25, between 0 and 1, except for the GPe pathway weights to the GPi/SNr, which were varied in steps of 0.2.

Table 2: **Thresholds.**

ϵ_{str}	0.2	ϵ_{in}	-0.2
ϵ_{stn}	-0.25	ϵ_{ta}	-0.2
ϵ_{ot}	-0.2	ϵ_{snr}	-0.2

Threshold values of the various nuclei and neural subpopulations used in the model.

Table 3: **Fixed synaptic weights.**

w_i^{str}	-1	w_i^{stn}	1
w_{d2-ot}^-	-1	w_{stn-ot}^+	0.8
w_{d2-in}^-	-1	w_{stn-in}^+	0.8
w_{d2-ta}^-	-1	w_{stn-ta}^+	0.8
w_{d1-snr}^-	-1	$w_{stn-snr}^+$	0.9

Synaptic weights of the pathways used in the model, which were fixed.

285

286 2.5. Simulations - guiding principles

287 The original GPR model had shown that the basic basal ganglia connectivity architecture when investigated from a systems-level, can behave like an effective selection mechanism.
 288 We incorporate more biological detail into the model, and are guided by the following principles
 289 while simulating and evaluating the model.
 290

291 *2.5.1. Enhancement of selectivity*

292 The model is driven by the hypothesis that action selection is a primary function of
293 the basal ganglia connectivity architecture, and with more biological detail we incorporate, there
294 must be an enhancement of the ability of the model to select. Selectivity is essentially the ability
295 of the model to ‘choose’ an action representation with the highest salience in a competition
296 between different action representations. We define a metric to quantify selection and evaluate it
297 which is detailed in subsequent sections.

298 *2.5.2. Mechanisms underlying selectivity*

299 Incorporation of significant biological detail also required us to investigate whether
300 new mechanisms of enforcing selectivity were generated. We observed for instance, in some mod-
301 els with the extended connectivity, there was a decrease in the channel output with increasing
302 salience, which could prevent the selection of that channel. ‘Reversal’, as we called this mech-
303 anism - was a new way through which the system could enforce selections in specific cases of
304 conflict. Reversal was able to resolve a conflict between two representations with high salience
305 (see also Sec 2.7.6).

306 *2.5.3. Roles of pathways*

307 The extended connectivity resulted in addition of a large number of biologically
308 grounded pathways. A primary question we addressed here, was to look into how these individual
309 pathways contributed to action selection. This was extended subsequently to neural populations
310 and then to the entire subnucleus (GPe).

311 *2.5.4. Role of dopamine*

312 Dopamine plays a crucial modulatory role in the basal ganglia, and to investigate
313 its influence on selection was another major goal of the simulations. We investigated the conse-
314 quences of different degrees of dopaminergic modulation in the striatum for each new pathway
315 modelled. This was pertinent, since dopamine loss and resultant oscillatory activity in the basal
316 ganglia underlies several pathological conditions like Parkinson’s. The aim was to investigate de-
317 pendency of selection on dopamine, but also to try to dissect out circuits which caused oscillatory
318 activity during lack of dopamine modulation.

319 *2.6. Experimental strategy*

320 The lack of decisive empirical evidence on the connectivity of the newly discov-
321 ered GPe sub-populations means that there is a proliferation of possible pathways, consistent with
322 the data. We therefore sought to investigate, as far as possible, the role of individual pathways
323 before bringing them together into a more realistic, but complex, configuration. We achieved
324 this by running a series of *Step-wise models* which simulated individual connections/pathways
325 added to the GPR model. The Step-wise models allowed us to tease out the contribution of every
326 new pathway we simulated, in action selection, from the new connectivity scheme we added on
327 in the GPe (See Fig 1D). This resulted in a Step-wise model for each new pathway modelled
328 (and named based on the pathway modelled) and whose performance was evaluated and com-
329 pared with the original GPR model (See Figs S1 & S2). Thus, for each subpopulation of GPe,
330 there are projections to other basal ganglia nuclei, projections to other GPe subpopulations, and
331 projections within the same population. Then, in a series of *Combined models*, we combined
332 connections in stages to simulate first, the entire projective connectivity of each subpopulation,

333 before repeating this with multiple subpopulations together. This enabled us to determine the
 334 functions for the various pathways and subpopulations of the GPe, as well as draw conclusions
 335 on the function of the GPe as a whole. Consequently, we present the simulation results broadly
 336 in three phases. In the first phase, we show step-wise models for the GPe TA subpopulation. In
 337 the second phase, we show a similar set of simulations of the GPe TI subpopulation. In the final
 338 phase, we draw these two subpopulations together in different ways into the extended architecture
 339 of GPe connectivity shown in Fig 1D.

340 2.7. Assessment and evaluation of selectivity

341 In order to assess the capabilities of each model variation, we established several
 342 metrics that described ‘selectivity’. Their definition builds on a simple pairwise competition
 343 protocol, the notions of ‘hard’ and ‘soft’ selection, and how these modes of selection vary with
 344 dopamine. We now describe the metrics and their construction in detail.

345 2.7.1. Basic selection procedure

346 In our simulations, we have actively driven two channels in a six channel model
 347 to replicate the stimulus protocols used in characterising the original GPR model (Gurney et al.,
 348 2001a, 2004). Selection was explored using a fixed protocol of salience variation of the two
 349 active channels (Fig 2). The selection threshold (θ_s) was set to 0 and the distortion threshold (θ_d)
 350 was set to $0.5 \times y_o^{snr}$, where y_o^{snr} was the tonic level of GPi/SNr (Fig 2A). In the time interval $t \leq 1$,
 351 the output reaches its ‘default’ or ‘equilibrium’ value which is the *tonic value* of the GPi/SNr (Fig
 352 2A). We further define time intervals 1 and 2 as $1 \leq t \leq 2$ and $2 \leq t$ respectively. We consider the
 353 two channel outputs during these intervals as $y_1^{snr}(1)$ and $y_2^{snr}(2)$. At time $t = 1$, channel 1 salience
 354 c_1 increases from 0 to 0.4 (*shown in blue*, Fig 2A). This induces a selection of channel 1 and an
 355 increase in $y_2^{snr}(2)$. At time $t = 2$, channel 2 increases its salience to 0.7 (*shown in red*, Fig 2B).
 356 This induces a selection of channel 2, and a clear deselection of channel 1 (since now, $y_1^{snr}(1) >$
 357 θ_d , Fig 2B). This particular outcome is called *Switching* (See description below). However, this
 358 dual threshold scheme and pairwise competition between two channels could result in several
 359 outcomes - *conditions of selectivity*, which are detailed below.

360 2.7.2. Conditions of selectivity

361 The six possible conditions of selectivity are described here (see also (Gurney
 362 et al., 2004)). They are the basic criteria used to classify selection possibilities. If \wedge stands for
 363 conjunction then,

- 364 1. *No Selection* No channel selected: $[y_1^{snr}(1) > \theta_s] \wedge [y_1^{snr}(2) > \theta_s] \wedge [y_2^{snr}(2) > \theta_s]$
- 365 2. *Single Channel Selection*: Each interval has a clear single channel selected with no interfer-
 366 ence, distortion or switching. Two possibilities:
 - 367 • Channel 1 selected: $[y_1^{snr}(1) \leq \theta_s] \wedge [y_1^{snr}(2) \leq \theta_s] \wedge [y_2^{snr}(2) > \theta_s] \wedge [y_2^{snr}(2) > \theta_d]$
 - 368 • Channel 2 selected: $[y_1^{snr}(1) > \theta_s] \wedge [y_1^{snr}(2) > \theta_s] \wedge [y_2^{snr}(2) \leq \theta_s] \wedge [y_1^{snr}(2) > \theta_d]$
- 369 3. *Switching*: Channel 2 is selected while channel 1 is deselected after being selected first,
 370 with no interference: $[y_1^{snr}(1) \leq \theta_s] \wedge [y_1^{snr}(2) > \theta_s] \wedge [y_2^{snr}(2) \leq \theta_s] \wedge [y_1^{snr}(2) > \theta_d]$
- 371 4. *Dual Channel Selection*: Channel 1 is selected in interval 1 and both channels are selected
 372 in interval 2: $[y_1^{snr}(1) \leq \theta_s] \wedge [y_1^{snr}(2) \leq \theta_s] \wedge [y_2^{snr}(2) \leq \theta_s]$

- 373 5. *Interference*: Channel 1 selected in interval 1. Channel 2 causes deselection of channel 1 in
374 interval 2, while it does not itself become selected: $[y_1^{snr}(1) \leq \theta_s] \wedge [y_1^{snr}(2) > \theta_s] \wedge [y_2^{snr}(2) >$
375 $\theta_s]$
- 376 6. *Distortion*: Single channel may be selected or switching might occur, the difference being
377 that the losing channel is not clearly deselected, i.e, it is less than θ_d . Three possibilities:
- 378 • Channel 1 selected: $[y_1^{snr}(1) \leq \theta_s] \wedge [y_1^{snr}(2) \leq \theta_s] \wedge [y_2^{snr}(2) > \theta_s] \wedge [y_2^{snr}(2) \leq \theta_d]$
 - 379 • Channel 2 selected: $[y_1^{snr}(1) > \theta_s] \wedge [y_1^{snr}(2) > \theta_s] \wedge [y_2^{snr}(2) \leq \theta_s] \wedge [y_1^{snr}(2) \leq \theta_d]$
 - 380 • Switching: $[y_1^{snr}(1) \leq \theta_s] \wedge [y_1^{snr}(2) > \theta_s] \wedge [y_2^{snr}(2) \leq \theta_s] \wedge [y_1^{snr}(2) \leq \theta_d]$

381 **Fig 2. Experimental protocol with pairwise competition.** Description of the basic selection
382 procedure (A) Channel 1 salience is increased to 0.4 which leads to its selection at $t = 1$ (B)
383 Channel 2 salience is then increased to 0.7 at $t = 2$, which leads to its selection and a clear
384 deselection of channel 1, a condition of selectivity called ‘switching’. Note that the output of
385 channel 1 at $t = 2$, is above the distortion threshold (θ_d) indicating its clear deselection.

386 2.7.3. *Hard and Soft selection through template matching*

387 The salience on the two competing channels was varied from 0 to 1 in steps of 0.1,
388 totalling 121 outcomes. We then observed which condition of selectivity, the pattern of outputs
389 defined, for each salience pairing. This was done for a fixed value of dopamine ratio. In the GPR
390 model, it was shown that for moderate levels of dopamine ($R_w = 1.83$) the outcomes favour *hard*
391 *selection*, which is dominated by single-channel selection (Gurney et al., 2001a, 2004). Hard
392 selection, was more crucial for a system working as a selection mechanism, as it was defined on
393 the basis of a clear winner amongst competing channels. An ideal selection mechanism would
394 normally require that there be a clear ‘winner’ of the competition for behavioural expression,
395 facilitated by intermediate levels of dopamine. At sufficiently low levels of dopamine ($R_w = 1$)
396 there is failure to select (See Figs 3C, 5A & B). This is consistent with the pathology of Parkin-
397 son’s disease in which low levels of dopamine (typically more than 80% loss, Roessner et al.
398 2011; Yoon et al. 2007) cause akinesia, which we interpret as a failure of action selection.

399 However, it may be desirable in some circumstances, that selection be more
400 ‘promiscuous’ so that inhibition is removed from multiple channels. We refer to this as *soft*
401 *selection* which consists largely of dual channel selection in the template description. Soft se-
402 lection is favoured at higher levels of dopamine ($R_w = 10$). In its extreme form, such selection
403 may be associated with undesired expression of actions simultaneously (or near simultaneous)
404 with the desired, as shown, for example, in Tourette’s syndrome, where undesirable behavioural
405 ‘tics’ accompany normal target behaviours (Roessner et al., 2011; Yoon et al., 2007). However,
406 there are other, more positive ways of interpreting soft selection and the nominal simultaneity of
407 selection, which we discuss below.

408 2.7.4. *Understanding behavioural correlates of soft selection*

409 Consider a model situation with dual channel selection. This is maintained in
410 the model only via the artefact of sustained application of fixed input saliences on the relevant
411 channels. In reality, if we close the environment-agent loop, the very act of committing an action
412 by the agent will modify the agents perceived environment, thereby facilitating a change in
413 salience which, in turn, may release any dual channel deadlock. This will also be assisted by any
414 neural noise which we have omitted in the current model for simplicity. In either case, the final
415 selection after this ‘symmetry breaking’ will be somewhat randomly obtained, and contingent

416 on small phasic disturbances in the agent or its dynamically evolving environment. This kind of
417 non-determinism in salience input will force the agent to *explore* a variety of actions in response
418 to a general environmental context, as required, if the agent is to undergo effective reinforcement
419 learning (Barto and Mahadevan, 2003; Barto, 1994). In our model, soft selection is favoured by
420 higher levels of dopamine, indicating more exploratory behaviour under these conditions. This
421 is consistent with some interpretations of the biological implications of increased dopamine; for
422 example, increased activity in the dopamine system has been associated with higher levels of
423 ‘risk’ taking during adolescence in human development (Wahlstrom et al., 2010). Furthermore,
424 modelling suggests that low to moderate levels of tonic dopamine activity in the striatum induces
425 *exploratory* behaviours (Humphries et al., 2012; Chakravarthy and Balasubramani, 2013), while
426 higher levels induce exploitive or ‘Go’ behaviours (Frank, 2006)

427 While the ‘symmetry breaking’ account of soft selection may apply to a single
428 competitive loop in the basal ganglia (the target of our model), soft selection may occur more
429 generally in the wider context of multiple, parallel (and competitively more independent)
430 loops. Parallel loops have been proposed in the basal ganglia for automatic and voluntary
431 behaviours (Kim and Hikosaka, 2015). These can mediate behaviours which can and do occur
432 simultaneously, in reward-seeking behaviours - as for instance eating and reaching out for food.
433 This would mean disinhibition of different pattern generator circuits devoted to specific types
434 of movements (Grillner et al., 1998). The basal ganglia output nuclei target all these motor
435 generating circuits (Grillner et al., 2005; Grillner, 2003; Kim and Hikosaka, 2015).
436

437 2.7.5. Quantifying selection

438 We quantify selection outcomes by comparing the degree of match of our own
439 experimental outcomes with ‘ideal’ templates for both hard and soft selection. The candidate
440 templates we used for these comparisons are shown in Fig 3A (hard selection) and Fig 3B (soft
441 selection, see also Gurney et al. 2001a, 2004). We thus used the comparison parameters, *Hard*
442 *selection match* P_h , and the *Soft selection match* P_s as,

$$443 P_h = \frac{N_h 100}{N}, P_s = \frac{N_s 100}{N} \quad (4)$$

444 where N_h and N_s were the salience value pairs for which the simulation outcomes matched their
445 counterparts in the ideal hard and soft selection templates respectively, and N , the total number of
446 salience value pairs. By repeating the 121 experiments in the ‘salience grid’ with several values
447 of λ ($0 < \lambda < 1$), we measured the P_h and P_s values across dopamine levels and plotted them
448 against R_w . The points were fit using a cubic spline and the maximum P_h and P_s (Max P_h , Max
449 P_s , peak of the corresponding spline, see Fig 3C) were calculated. The value of the dopamine
450 ratio at which the $P_{h(R_w)}$ and $P_{s(R_w)}$ trajectories cross was defined as the *Cross-over point* W_c (Fig
451 3C).

451 **Fig 3. Selection templates and performance trajectories.** (A) Ideal *Hard* and (B) *Soft*
452 selection templates used for comparisons of our simulation outcomes. (C) Hard and soft
453 trajectories across dopamine range, of the best performance of the GPR model, which highlights
454 the desirable trajectories of P_h and P_s , each having high values and sufficient difference
455 between them. The values are Max $P_h = 65.22$, Max $P_s = 86.78$ and the cross-over point
456 $W_c = 2.35$ (D) shows a model run with a biologically implausible weight from one of our
457 step-wise models, indicates the failure of the model-the hard and soft curves nearly overlap.
458 The curves are cubic spline fits to data.

459 The general metric was to compare P_h and P_s values of our models with the corresponding
 460 values of the best performance simulation of the GPR model (Gurney et al., 2001b). We defined
 461 performance from a computational perspective based on the *ability* of the selection mechanism
 462 to perform better hard selection. Thus, an increase in Max P_h compared to the Max P_h of the
 463 GPR model (65.22, Fig 3C, Gurney et al. 2001a, 2004) was taken to be a performance increment.
 464 However, the selection system was also required to demonstrate large values of P_s similar to the
 465 GPR model, ensuring sufficient access to both hard and soft selection regimes. We thus took
 466 minimal deviation of the Max P_s value, or an increase from that of the GPR model (86.78, Fig
 467 3C) as another indicator of model performance.

468 We also evaluated the general trajectories of both P_h and P_s plots across R_w in
 469 terms of their resemblance to what was seen in the GPR model (Fig 3C). In general, the P_h
 470 trajectory $> P_s$ for low dopamine, must cross each other subsequently at a point defined as the
 471 crossover-point W_c , and for higher dopamine values $P_s > P_h$. This translates to the function
 472 $P_h(R_w)$ increasing from $P_h(1)$ reaching its peak Max P_h at relatively small values of R_w and
 473 then decreasing gradually with increase in R_w . The function $P_s(R_w)$ on the other hand, increased
 474 monotonically from $P_s(1)$ reaching the peak value Max P_s at large values of R_w . The cross-
 475 over point W_c essentially determined that for $1 < R_w < W_c$, $P_h > P_s$ the system was in the *hard*
 476 *selection regime*. For $R_w > W_c$, $P_s > P_h$ the system was in the *soft selection regime*. Thus, there
 477 had to be a clear distinction and difference between the fits of P_h and P_s across R_w , and any
 478 overlap was considered as a failure of the model (Fig 3D, See also Gurney et al. 2004). This
 479 was important in that it forced a clear distinction in the models behaviour in terms of hard and
 480 soft selection. The cross-over point in addition, also determined the range of dopamine values
 481 through which hard selection may be accessed by the model, and its value being equal to or
 482 greater than that of the GPR model (2.35, Fig 3C), was also an additional determinant of model
 483 performance.

484 Each of the three parameters defined - Max P_h , Max P_s and W_c , represented a
 485 feature of the model and contributed in its own right towards the assessment of the performance
 486 of the model. We thus had the feature set $F = \{\text{Max } P_h, \text{Max } P_s, W_c\}$. However, the basis of
 487 our performance metric was changes of performance in relation to that of the GPR model. We
 488 therefore defined these features relative to those of the GPR model as $R_i = \log(r_i)$, where $r_i =$
 489 f_i/f_{GPR} with $f_i \in F$, and where f_{GPR} was the value of the corresponding feature in the GPR model.
 490 This resulted in the defining of relative features to the three features $F = \{\text{Max } P_h, \text{Max } P_s, W_c\}$
 491 as $\{R_i\} = \{H_{MAX}^*, S_{MAX}^*, W_c^*\}$ respectively. Bringing these ideas together allows us to define a
 492 single scalar metric Q^* which added up the three relative features as,

$$Q^* = \sum_i \log(r_i) \quad (5)$$

493 Thus, an increase in Q^* following any addition of a biologically plausible pathway to the GPR
 494 model would indicate an increment in performance, implying greater support for the action se-
 495 lection hypothesis.

496 2.7.6. Reversal phenomenon

497 In the extended architecture simulated in this study, we observed a hitherto unseen
 498 ‘reversing’ of tendency of a particular channel to get selected, with increasing salience. In gen-
 499 eral, as the salience is increased for a particular channel, its output decreases and approaches the
 500 selection threshold (which is zero). However, in some models with newly included pathways

501 here, it was observed that across a range of high salience values, with increasing salience values,
 502 when the salience on one channel was kept constant and that on the second increased, the output
 503 of the latter channel increased, rather than decrease (and thereby approach the selection thresh-
 504 old) *reversing* the tendency to get selected. We defined a value to quantify this phenomenon - a
 505 *Reversal* R_v which was given by,

$$R_v = \frac{N_r 100}{N} \quad (6)$$

506 where N_r was the number of channel 1 and channel 2 salience value pairs for which reversal
 507 occurs and N the total number of salience value pairs (within the experimental ‘salience grid’
 508 defined previously). This unitary phenomenon (increase in output with increased salience), re-
 509 sulted in four possible cases: *Single Ch selection* \rightarrow *No Selection*, *Dual channel selection* \rightarrow
 510 *Interference/Distortion/Switching*, *Switching* \rightarrow *Interference/Distortion* and *Distortion* \rightarrow *Inter-*
 511 *ference*. Some of these cases are illustrated in Fig 4. These various cases were seen in control
 512 models of pathways underlying reversal (see reversal architecture, Fig 10B). In the final model,
 513 only the cases resulting in *Dual channel selection* \rightarrow *Interference/Distortion/Switching*, were
 514 seen, largely in the soft selection regime (see Fig 7F and Discussion). We do not detail the types
 515 of reversal in different models, but present its occurrence in terms of Reversal value defined here.

516 Thus, mechanistically, reversal by large, enables soft selection outcomes (dual
 517 channel selection) being reversed to hard selection outcomes (single channel outcomes). Since
 518 reversal occurred across a range of high salience values, we speculate that it may be indicative
 519 of exploratory behaviours (Humphries et al., 2012; Chakravarthy and Balasubramani, 2013) but
 520 also resolution of ‘flight-fight’ instances of behavioural decision-making.

521 **Fig 4. Reversal phenomenon.** Reversal seen here on the selection outcomes from (A) one of
 522 the control models (1,2, green dotted box) shows the case where after *switching* the selected
 523 channel is pulled back causing *interference*. In (2) *distortion* is followed by *interference* instead
 524 of the normal *switching*. These types of reversal cases were only seen in control models. (B)
 525 Reversal in the final model, in (3) *dual channel selection* is followed by *distortion* and *switching*
 526 while in (4) it is followed by *distortion* and *interference*. These cases aid in better action
 527 selection performance in that they lessen the number of more promiscuous selections. (C-D)
 528 Time course of a typical reversal case occurring in the final model as per the sequence seen in
 529 (3), in (C) channel 1 is selected upon reaching the selection threshold, following which in (D)
 530 the salience of channel 2 increases sufficiently to result in its selection as well - *dual channel*
 531 *selection*. Reversal kicks in, and in (E) channel 2 output can be seen to increase (*black arrow*),
 532 causing *distortion* (its output is still lesser than the distortion threshold). Subsequently however
 533 in (F), the channel 2 output increases above the distortion threshold, resulting in its clear
 534 deselection, resulting in *switching*. Thus reversal resulted in a reversion back to a clear selection
 535 of channel 1 from the scenario where both channel 1 & 2 were selected.

536 2.7.7. Other features

537 As well as determining the values of metrics such as Q^* and R_v , we also report a
 538 range of features about model behaviour, such as presence or absence of oscillations, changes in
 539 tonic rates of the GPI/SNr. We also attempt to dissect out neural connectivity underlying some of
 540 these features and identify the roles of different pathways in these features, which are tabulated
 541 in Table 4.

542 2.8. Extended Architecture - omissions

543 The extended architecture incorporates most of the neural subpopulations and in-
544 trinsic connectivity of the GPe known. However, not all logically possible pathways are inves-
545 tigated as we had to limit the combinatorics to be tractable. The rationale for omissions is as
546 follows: The projections from striatal D1 neurons to GPe TI and GPe TA have been omitted,
547 since their primary role is in relation to the direct pathway. With respect to the projections of
548 the GPe TA neurons to the striatum, we have modelled only the projections to the SPNs. The
549 extent and distribution of the GPe TA neuronal projections to the striatum is not yet completely
550 clear, although they are known to target both the SPNs and the interneurons (Mallet et al., 2012;
551 Hegeman et al., 2016; Burke et al., 2017). Furthermore, there are some indications that GPe
552 TA input to striatum D2 SPNs is stronger (Glajch et al., 2016), however, we have not varied
553 the relative strengths of GPe TA projections to D1 and D2 SPNs. We have also not modelled
554 the GPe TA local collaterals to the GPe TI, whereas the reverse connection has been included.
555 There is recent evidence from modelling that GPe TA neurons receive inputs from the GPe TI
556 (Lindahl and Hellgren Kotaleski, 2016), which agrees with our own modelled connectivity. The
557 final form of the new extended architecture is seen in Fig 1D. The TI and TA neurons are shown
558 within the GPe boundary, whereas the outer and inner neurons are shown within the TI boundary.
559 The extrinsic connections of both the outer and inner neurons are commonly represented by the
560 TI, except for the distinguishing connection between the outer and inner neurons.

561 3. Results

562 Recall from the methods that we make use of step-wise and combined models,
563 investigating single and multiple pathways respectively, and that their deployment is carried out
564 in three modeling phases. This approach is reflected here in reporting the Results.

565 3.1. Phase 1: TA step-wise models

566 In phase 1, the GPe TA neurons were added to the GPR model. The results of each
567 of the step-wise models are described below. The different weights used in each of the step-wise
568 models are tabulated in Appendix S2.

569 3.1.1. GPe TA - GPe TA step-wise model

570 This model tested the feedback pathways of the GPe TA neurons (pathway 1 in
571 Fig 1B). The feedback loop of the GPe TI w_{ii}^- , was set to 0 to isolate the GPe TA - GPe TA
572 pathway as much as possible. Only w_{ta-ta}^- was varied. The projections to striatum, w_{ta-d1}^- and
573 w_{ta-d2}^- were set at -1, while the w_{ti-ta}^- was set at -1. w_{ta-ta}^- had no effect on P_h or P_s , as it was
574 varied. H_{MAX}^* and W_c^* were slightly higher than the GPR values while S_{MAX}^* was unchanged.
575 The performance Q^* was only slightly higher than the GPR model (Fig 6A-D). There was no
576 change in tonic level of GPI/SNr. This pathway has no significant influence on selection as the
577 $P_{h(R_w)}$ and $P_{s(R_w)}$ trajectories were similar to that of the GPR model (Fig S1A). Reversal was also
578 not noticed; this path had no role in reversal phenomenon. The model produced oscillations,
579 and in order to find the source of oscillations more precisely, w_{ta-d1}^- and w_{ta-d2}^- were varied.
580 It was found that oscillations were sustained for $w_{ta-d1}^- = w_{ta-d2}^- = -1$, indicating that both the
581 arky pallido-striatal components were required to generate them (see Table 4). Oscillations were
582 sustained at lower DA levels and were maximum when there was no dopamine activity (DA =
583 0, Fig 5A). They reduced in amplitude as DA level increased $DA \leq 0.3$ (Fig 5B & C), and were

584 completely suppressed for $DA \geq 0.4$ (Fig 5D). The oscillations had a frequency of 4.7 Hz and
 585 were therefore classified as being in the theta band. Furthermore, for $DA = 0$, the outputs at
 586 the level of GPe subpopulations and STN were also evaluated. Both the GPe subpopulations -
 587 arky pallidal and prototypical neurons were oscillating (Fig 5G) as well as STN (Fig 5H). Thus
 588 the entire STN - GPe - GPi/SNr network oscillates.

589 *STN stimulation.* We checked whether over activation of the STN in the model conditions which
 590 produced oscillations, could relieve oscillations. All the weights associated with the STN were
 591 set to +1 to capture the conditions of STN stimulation. The model performance was tested for
 592 $DA = 0$ and the model was able to select and the oscillations were suppressed (Fig 5G, see also
 593 Fig S4B&D, for weights of different pathways see ‘STN - DBS model’ in Appendix S2). The
 594 Max P_h value was higher than the oscillating condition (Fig S4D).

595 *STN lesion.* We furthermore checked whether the lesioning of STN could provide similar out-
 596 comes - in this case all the weights associated with STN were set to 0). Interestingly, for $DA =$
 597 0, the model was able to select as well as suppress oscillations (Fig 5H, see also Fig S4C&D, for
 598 weights of different pathways see ‘STN - lesion model’ in Appendix S2). The Max P_h value was
 599 higher than the oscillating condition (Fig S4D).

600 **Fig 5. Theta oscillations induced by lack of dopamine.** Oscillations across dopamine levels,
 601 Max Amplitude at (A) $DA = 0$, Intermediate levels (B) $DA = 0.2$ and (C) $DA = 0.3$, Suppressed
 602 at (D) $DA = 0.4$. The oscillations were due to the arky pallidal TA projections to the striatum.
 603 (E) Oscillations at $DA = 0$, also at the level of GPe subpopulations - both the arky pallidal and
 604 prototypical neurons. (F) Oscillations also at the level of STN for $DA = 0$. (G) Suppression of
 605 oscillations and selection induced for $DA = 0$ for maximum weights on STN mimicking STN -
 606 deep brain stimulation conditions. (H) Similar suppression of oscillations and selection when
 607 STN weights are made zero reflecting ‘STN - lesion’ condition.

608 **Fig 6. Performance metrics.** Performance metrics for the step-wise models (A) H_{MAX}^* values
 609 showing the relative change in Hard selection of the step-wise models to that of the GPR model
 610 (B) S_{MAX}^* values showing the relative change in Soft selection of the step-wise models to that of
 611 the GPR model (C) W_c^* values showing the relative change in cross-over point of the step-wise
 612 models to that of the GPR model (D) Q^* Performance metric values of step-wise models
 613 relative to the GPR model. In all, red plots indicate increment in value while blue plots indicate
 614 decrement in value.

615 3.1.2. GPe TA - STR step-wise model

616 This model tests the diffuse projections of the GPe TA neurons to the striatum
 617 (pathway 2 in Fig 1B). The weights w_{ta-d1}^- and w_{ta-d2}^- were varied but were kept equal. The GPe
 618 TI - GPe TA pathway weight w_{ti-ta}^- was also varied. GPe TI was necessary since the GPe TA
 619 neurons have no efferents to the GPi/SNr. To test the pathways in as much isolation as possible,
 620 the feedback weights of GPe TI and GPe TA neural populations were ‘lesioned’, $w_{ti-ti}^- = w_{ta-ta}^- =$
 621 0. H_{MAX}^* was lower than the GPR value showing this projection reduced the performance of the
 622 model in the hardness regime. However, with increase in W_c^* , it increased the range of the
 623 hardness regime across dopamine values. S_{MAX}^* was also reduced. The performance Q^* was
 624 higher than the GPR model, largely due to the marked increase of W_c^* (Fig 6A-D). Oscillations
 625 were observed for $w_{ti-ta}^- = -1$ and $w_{ta-d1}^- = w_{ta-d2}^- = -1$, just as they were observed in the

626 GPe TA - GPe TA step-wise model. It was confirmed that these pathways were responsible
627 for oscillations (see Table 4). The dependence of oscillations on low dopamine levels was also
628 confirmed. Even for the values of best performance, $w_{ti-ta}^- = -0.75$ and $w_{ta-d1}^- = w_{ta-d2}^- = -0.25$,
629 the $P_{h(R_w)}$ and $P_{s(R_w)}$ trajectories overlapped (Fig S1B). This was a failure of the model - indicating
630 that the connectivity was incomplete and not fit for optimum action selection. Reversal was not
631 observed indicating that these pathways had no role in reversal phenomenon.

632 *GPe TI - TA step-wise model*

633 This model tested the GPe TI - GPe TA pathway w_{ti-ta}^- , which was added to the
634 GPR model (pathway 3 in Fig 1B). This would be analogous to the GP-outer to GP-TA connec-
635 tion in future models. Both w_{ti-ti}^- and w_{ta-ta}^- were set to 0 or 'lesioned' to provide for exclusive
636 testing. The TA projections to the striatum, w_{ta-d1}^- and w_{ta-d2}^- were set to -1. H_{MAX}^* was higher
637 the GPR value which resulted in the performance Q^* being slightly higher than the GPR. S_{MAX}^*
638 and W_c^* were unchanged (Fig 6A-D). The model showed no selection till $w_{ti-ta}^- = -0.75$, and
639 selection was observed at $w_{ti-ta}^- = -1$ (Fig S1C). There was no influence on the GPi/SNr tonic
640 level or any significant influence on selection. There was no role of this pathway in reversal,
641 which was not noticed. This pathway allows the prototypical TI neurons to maintain control on
642 the arkipallidal TA neurons, inturn allowing them to influence striatal activity (see Table 4).

643 *3.1.3. GPe TI - TI step-wise model*

644 This model tested the local inhibitory connections of GPe TI neurons, considered
645 as a single homologous population (pathway 4 in Fig 1B, analogous also to pathway *, GPe
646 outer - GPe outer in Fig 1C). This didnt include the GPe TA neurons or the outer/inner neuron
647 distinction of GPe TI neurons. The GPe TI-SNr weight was fixed at $w_{ti-snr}^- = -0.4$. The GPe TI-
648 GPe TI feedback weight, w_{ti-ti}^- was varied. Both H_{MAX}^* and S_{MAX}^* were reduced, however W_c^* was
649 increased which yielded in an increased performance Q^* than the GPR model (Fig 6A-D). Max
650 P_h occurred for $w_{ti-ti}^- = 0$, which was the same as the GPR model. Clearly this pathway was, at
651 this stage not useful for action selection. This indicated lack of sufficient circuitry modelled. We
652 have, however, shown the simulation result with $w_{ti-ti}^- = -0.25$ (Fig S1D), which was the weight
653 of this pathway, for best performance in the final model (see below). Reversal was observed
654 for $w_{ti-ti}^- > 0$ (see Fig 7A) showing that the TI neurons play a role in reversal. Tonic value of
655 GPi/SNr increased with increase in w_{ti-ti}^- (see Fig 8A and Table 4). The pathway thus influences
656 selection by setting the tonic value of GPi/SNr.

657 **Fig 7. Reversal phenomenon generated by prototypical GPe neurons.** Reversal (in %)
658 across dopamine levels with change in the weights of (A) w_{ot-ot}^- (B) w_{in-in}^- (C) w_{ot-in}^- (D) w_{ot-d1}^-
659 & w_{ot-d2}^- (E) w_{in-d1}^- & w_{in-d2}^- . (F) shows reversal observed in the final model across dopamine
660 values, occurring largely in the soft selection regime.

661 *3.2. Phase 2: TI step-wise models*

662 In phase 2, the GPe TI neurons with the outer - inner dichotomy were added to
663 the GPR model. The results of each of the step-wise models are described below. The different
664 weights used in each of the step-wise models are tabulated in Appendix S2.

665 3.2.1. GP IN - GP IN step-wise model

666 This was the first model incorporating the dichotomy of GPe TI neural population
667 - the outer and inner neurons. The GPe TI - GPe TI step-wise model was equivalent to GPe outer
668 - GPe outer step-wise model, so we start from investigating the GPe inner - GPe inner step-wise
669 model (pathway 5 in Fig 1C). To investigate this pathway exclusively, we set the GPe outer -
670 GPe outer (TI -TI) weight, $w_{ot-ot}^- = -1$ and the GPe outer - GPe inner weight $w_{ot-in}^- = -1$, and
671 varied w_{in-in}^- . We also 'lesioned' the GPe outer - SNr pathway $w_{ot-snr}^- = 0$, so as to have only
672 the output of GPe inner neurons to the GPi/SNr. Both H_{MAX}^* and S_{MAX}^* were reduced, however
673 W_c^* was increased which yielded in an increased performance Q^* than the GPR model (Fig 6A-
674 D), similar to the GPe TI - GPe TI model, indicating these two pathways may be involved in
675 similar functions. Reversal was noticed, even when $w_{ot-ot}^- = 0$ (Fig 7B) indicating this pathway
676 and by extension - the inner neuron play a role in generating reversal (see Table 4). Tonic
677 value of GPi/SNr increased with increase in w_{in-in}^- (Fig 8A) also implicating the inner neurons
678 in influencing the tonic output of the GPi/SNr (see Table 4). Max P_h occurred for $w_{in-in}^- = -0.5$.
679 However, there was a near overlap of $P_{h(R_w)}$ and $P_{s(R_w)}$ trajectories, which was clearly undesirable
680 (Fig S1E) and indicated incomplete connectivity. In the final model (see below) a weight of
681 $w_{in-in}^- = -0.75$ was used, which yielded best performance.

682 **Fig 8. Effects of prototypical GPe neuron projections on tonic level of GPi/SNr.** Step
683 changes in GPi/SNr tonic levels with change in the weights of (A) w_{ot-ot}^- , w_{in-in}^- & w_{ot-in}^- (B)
684 w_{ot-snr}^- & w_{in-snr}^- .

685 3.2.2. GP OT - GP IN step-wise model

686 This model investigated the crucial GPe outer - GPe inner link, which was the
687 inhibitory connection between the GPe outer and GPe inner neuron populations (pathway 6 in
688 Fig 1C). w_{ot-in}^- was varied, whereas same population inhibitory connection weights were set
689 to, $w_{ot-ot}^- = w_{in-in}^- = -1$. H_{MAX}^* was unchanged from that of the GPR model, while S_{MAX}^*
690 was reduced. W_c^* was increased which yielded in an increased performance Q^* (Fig 6A-D).
691 When $w_{ot-in}^- = 0$, the model behaved like the GPR model, which was also the best performance
692 (Fig S1F). However we used a value of $w_{ot-in}^- = -0.25$ in the final model, which gave best
693 performance, which we have shown here as well. Reversal was noticed across the values of
694 w_{ot-in}^- (Fig 7C). However, when the same population inhibitory weights were 'lesioned', i.e.,
695 $w_{ot-ot}^- = w_{in-in}^- = 0$, no reversal was noticed. Thus, this pathway had no role in generating
696 reversal. Tonic level of GPi/SNr increased with increase in w_{ot-in}^- (see Fig 8A and Table 4).

697 3.2.3. GP OT - SNr step-wise model

698 This model investigated the efferents of the GPe outer neurons to the GPi/SNr (part
699 of pathway 7 in Fig 1C, considering only GPe outer). The same population inhibitory weight was
700 set at $w_{ot-ot}^- = -1$. The GPe outer - SNr weight w_{ot-snr}^- was varied. Both H_{MAX}^* and S_{MAX}^* were
701 reduced. W_c^* was increased which resulted in an increased performance Q^* (Fig 6A-D). This
702 pathway decreased the tonic level of GPi/SNr markedly with increase in w_{ot-snr}^- (Fig 8B, see also
703 Table 4). Clearly, this would facilitate selection, since a lower salience would be sufficient to
704 ensure selection. Thus, the outer neurons made it easier for competing channels to be selected
705 - *soft selectors* (Fig 10D, see Discussion). Although reversal was observed, this was due to the
706 same population inhibitory weight being $w_{ot-ot}^- = -1$. When $w_{ot-ot}^- = 0$, no reversal was seen.
707 Thus, this pathway does not generate reversal but executes it (see Table 4), as it is the pathway

708 targeting the output nuclei. Best performance occurred for $w_{ot-snr}^- = -0.6$ (Fig S2A), and Max
 709 P_h increased with increasing w_{ot-snr}^- till -0.6 and then decreased.

710 3.2.4. GP IN - SNr step-wise model

711 This model investigated the efferents of the GPe inner neurons to the SNr (part of
 712 pathway 7 in Fig 1C, considering only GPe inner). The same population inhibitory weight was
 713 set at $w_{in-in}^- = -1$ and that of GPe outer neurons $w_{ot-ot}^- = -1$ as well. The GPe outer - GPe
 714 inner weight was set at $w_{ot-in}^- = -1$. The GPe inner - SNr weight w_{in-snr}^- , was varied. The GPe
 715 outer - SNr pathway was ‘lesioned’, $w_{ot-snr}^- = 0$, so as to enable examination of GPe inner - SNr
 716 pathway in isolation. Both H_{MAX}^* and S_{MAX}^* were reduced. W_c^* was increased which resulted in
 717 an increased performance Q^* , the metrics resemble those of the GPe outer - SNr step-wise model
 718 (Fig 6A-D). The tonic level of GPi/SNr, like with their GPe outer counterparts, decreased with
 719 increase in w_{in-snr}^- (Fig 8B, see also Table 4), indicating similar roles for these pathways in setting
 720 the tonic level of GPi/SNr, although the decrease was lesser compared to the latter. Thus, the
 721 inner neurons made it less easier for channels to be selected, since they required higher salience
 722 in comparison to the outer neurons. This made the inner neurons - *hard selectors* (Fig 10D,
 723 see Discussion). Reversal was observed, even when both same population inhibitory pathways
 724 were set to $w_{ot-ot}^- = w_{in-in}^- = 0$. However GPe outer - GPe inner weight was high $w_{ot-in}^- = -1$.
 725 When $w_{ot-in}^- = 0$, reversal disappeared. Thus, this pathway had no role in generating reversal but
 726 executed it (see Table 4), just like its GPe outer - SNr counterpart. Best performance occurred
 727 for $w_{in-snr}^- = -0.6$ (Fig S2B).

728 3.2.5. GP OT - STRD1 step-wise model

729 This model investigated the effect of the projections of GPe outer neurons to the
 730 striatum, in this case, striatum D1 (part of pathway 8 in Fig 1C, considering only GPe outer
 731 to STRD1). These projections were modelled as excitatory, since they innervate the FSNs in
 732 the striatum. This model investigates the effect on the selection pathway. We vary the weight
 733 w_{ot-d1}^+ . The same population inhibitory weight was set to $w_{ot-ot}^- = 0$. All features, H_{MAX}^* , S_{MAX}^*
 734 and W_c^* showed a decrement in performance which consequently reduced Q^* (Fig 6A-D). This
 735 indicated that this pathway was not favourable for action selection. However, this was due to
 736 lack of more complete circuitry. Although best selection occurred for $w_{ot-d1}^+ = 0$, we use a value
 737 of $w_{ot-d1}^+ = 0.5$, which gave best performance in the final model (Fig S2C). At a high weight,
 738 $w_{ot-d1}^+ = 1$, at DA = 0, distortion and interference was noticed across saliences, while at high DA,
 739 dual channel selection across saliences was observed. Tonic level of GPi/SNr remained constant
 740 till $w_{ot-d1}^+ = 0.5$ and then increased for subsequent higher weights. Clearly, high weights on this
 741 pathway were detrimental to action selection (see Discussion). Reversal was observed for DA \leq
 742 0.3, indicating its role in causing reversal in the hard selection regime (Fig 7D, see Table 4).

743 3.2.6. GP OT - STRD2 step-wise model

744 This model investigated the effect of the projections to the GPe outer neurons to
 745 the control pathway - striatum D2 (part of pathway 8 in Fig 1C, considering only GPe outer to
 746 STRD2). All the conditions of the previous model remained, except for the GPe outer projections
 747 to the selection pathway, which were ‘lesioned’ $w_{ot-d1}^+ = 0$. H_{MAX}^* and S_{MAX}^* showed a decrement
 748 while W_c^* showed a marked increase consequently improving performance Q^* (Fig 6A-D). This
 749 shows that this pathway is more favourable for action selection unlike its sister projections which
 750 affects striatum D1 SPNs (see Discussion). Reversal was noticed for $w_{ot-in}^- = -0.25$ and $w_{ot-d2}^+ \leq$

751 0.5 and $DA \geq 0.3$, indicating its role in causing reversal largely in the soft selection regime (Fig
752 7D, see Table 4).

753 3.2.7. GP IN - STRD1 step-wise model

754 This model investigated the projections of GPe inner neurons to striatum D1, to
755 the selection pathway, which were modelled as excitatory due to their targeting FSNs (part of
756 pathway 8 in Fig 1C, considering only GPe inner to STRD1). The weight of the GPe outer - GPe
757 inner pathway, w_{ot-in}^- , was varied as well. The output of the GPe outer neurons was ‘lesioned’
758 $w_{ot-snr}^- = 0$, to isolate GPe inner output. H_{MAX}^* and S_{MAX}^* showed a marked decrement. Although
759 W_c^* showed a slight increase, there was a decrease of performance Q^* (Fig 6A-D). Again this
760 is an undesirable pathway for action selection similar to GP OT - STRD1. The model had best
761 performance for $w_{in-d1}^+ = w_{ot-in}^- = 0$, equal to GPR model. However, we used weight of $w_{in-d1}^+ =$
762 0.25 and $w_{ot-in}^- = -0.25$ (Fig S2E) in the final model which yielded best performance. Tonic
763 level of GPi/SNr remained constant till $w_{in-d1}^+ = 0.5$ then decreased. Reversal was noticed for
764 $w_{ot-in}^- = -0.25$ and $w_{in-d1}^+ \leq 0.5$, and for $DA \leq 0.6$ (Fig 7E), indicating its role in causing reversal
765 largely in the hard selection regime and at intermediate dopamine levels (see Table 4).

766 3.2.8. GP IN - STRD2 step-wise model

767 This model investigated the projections of GPe inner neurons to striatum D2, to
768 the control pathway (part of pathway 8 in Fig 1C, considering only GPe inner to STRD2). The
769 weight of the GPe outer - GPe inner pathway, w_{ot-in}^- , was varied as well. The output of the
770 GPe outer neurons was ‘lesioned’ $w_{ot-snr}^- = 0$, to isolate GPe inner output. H_{MAX}^* and S_{MAX}^*
771 show a decrement while W_c^* showed a marked increase, consequently improving performance
772 Q^* (Fig 6A-D). This shows that this pathway is more favourable for action selection similar to
773 GP OT - STRD2. The model had best performance for $w_{in-d2}^+ = w_{ot-in}^- = 0$, equal to GPR model.
774 However we used the weight of $w_{in-d2}^+ = 0.25$ and $w_{ot-in}^- = -0.25$ (Fig S2F) in the final model,
775 which yielded best performance. Tonic level of GPi/SNr remained constant till $w_{in-d2}^+ = 0.5$ then
776 increased. Reversal was noticed for $w_{ot-in}^- = -0.25$ and $w_{in-d2}^+ \leq 0.5$ and for $DA \geq 0.4$ indicating
777 its role in causing reversal largely in the soft selection regime (Fig 7E and Table 4), similar to
778 GP OT - STRD2.

779 3.3. Phase 3: Combined model - I

780 In the third phase, combinations of connections were simulated to dissect out their
781 function. This gave rise to a large number of simulations but essentially it was accomplished in
782 two broad ways. We first captured the dichotomy of the GPe TI neural population - outer and
783 inner neurons added together onto the GPR model which had a single homologous GPe, which
784 we called *Combined model - I* and we present here two instantiations of the same as Case A and
785 Case B.

786 3.3.1. Combined model - I: Case A

787 In Case A, the GPe TI projections to striatum, w_{ot-d1}^+ , w_{ot-d2}^+ , w_{in-d1}^+ , w_{in-d2}^+ ,
788 along with GPe outer - GPe inner pathway w_{ot-in}^- , were varied (pathways 8 + 6 in Fig 1C).
789 The inhibitory same population weights were ‘lesioned’ $w_{ot-ot}^- = w_{in-in}^- = 0$. H_{MAX}^* showed
790 a marked increase while S_{MAX}^* was reduced. W_c^* shows a marked decrease. Overall, there
791 was a decrement of performance Q^* (Fig 9A-D). The model showed best performance for
792 $w_{ot-in}^- = -0.5$, $w_{ot-d1}^+ = w_{ot-d2}^+ = 0.5$ and $w_{in-d1}^+ = w_{in-d2}^+ = 0.25$ (Fig S3A). Reversal was
793 also noticed implicating the modelled pathways in causing it (see Table 4).

794 **Fig 9. Performance metrics.** Performance metrics for the combined models (A) H_{MAX}^* values
795 showing the relative change in Hard selection of the combined models to that of the GPR model
796 (B) S_{MAX}^* values showing the relative change in Soft selection of the combined models to that of
797 the GPR model (C) W_c^* values showing the relative change in cross-over point of the combined
798 models to that of the GPR model (D) Q^* Performance metric values of combined models
799 relative to the GPR model. In all, red plots indicate increment in value while blue plots indicate
800 decrement in value.

801 3.3.2. Combined model - I: Case B

802 In Case B, the GPe TI projections to striatum were fixed $w_{ot-d1}^+ = w_{ot-d2}^+ = 0.5$
803 and $w_{in-d1}^+ = w_{in-d2}^+ = 0.25$. The inhibitory same population weights were varied w_{ot-ot}^- , w_{in-in}^-
804 along with GPe outer GPe inner pathway w_{ot-in}^- (pathway 4 in Fig 1B + pathways 5 + 6 in
805 Fig 1C). H_{MAX}^* showed an increase while S_{MAX}^* showed a marked reduction. W_c^* also showed
806 a marked decrease, causing a decrement of performance Q^* (Fig 9A-D). The model shows best
807 performance for $w_{ot-ot}^- = w_{in-in}^- = w_{ot-in}^- = -0.25$ (Fig S3B). Reversal and changes in tonic value
808 of GPi/SNr were noticed implicating these pathways in both of these functions (see Table 4).

809 3.4. Phase 3: Combined model - II

810 This second major part of combined model simulations, called *Combined model -*
811 *II* augmented the combination model - I, with GPe TA neurons. We divided the model into three
812 stages, each of which is detailed below.

813 3.4.1. Stage 1: Inter-Population Connections

814 This model focussed on varying the weights of the inter-population inhibitory
815 weights within the GPe. The weights w_{ot-in}^- , the pathway between GPe outer and GPe inner
816 neurons, w_{ot-ta}^- , the pathway between GPe outer and GPe TA neurons, w_{in-ta}^- , the pathway be-
817 tween GPe inner and GPe TA neurons were varied (pathway 3 in Fig 1B + pathway 6 in Fig 1C).
818 The GPe TI projections to striatum, were set to zero, $w_{ot-d1}^+ = w_{ot-d2}^+ = w_{in-d1}^+ = w_{in-d2}^+ = 0$.
819 H_{MAX}^* and S_{MAX}^* showed an increase. W_c^* however, showed a marked decrease resulting in a
820 decrement of performance Q^* (Fig 9A-D). Best performance of the model was for the weights
821 $w_{ot-in}^- = 0$ and $w_{ot-ta}^- = w_{in-ta}^- = -1$ (Fig S3C). The role of GP OT - GP IN pathway in reversal
822 as well as in influencing tonic value of GPi/SNr were confirmed. It also became apparent here
823 that using the other two pathways GP OT - GPe TA and GP IN - GPe TA, the GPe TI neurons
824 control the activity of the TA neurons and maintain their influence over the striatum.

825 3.4.2. Stage 2: Intra-Population Connections

826 This model added onto stage 1, the within population inhibitory pathways, which
827 were fixed in the former. The weights in stage 1 along with w_{ot-ot}^- , w_{in-in}^- and w_{ta-ta}^- were varied
828 (pathways 3 + 4 + 1 in Fig 1B + pathways 6 + 5 in Fig 1C). This led to a large number of
829 simulations with many instantiations having performances greater than the GPR model. Only
830 the projections from the GPe TI neurons to the striatum were 'lesioned', $w_{ot-d1}^+ = w_{ot-d2}^+ =$
831 $w_{in-d1}^+ = w_{in-d2}^+ = 0$. H_{MAX}^* and S_{MAX}^* showed an increase. W_c^* however showed a marked
832 decrease resulting in a decrement of performance Q^* (Fig 9A-D). Best performance occurs for
833 $w_{ot-in}^- = w_{ot-ot}^- = w_{in-in}^- = w_{ta-ta}^- = -0.25$ and $w_{ot-ta}^- = w_{in-ta}^- = -0.5$ (Fig S3D). The intra-
834 population connections of the GPe TI neurons were confirmed to be involved in influencing the
835 tonic value of GPi/SNr and in reversal. However, the GPe TA - GPe TA pathway did not seem to
836 partake in any function nor contribute to selection (see Table 4).

837 *3.4.3. Stage 3: Extended Architecture*

838 This model incorporated the extended architecture we planned to simulate (Fig
839 1D). The set of weights for best performance selected from this model is presented as the final
840 model.

841 *3.5. Final Model*

842 The weights were $w_{ta-d1}^- = w_{ta-d2}^- = -0.75$, $w_{ot-in}^- = -0.3$, $w_{ot-ta}^- = w_{in-ta}^- = -0.5$
843 and $w_{ot-ot}^- = w_{in-in}^- = w_{ta-ta}^- = -0.75$. The GPe outer and GPe inner to SNr, output pathway
844 weights were set to $w_{ot-snr}^- = w_{in-snr}^- = -0.4$. We called this model Fin 1 (Fig S3E). We also show
845 a variant of the final model which had a higher Max P_h when there was a difference in the output
846 weights to SNr from the GPe outer and GPe inner neurons, $w_{ot-snr}^- = -1$ $w_{in-snr}^- = -0.2$. We
847 called this model Fin 2 (Fig S3F).

848 *Fin 1.* H_{MAX}^* showed an increase while S_{MAX}^* showed a slight decrease. W_c^* showed a slight
849 decrease, but the overall performance Q^* showed a slight but clear increase than the GPR model
850 (Fig 9A-D). Of all the combined models, this was the only model which showed an increase in
851 performance indicating that the complete architecture was necessary to perform optimal action
852 selection. The model also had reversal largely in the soft selection regime (Fig 7F), thus reducing
853 promiscuous selection. Thus, the model performs better selection *per se* than the GPR model,
854 along with the added functionalities derived from the extended connectivity which are detailed
855 below.

856 *Fin 2.* This model tested the differences in output weights to GPi/SNr from GPe TI neurons.
857 Best performance occurred for $w_{ot-snr}^- = -0.8$ and $w_{in-snr}^- = -0.2$. Although H_{MAX}^* showed an
858 increase, S_{MAX}^* and W_c^* showed a decrement bringing down the model performance Q^* (Fig 9A-
859 D). The results confirmed the step-wise model results and showed that higher weights on outer
860 neuron projections to the output nuclei promoted easier selection, compared to the inner neuron
861 projections to the output nuclei.

862 *3.6. New control functions of GPe*

863 In the original GPR model, routes through GPe were interpreted as 'control path-
864 ways' since GPe supplied signals to ensure that the main 'selection pathway' worked correctly
865 (Fig 1A). Some of our modelling results have an interpretation within this context, highlighting
866 new control properties of the GPe.

867 *3.6.1. The striatal switch network*

868 The arkyvallidial TA neurons can act as a 'striatal switch' and with increased activ-
869 ity, can essentially 'switch off' the striatum (Table 4). The prototypical outer and inner neurons
870 maintain control over the striatum through the TA neurons and by inhibiting their activity can
871 'turn on' the striatum. The crucial link is the TI (outer/inner) - TA connection through which
872 the TI neurons can operate the 'switch'. STN also plays an important role in the operation of
873 the switch, in that by exciting the TA neurons they can 'switch off' the striatum (see also Dis-
874 cussion). Thus, we can dissect out the 'striatal switch network' consisting of the striatal D2 -
875 GPe TA pathway which initiates the network, the GPe TI - GPe TA and STN - GPe TA pathways
876 which operate the switch and the GPe TA - STR pathways which execute the function of the
877 'switch' (See Table 4 and Fig 10A). This is also the network which produces oscillations for low
878 dopamine values, and hence could be a potential source for Parkinsonian oscillations (Fig 5).

879 **Fig 10. Functional roles of the control pathway.** Functional networks (in orange) (A) Striatal
 880 switch (B) SNr Control (C) Reversal (D) Population functions - the GPe inner neurons (red) are
 881 *hard selectors*, the GPe outer neurons (blue) are *soft selectors* and the GPe TA neurons (green)
 882 are the *striatal switch*.

883 3.6.2. SNr control network

884 The TI (outer/inner) neurons control the GPi/SNr - the output nuclei, by setting the
 885 tonic level of inhibition the GPi/SNr have on their efferents, in turn, maintaining control over the
 886 basal ganglia output. Through the same population inhibitory pathways and the GPe OT - GPe
 887 IN pathway, the outer and inner neurons can increase the tonic activity of the output nuclei (Fig
 888 8A, Table 4). Through their projections to the output nuclei, the outer and inner neurons can turn
 889 down the activity of GPi/SNr (Fig 8B, Table 4). This ability to influence basal ganglia output
 890 gives the GPe prototypical neurons effective control of selection. In this, the outer neurons are
 891 ‘soft selectors’ since they facilitate selection at lower saliences, while the inner neurons are ‘hard
 892 selectors’ owing to their requiring higher saliences to result in selection (Fig 10D). The network
 893 of these pathways which form the ‘SNr control network’ are shown in Fig 10B.

894 3.6.3. Reversal network

895 Through their same population inhibitory connections, the TI (outer/inner) neurons
 896 give rise to the reversal phenomenon (Fig 7A & B, Table 4). They maintain reversal across
 897 dopamine levels through their projections to the striatum (Fig 7D & E, Table 4). The outer-inner
 898 pathway does not generate reversal, but is crucial to sustain it (Fig 7C, Table 4), and if ‘lesioned’,
 899 reversal phenomenon is lost. This is due to upsetting of the two-stage processing of outer and
 900 inner neurons (Fig 10D, see Discussion). The pathways comprising the ‘reversal network’ are
 901 shown in Fig 10C.

Table 4: **Functions of different pathways**

Pathway	Oscillations	Striatal Switch	Reversal	Tonic level of GPi/SNr	Network
GPe TA to striatum D1	Generates	Executes	-	-	Striatal switch
GPe TA to striatum D2	Generates	Executes	-	-	Striatal switch
GPe TA to GPe TA	-	-	-	-	-
GPe TI (outer/inner) to GPe TA	-	Operates	-	-	Striatal switch
STN to GPe TA	-	Operates	-	-	Striatal switch
GPe outer to GPe outer	-	-	Generates	Increases	Reversal/ GPi/SNr control
GPe inner to GPe inner	-	-	Generates	Increases	Reversal/ GPi/SNr control

GPe outer to GPe inner	-	-	Sustains	Increases	Reversal/ GPi/SNr control
GPe outer to GPi/SNr	-	-	Executes	Decreases	Reversal/ GPi/SNr control
GPe inner to GPi/SNr	-	-	Executes	Decreases	Reversal/ GPi/SNr control
GPe outer to striatum D1	-	-	In the hard selection regime	-	Reversal
GPe outer to striatum D2	-	-	In the soft selection regime	-	Reversal
GPe inner to striatum D1	-	-	In the hard selection regime and intermediate DA	-	Reversal
GPe inner to striatum D2	-	-	In the soft selection regime	-	Reversal
Striatum D2 to GPe TI (outer/inner)	-	-	Initiates	Initiates	Reversal/ GPi/SNr control
Striatum D2 to GPe TA	Initiates	Initiates	-	-	Striatal switch
Striatum D1 to GPi/SNr	-	-	-	-	Direct pathway
STN to GPe TI (outer/inner)	-	Operates	-	-	Striatal switch
STN to GPi/SNr	-	-	-	-	Hyperdirect pathway

902 Functions of the different pathways simulated in our models and the network architecture that
903 they belong to. The GPe TA projections give rise to oscillations but input from the striatum D2
904 to the GPe TA initiates them. The ‘Striatal switch’ function is executed via the GPe TA
905 prjections to the striatal SPNs. The ‘switch’ is operated by both the STN and GPe
906 TI(outer/inner). ‘Reversal’ is generated by the same subpopulation inhibitory connections of the
907 GPe TI (outer/inner) neurons, while the outer-inner projection is needed to maintain it. The
908 striatal projections of the outer/inner neurons ensure that reversal occurs across the range of
909 dopamine activity in the striatum, while reversal eventually occurs via the GPe TI projections to
910 the output nuclei GPi/SNr.

911 **4. Discussion**

912 We have investigated the newly discovered intrinsic connectivity of GPe in consid-
913 erable detail. Quantitative evaluation of selection performance in this model has revealed several
914 new functions of GPe that may be understood within the selection framework. The prototypical
915 neurons have been shown to be the principal subpopulation influencing action selection. The
916 arky pallidal neurons are used by both the prototypical neurons and the STN, to modulate the
917 activity of the striatum. These arky pallidal neurons are also revealed as a novel source of theta
918 oscillations in the absence of dopaminergic modulation in the striatum. The prototypical neurons
919 furthermore, exert their influence on the output nuclei GPi/SNr, by setting the level of their tonic
920 activity. We can thus infer from the results, that the GPe is a nucleus of vital importance for
921 action selection playing a range of roles in its control and modulation.

922 *4.1. Support for action selection hypothesis*

923 The action selection hypothesis (Gurney et al., 2004) is further supported by the
924 present results. The incorporation of more anatomically plausible detail (compared with the
925 original, GPR model), and the optimization of the model on action selection capabilities show
926 quantitative improvement in selection. Moreover, new functional roles of the control pathway
927 have emerged along with a greater understanding of the roles of neural subpopulations within
928 the GPe. Earlier models with the classical connectivity of the basal ganglia did demonstrate the
929 ability to perform action selection. However, this had not been addressed with the newly revealed
930 projections and connectivity of the GPe.

931 *4.2. TA neurons can turn up or turn down striatal activity*

932 Our results indicate that the arky pallidal TA neurons, through their activity, can
933 turn down activity in the striatum and can be regarded as a sort of striatal ‘switch’ (Fig 10D).
934 Furthermore, the prototypical TI neurons through their modulation of the TA neuronal excitabil-
935 ity, can restore striatal activity. The GPe TI - GPe TA pathway seems to be the crucial link
936 through which the TI neurons control the TA neurons, in turn maintaining operational control
937 over the striatum. There is some evidence from modelling indicating a strong GPe TI - TA
938 projection (Lindahl and Hellgren Kotaleski, 2016). In our simulations, for high weights on the
939 arky pallidal projections to striatum, activity in striatum was very low, and the TA neurons had
940 effectively turned striatum ‘off’. This resulted in no selection occurring. As soon as the weights
941 on the arky pallidal projections to striatum were reduced, activity in the striatum was restored and
942 selection was induced, with performance metric Q^* higher than the GPR model. The striatum
943 had been turned ‘on’.

944 These results are supported by a recent study which showed that arky pallidal TA
945 neurons in the GPe, send a ‘Stop’ signal and can essentially curtail developing action representa-
946 tions in the striatum (Mallet et al., 2016). Although it is not clear whether the arky pallidal cells
947 are the source or simply relay this ‘Stop’ signal as noted in (Mallet et al., 2016), our simulations
948 suggest that the GPe TI prototypical cells could have a role in determining when the arky pallidal
949 cells can ‘turn off’ the striatum.

950 Another factor to consider here is the role of the STN, which is known to generate
951 a stop signal via the hyperdirect pathway (Gillies and Willshaw, 1998; Frank, 2006) and the in-
952 direct pathway. STN and GPe TA neurons fire in phase with cortical activity (Mallet et al., 2012)
953 and there is also computational evidence indicating that STN might target GPe TA neurons more
954 strongly than GPe TI (Nevado-Holgado et al., 2014). Thus, the STN could clearly activate the

955 GPe TA neurons, thereby switching-off the striatum. However, the GPe TI neurons can inhibit
956 the GPe TA as well as the STN, thereby stopping the ‘stop’ signal from the STN - GPe TA net-
957 work, given that the GPe TI neurons fire out of phase with cortical activity (Mallet et al., 2012).
958 Thus, both the STN and the GPe TI contribute to the striatal switch network, and they *operate*
959 the switch - in that STN can turn the switch ‘on’, while the GPe TI can turn it ‘off’. This also
960 suggests the possibility of both the STN and the prototypical GPe neurons being involved in *ex-*
961 *plorative* behaviour. Along with the tonic dopaminergic modulation of the striatum, there have
962 been suggestions of the involvement of the STN - GPe network, as well as the lateral intrinsic
963 connectivity within the STN in explorative behaviour (Chakravarthy et al., 2010; Gillies et al.,
964 2002; Kalva et al., 2012; Mandali et al., 2015). More work is required with our model to explore
965 these possibilities, but the model provides a basis for doing so in future simulations.

966 4.3. *Oscillations from TA neuronal projections - consistent with Parkinsons disease*

967 Modelling of the arky pallidal TA neurons has revealed low-frequency theta oscil-
968 lations (3-10 Hz) which are reliant on the GPe TA - striatal pathway. Low frequency oscillations
969 have been associated with Parkinsons disease and are said to be in synchrony with tremor (Bevan
970 et al., 2002). Oscillations around this range are said to arise in the basal ganglia and spread to
971 the cortex, producing an ‘antikinetic’ effect (Hutchison et al., 2004). Loss of dopamine has been
972 associated to these oscillations (Rivlin-Etzion et al., 2006; Weinberger and Dostrovsky, 2011).
973 Furthermore, modelling also suggests that increase in oscillations interfering with information
974 processing in the basal ganglia is characteristic of Parkinsonian conditions (Bergman et al., 1998;
975 Lindahl and Hellgren Kotaleski, 2016). Our model shows that the oscillations have maximum
976 amplitude for no dopamine activity ($DA = 0$) consistent with Parkinsons disease, and are sup-
977 pressed for higher dopamine values. The model reveals TA projections to the striatum to be the
978 source of these low frequency oscillations, but high inhibitory input from the prototypical TI
979 neurons are also necessary to sustain them. The model also shows better performance for a cor-
980 responding high inhibitory weight of TI (outer/inner) - TA pathways, which are accordingly set
981 high in the final model. Furthermore, the GPe TI neurons are known to have have more axonal
982 collaterals within GPe, targeting GPe TA neurons (Sadek et al., 2007; Lindahl and Hellgren Ko-
983 taleski, 2016). There is also evidence implicating the GPe TA neurons as well as the GPe-STN
984 network in inducing oscillations (Nevado-Holgado et al., 2014; Lindahl and Hellgren Kotaleski,
985 2016). In summary, we can conclude from our results that the anatomical substrate exists to
986 sustain these oscillations, and without dopamine, there may be no stopping them.

987 While beta oscillations are discussed more often in relation to Parkinson’s disease,
988 theta oscillations are associated with a very characteristic pathological deficit - freezing of gait.
989 Clinical studies show an increase of theta oscillations with freezing, referred to as ‘trembling in
990 place’ (Plamen et al., 2006; Shine et al., 2014). It has been hypothesised that oscillatory inter-
991 action in the STN-GPe network underly these oscillations (Shine et al., 2013). Our results show
992 that the oscillations manifest when there is competition between two action representations (See
993 Fig 5).

994 It thus appears that the arky pallidal TA neurons are a novel potential source of
995 theta oscillations under dopamine depleted conditions, similar to pathophysiological conditions
996 of Parkinsons disease. But how are they generated? Our results clearly reveal the cause - lack
997 of dopamine. Dopamine is well known to modulate excitability of the SPNs in the striatum
998 (Humphries et al., 2009a; Jr and Zigmond, 1997) and our results show that the arky pallidal neu-
999 rons are able to turn up or turn down the activity of the SPNs via their massive projections. Our
1000 results indicate that removing dopamine could alter the excitability of SPNs during high salience

1001 competing inputs, resulting in a continuous switching between the ‘striatum on’ and ‘striatum
1002 off’ conditions (translates to switching between their ‘up’ and ‘down’ states (Wilson and Groves,
1003 1981; Kasanetz et al., 2006)), which would also engage the STN - GPe, inducing the theta os-
1004 cillations in the network. This possibility is corroborated by the suggestion that rhythmic inputs
1005 from striatum, but also from cortex and thalamus could engage STN-globus pallidus network in
1006 Parkinsonian oscillations (Nevado-Holgado et al., 2014). Furthermore, these oscillations seen in
1007 the STN - GPe - GPi/SNr network (see Figure 5E & F) agree with the evidence of high level
1008 of synchronous oscillations, including the theta band, observed in these nuclei in Parkinsonian
1009 conditions (Weinberger and Dostrovsky, 2011; Tachibana et al., 2011).

1010 Our model also suggests a possible explanation for a long standing paradox in PD
1011 treatment. Current treatment therapies to alleviate parkinsonian deficits by lesions and deep-
1012 brain stimulations of the STN present an incongruity - in that both lesioning of the STN, or its
1013 increased activity (by high frequency deep brain stimulation) reduces Parkinsonian symptoms
1014 (Okun and Vitek, 2004; Benabid et al., 2009). Our results also indicated that mimicking these
1015 conditions in the model which produced the oscillations under dopamine depleted conditions
1016 could remove the oscillations and improve selection (See Results and Fig 5G,H and S4). Our
1017 network architecture for the striatal-switch (Fig 10A) suggests that lesioning STN, would result
1018 in the lesser activation of the GPe TA, preventing the inhibition of SPNs, which means that the
1019 striatal switch architecture would simply be bypassed - thus preventing oscillations in the net-
1020 work. This hypothesis is supported by several of our step-wise models, which lacked the GPe
1021 TA neurons, for instance, the GPe TI - GPe TI step-wise model. Although the striatal switch
1022 network was absent, the model could perform action selection *per se*, as well as the GPR model
1023 (Fig 6A-D).

1024 On the other hand, high-frequency stimulation of the STN would ‘switch-on’ the
1025 GPe TA - but this would also activate the GPe TI neurons, which would play their part in con-
1026 trolling STN excitation as well as in inhibition and ‘switch-off, of the GPe TA neurons. We
1027 speculate that this activation of the GPe TA from STN and the consequent modulation of their
1028 excitability by the TI neurons, would inhibit the SPNs in striatum to prevent their oscillatory
1029 swapping between ‘on’ and ‘off’ states caused by lack of dopamine.

1030 Lastly, with respect to the preferential targets of the massive arky pallidal projec-
1031 tions to striatum, there is by far, no clear consensus. However, there is evidence suggesting that
1032 they target not only the spines of the SPNs, but also different interneuron subtypes (Mallet et al.,
1033 2012; Glajch et al., 2016; Hegeman et al., 2016; Burke et al., 2017). We have modelled only the
1034 diffuse arky pallidal inhibitory projections to the SPNs. The final model gave best performance
1035 for a lower weight of the arky pallidal projections to SPNs (see Results), which corroborates
1036 anatomical evidence indicating that the projections are not exclusive to the striatal SPNs.

1037 4.4. GPe TA predominantly receive local collaterals from GPe TI neurons

1038 Our results indicated that the probability of GPe TI - GPe TA connections were
1039 more likely, rather than GPe TA - GPe TA connections. While in the step-wise models, both the
1040 pathways showed similar performance (see Fig 6A-D), subsequent combined models revealed
1041 no role for the GPe TA - GPe TA pathway. Furthermore, change of weights of the TA - TA did
1042 not result in any change in performance. However, the GPe TI - GPe TA pathway was a vital
1043 component of the striatal switch network, enabling the TI neurons to control the TA neurons.
1044 While it is generally known that GPe neurons receive local collaterals, the organisation of local
1045 collateral inputs to the GPe TA neurons is not yet clear. However, it is known that the TI neurons
1046 send out more local collaterals than the TA neurons (Mallet et al., 2012), and that they are also

1047 the predominant subpopulation, indicating a stronger TI - TA connection probability. This allows
1048 us to predict that a TI - TA pathway is more likely, which also agree with those of (Lindahl and
1049 Hellgren Kotaleski, 2016), which predict a stronger TI - TA connection.

1050 *4.5. Prototypical TI neurons promote better hard selection through reversal*

1051 Reversal phenomenon noticed in these simulations was another significant result.
1052 The GPR model had shown only a monotonic decrease in channel output with increase in salience
1053 or input. With the inclusion of the reversal network (Fig 10C), which are essentially the proto-
1054 typical neurons (see subsequent section), this trend can be reversed.

1055 Reversal can occur as several cases, some of which can be detrimental to a selection
1056 mechanism. For instance, in the case which resulted in the deselection of a selected channel
1057 (Single Ch selection → No Selection). However, these cases were only seen in step-wise models
1058 and were not observed in the final model, indicating that they were due to an incomplete model-
1059 led architecture. In the final model, reversal cases comprised entirely of Dual channel selection
1060 → Interference/Distortion/Switching occurring in both the hard and soft selection regimes, al-
1061 though largely in the soft selection regime (Fig 7F). This contributed to the better performance
1062 of the model than the GPR model, in that some of the soft selection outcomes were reversed into
1063 hard selection outcomes. This also indicated that the prototypical neurons aid in better *decision-*
1064 *making* by making a ‘choice’ between competing channels of high salience. Thus, when faced
1065 between two possible action outcomes, the prototypical neurons can essentially ‘choose’ one at
1066 a time.

1067 The simulations have shown that within population inhibitory connections of outer
1068 and inner neurons, are responsible for causing the reversal phenomenon (Fig 7 and Table 4). It is
1069 also evident that with higher weights they ensure reversal occurring across the range of dopamine
1070 values. High weights are also necessary for reversal to occur in subsequent combined models,
1071 in addition to their contribution for better performance. It is with this view that higher weights
1072 were fixed for these pathways in combined models, which in addition, agrees with anatomical ev-
1073 idence showing prototypical neurons having more extensive local collaterals (Sadek et al., 2007).
1074 In addition to the within inhibitory projections of the outer and inner neurons, the outer to inner
1075 neuron inhibitory projections are also vital for reversal, as well as for improving the performance
1076 of the model. These three pathways form the core aspect of the reversal network (Fig 10C).

1077 *4.6. Striatal projections of prototypical TI neurons facilitate reversal over a range of dopamine* 1078 *levels*

1079 The striatal projections of outer and inner neurons seem to play the crucial role of
1080 spreading the reversal phenomenon across dopamine levels (Fig 7 and Table 4). The projections
1081 of outer neurons to the selection pathway (STRD1) cause reversal at low dopamine levels $DA \leq 0.3$,
1082 The outer neuron projections to the control pathway (STRD2) cause reversal for $DA \geq 0.3$
1083 onwards. Striatal projections of inner neurons to both the selection and control pathways, cause
1084 reversal for mid-valued dopamine ($0.2 \leq DA \leq 0.8$). This allows for ‘reversal’ of promiscuous
1085 selections into hard selection outcomes occurring at different levels of dopamine activity - aiding
1086 in more optimal selection.

1087 Regarding the striatal projections of the prototypical neurons, from (Sadek et al.,
1088 2007), we have data indicating every 4/8 outer neurons and 2/9 inner neurons projecting to the
1089 striatum. The final model yielded best performance for matching corresponding weights at 0.5
1090 and 0.25 respectively. Having higher weights on outer neuron striatal projections resulted in

1091 complete soft selection, while higher weights on inner neuron striatal projections resulted in no
1092 selection occurring. Thus, the best performance weights in the final model shows a degree of
1093 agreement on available biological data on these pathways.

1094 *4.7. Differences in prototypical TI neural population influences*

1095 The outer neurons seem to be associated more with soft selection owing to
1096 the decreased tonic level of the GPi/SNr they set, through their efferents. This allows action
1097 representations with relatively lower saliences to be selected. This was further substantiated
1098 in the final model, wherein an increased weight of outer-SNr pathway and decreased weight
1099 of inner-SNr pathway increased the hard selection performance H_{MAX}^* (Fin 2, see Results).
1100 Although H_{MAX}^* was increased, there was a decrease of W_c^* and the performance was less than
1101 the GPR model. The range of dopamine values where hard selection dominates was reduced
1102 considerably (Fig S3F) because this condition allows for more promiscuous selection, which
1103 decreases performance. Overall, this indicates that the outer neurons can help in easier selection
1104 making them ‘soft selectors’ (Fig 10D).

1105 In contrast, the inner neurons seem to be more associated with hard selection (Fig
1106 10D), since they reduce the tonic level of GPi/SNr to a much less extent than the outer neurons.
1107 Thus, the inner neurons encourage only actions with stronger saliences to be selected thus
1108 reducing promiscuous selection - making them ‘hard selectors’. Additionally, we verified this
1109 by running a variant of the Fin 2 model with higher inner neuron to GPi/SNr and reduced outer
1110 to GPi/SNr weights. The extent of hard selection regime across dopamine values did increase.
1111 However, maximum value of hard selection was less than that of the Fin 1 model which had the
1112 outer and inner neuron to GPi/SNr weights equal.

1113 The overall conclusion was that both the differential influences of the outer and
1114 inner neurons, on soft and hard selection are necessary to promote optimal selection. In the
1115 final model, the best performance was for having equal weights on these two pathways. This
1116 allows us to predict that the outer and inner neuron efferents to the GPi/SNr are relatively
1117 equal in magnitude and strength. There is no evidence so far to support any differences in
1118 the relative strengths of the extrinsic efferents of outer and inner neurons to the GPi/SNr, as of yet.

1119

1120 *4.8. GPe influence on the GPi/SNr*

1121 The within population inhibitory pathways of the outer and inner neurons and the
1122 outer - inner pathway, increase the tonic value of GPi/SNr with increasing weights which results
1123 in higher salience being required to reach the selection threshold (Fig 8A). The extrinsic efferents
1124 of the GPe outer and inner neurons to GPi/SNr, tend to decrease the tonic value of GPi/SNr,
1125 making it easier to reach the threshold (Fig 8B). Since the weight change in the semilinear
1126 neuron is equivalent to changing afferent drive, this indicates a ‘push-pull’ mechanism, wherein,
1127 based on the relative ‘importance’ of a particular action, the feasibility of its selection can be
1128 enhanced or decreased by the prototypical neurons. This reveals an additional mechanism,
1129 through which the GPe can maintain an operational control over the GPi/SNr; without the GPe
1130 prototypical neurons, there would be no modulation of the level of tonic activity of the GPi/SNr.
1131 Lesion studies of the GPe result in a marked increase in the level of tonic activity of the GPi/SNr,
1132 as well as exacerbated Parkinsonian symptoms (Zhang et al., 2006). Our results agree in that
1133 lesions of the outer-SNr and inner-SNr pathways leads to the loss of the ‘push’ mechanism,
1134 and hence induces difficulty in selection. The outer-SNr pathway lesion reduces the ability for

1135 soft selection, while the inner-SNr pathway lesion results in reduced ability for hard selection.
1136 Lesions of outer-outer and inner-inner pathways result in loss of the ‘pull’ mechanism - as well
1137 as loss of reversal.
1138

1139 5. Concluding remarks

1140 The simulations have thrown light on the importance of the GPe in the basal gan-
1141 glia, and its crucial and myriad role in action selection. It seems to be a ‘control centre’ of the
1142 basal ganglia with considerable influence on the functioning of other basal ganglia nuclei. The
1143 results show the GPe controlling the striatum, the GPi/SNr and as shown also in previous mod-
1144 els, the STN (Gurney et al., 2001a). In particular, the prototypical GPe TI (outer/inner) neurons,
1145 seem to be the ‘controllers’, maintaining operational control over different subnuclei, and on
1146 striatum via the arky pallidal TA neurons. They can use the arky pallidal neurons to turn on or
1147 turn off the striatum, can effect selection by setting the level of tonic activity of the GPi/SNr, and
1148 can contribute to optimizing action selection via reversal.

1149 The implication is that the GPe cannot be modelled as a simple uniform relay nu-
1150 cleus. On the contrary, each subpopulation plays a distinct and direct role in action selection.
1151 The arky pallidal neurons clearly have a massive influence on the striatum and when more data
1152 is available on their connectivity, they must be incorporated in future models. Our model has
1153 allowed for the unification of the two levels of neuronal organization in the GPe - the prototyp-
1154 ical neurons and the outer/inner neurons. These subtypes of the prototypical neurons also have
1155 differences in their influence on action selection. The prototypical neurons along with the tonic
1156 dopaminergic activity from the SNc in striatum, may also play a role in explorative behaviours.
1157 Furthermore, their ability to regulate the tonic level of activity of the output nuclei (GPi/SNr) in
1158 a ‘push-pull’ manner could also indicate a role in learning. Thus, the indirect pathway would
1159 seem to have a wider scope of functionality in addition to being the classical ‘no-go’ pathway.
1160 Overall, the simulations have reinforced the hypothesis of action selection as a primary function
1161 of the basal ganglia.

1162 Looking forward, the simulation results open up new questions. For instance, the
1163 ability of the arky pallidal neurons to suppress action representations and the ability of the STN-
1164 GPe prototypical network to ‘use’ this function, leads to the question whether these decisions
1165 are made at the level of the basal ganglia? Does the GPe, and more specifically the prototypical
1166 neurons themselves, have a part in the decision-making? Or are they merely relaying inputs?
1167 The range of roles the GPe has in action selection as suggested by our simulation results, hint at
1168 a more proactive role in decision-making rather than being just a relay of decisions made else-
1169 where. Although we have modelled to a considerable extent, the intrinsic connectivity of the
1170 GPe known till date, we are yet to capture the connectivity *in toto*. The extended architecture
1171 proposed however, must be simulated in the much wider contexts of cortical and thalamic loops
1172 as well as the intrinsic and extrinsic connectivity of other basal ganglia nuclei.

1173 Finally, the involvement of the GPe-STN-GPi/SNr network in generating oscilla-
1174 tions and in particular, the arky pallidal projections to striatum, demand for more comprehensive
1175 circuit investigations in pathological conditions of the basal ganglia like Parkinson’s disease.
1176 These results can act as useful pointers for clinical assessment as well as remedy for these patho-
1177 logical conditions. However, as with all our results, we look forward to their being extended and
1178 tested further against new data.

1179 **Supporting information**

1180 **Fig S1. Step-wise model simulation plots.** Step-wise model P_h and P_s plots (cubic spline fits)
1181 across dopamine levels and parameter values: **(A)** TA - TA model **(B)** TA -STR model **(C)** TI -
1182 TA model **(D)** TI - TI model **(E)** IN - IN model **(F)** OT - IN model.

1183 **Fig S2. Step-wise model simulation plots.** Step-wise model P_h and P_s plots (cubic spline fits)
1184 across dopamine levels and parameter values: **(A)** OT - SNR model **(B)** IN - SNR model **(C)** OT
1185 - STRD1 model **(D)** OT - STRD2 model **(E)** IN - STRD1 model **(F)** IN - STRD2 model.

1186 **Fig S3. Combined model simulation plots.** Combined model P_h and P_s plots (cubic spline fits)
1187 across dopamine levels and parameter values: **(A)** OT IN Case A **(B)** OT IN Case B **(C)** Stage 1
1188 **(D)** Stage 2 **(E)** and **(F)** Two versions of the final model.

1189 **Fig S4. Selection templates for STN DBS/Lesion models** **(A)** Selection template for the model
1190 with $DA = 0$, producing oscillations (see also Fig 5A) **(B)** Selection template for the STN – DBS
1191 model **(C)** Selection template for the STN – lesion model **(D)** Max P_h values for the oscillating,
1192 STN – DBS and STN – lesion models. Both the STN – DBS and STN – lesion models show
1193 better hard selection than the oscillating model.

1194 **Appendix A1. Detailed modelling formalism of the various subnuclei.** Activation and output
1195 functions of the various subpopulations and subnuclei are presented here.

1196 **Appendix A2. Synaptic weights.** Synaptic weights used in various step-wise and combined
1197 models are tabulated here.

1198 **Acknowledgments**

1199 We acknowledge the following grant sponsors: European Horizon 2020 Frame-
1200 work Programme [Grant 720270 (Human Brain Project SGA1), Grant 785907 (Human Brain
1201 Project SGA2)], the Swedish Research Council and the Swedish e-Science Research Center. We
1202 are also grateful for comments on the manuscript by Dr. Brita Robertson and Associate professor
1203 Dr. Peter Wallén.

1204 **References**

- 1205 Abdi, A., Mallet, N., Mohamed, F. Y., Sharott, A., Dodson, P. D., Nakamura, K. C., Suri, S., Avery, S. V., Larvin,
1206 J. T., Garas, F. N., Garas, S. N., Vinciati, F., Morin, S., Bezard, E., Baufreton, J., Magill, P. J., 2015. Prototypic and
1207 arky pallidal neurons in the dopamine-intact external globus pallidus. *Journal of Neuroscience* 35 (17), 6667–6688.
1208 Akkal, D., Burbaud, P., Audin, J., Bioulac, B., 1996. Responses of substantia nigra pars reticulata neurons to intrastriatal
1209 d1 and d2 dopaminergic agonist injections in the rat. *Neuroscience Letters* 213 (1), 66 – 70.
1210 Alexander, G. E., DeLong, M. R., , Strick, P. L., 1986. Parallel organization of functionally segregated circuits linking
1211 basal ganglia and cortex. *Annual Review of Neuroscience* 9 (1), 357–381, PMID: 3085570.
1212 Bahuguna, J., Tetzlaff, T., Kumar, A., Hellgren Kotaleski, J., Morrison, A., 2017. Homologous basal ganglia network
1213 models in physiological and parkinsonian conditions. *Frontiers in Computational Neuroscience* 11, 79.
1214 Barto, A. G., 1994. Reinforcement learning control. *Current Opinion in Neurobiology* 4 (6), 888–893.
1215 URL <http://www.sciencedirect.com/science/article/pii/0959438894901384>
1216 Barto, A. G., Mahadevan, S., 2003. Recent advances in hierarchical reinforcement learning. *Discrete Event Dynamic*
1217 *Systems* 13 (4), 341–379.
1218 URL <https://doi.org/10.1023/A:1025696116075>

- 1219 Beiser, D. G., Houk, J. C., 1998. Model of cortical-basal ganglionic processing: Encoding the serial order of sensory
1220 events. *Journal of Neurophysiology* 79 (6), 3168–3188.
- 1221 Benabid, A. L., Chabardes, S., Mitrofanis, J., Pollak, P., 2009. Deep brain stimulation of the subthalamic nucleus for the
1222 treatment of parkinson’s disease. *The Lancet Neurology* 8 (1), 67 – 81.
1223 URL <http://www.sciencedirect.com/science/article/pii/S1474442208702916>
- 1224 Bergman, H., Feingold, A., Nini, A., Raz, A., Slovin, H., Abeles, M., Vaadia, E., 1998. Physiological aspects of infor-
1225 mation processing in the basal ganglia of normal and parkinsonian primates. *Trends in Neurosciences* 21 (1), 32 – 38.
1226 URL <http://www.sciencedirect.com/science/article/pii/S016622369701151X>
- 1227 Berthet, P., Lindahl, M., Tully, P. J., Hellgren-Kotaleski, J., Lansner, A., 2016. Functional relevance of different basal
1228 ganglia pathways investigated in a spiking model with reward dependent plasticity. *Frontiers in Neural Circuits* 10,
1229 53.
- 1230 Bevan, M. D., Booth, P. A. C., Eaton, S. A., Bolam, J. P., 1998. Selective innervation of neostriatal interneurons by a
1231 subclass of neuron in the globus pallidus of the rat. *Journal of Neuroscience* 18 (22), 9438–9452.
- 1232 Bevan, M. D., Magill, P. J., Terman, D., Bolam, J., Wilson, C. J., 2002. Move to the rhythm: oscillations in the subthala-
1233 mic nucleus–external globus pallidus network. *Trends in Neurosciences* 25 (10), 525 – 531.
- 1234 Blenkinsop, A., Anderson, S., Gurney, K., 2017. Frequency and function in the basal ganglia: the origins of beta and
1235 gamma band activity. *The Journal of Physiology* 595 (13), 4525–4548.
- 1236 Bogacz, R., Martin Moraud, E., Abdi, A., Magill, P. J., Baufreton, J., 07 2016. Properties of neurons in external globus
1237 pallidus can support optimal action selection. *PLOS Computational Biology* 12 (7), 1–28.
1238 URL <https://doi.org/10.1371/journal.pcbi.1005004>
- 1239 Bolam, j. p., hanley, j. j., booth, p. a. c., bevan, m. d., 2000. Synaptic organisation of the basal ganglia. *Journal of*
1240 *Anatomy* 196 (4), 527–542.
1241 URL <http://dx.doi.org/10.1046/j.1469-7580.2000.19640527.x>
- 1242 Brown, J. W., Bullock, D., Grossberg, S., 2004. How laminar frontal cortex and basal ganglia circuits interact to control
1243 planned and reactive saccades. *Neural Networks* 17 (4), 471 – 510.
- 1244 Burke, D. A., Rotstein, H. G., Alvarez, V. A., 2017/11/22 2017. Striatal local circuitry: A new framework for lateral
1245 inhibition. *Neuron* 96 (2), 267–284.
1246 URL <http://dx.doi.org/10.1016/j.neuron.2017.09.019>
- 1247 Calabresi, P., Picconi, B., Tozzi, A., Ghiglieri, V., Di Filippo, M., 08 2014. Direct and indirect pathways of basal ganglia:
1248 a critical reappraisal. *Nat Neurosci* 17 (8), 1022–1030.
1249 URL <http://dx.doi.org/10.1038/nn.3743>
- 1250 Chakravarthy, V. S., Balasubramani, P. P., 2013. *Basal Ganglia System as an Engine for Exploration*. Springer New York,
1251 New York, NY, pp. 1–15.
- 1252 Chakravarthy, V. S., Joseph, D., Bapi, R. S., 2010. What do the basal ganglia do? a modeling perspective. *Biological*
1253 *Cybernetics* 103 (3), 237–253.
1254 URL <https://doi.org/10.1007/s00422-010-0401-y>
- 1255 Chang, H., Wilson, C., Kitai, S., 1981. Single neostriatal efferent axons in the globus pallidus: a light and electron
1256 microscopic study. *Science* 213 (4510), 915–918.
- 1257 Chersi, F., Mirolli, M., Pezzulo, G., Baldassarre, G., 2013. A spiking neuron model of the cortico-basal ganglia circuits
1258 for goal-directed and habitual action learning. *Neural Networks* 41 (Supplement C), 212 – 224, special Issue on
1259 *Autonomous Learning*.
- 1260 Corbit, V. L., Whalen, T. C., Zitelli, K. T., Crilly, S. Y., Rubin, J. E., Gittis, A. H., 2016. Pallidostriatal projections
1261 promote beta oscillations in a dopamine-depleted biophysical network model. *Journal of Neuroscience* 36 (20), 5556–
1262 5571.
- 1263 Damodaran, S., Cressman, J. R., Jedrzejewski-Szmek, Z., Blackwell, K. T., 2015. Desynchronization of fast-spiking
1264 interneurons reduces beta band oscillations and imbalance in firing in the dopamine-depleted striatum. *Journal of*
1265 *Neuroscience* 35 (3), 1149–1159.
- 1266 Dodson, P. D., Larvin, J. T., Duffell, J. M., Garas, F. N., Doig, N. M., Kessar, N., Duguid, I. C., Bogacz, R., Butt,
1267 S. J., Magill, P. J., 2015. Distinct developmental origins manifest in the specialized encoding of movement by adult
1268 neurons of the external globus pallidus. *Neuron* 86 (2), 501 – 513.
- 1269 Frank, M. J., 2005. Dynamic dopamine modulation in the basal ganglia: A neurocomputational account of cognitive
1270 deficits in medicated and nonmedicated parkinsonism. *Journal of Cognitive Neuroscience* 17 (1), 51–72.
- 1271 Frank, M. J., 2006. Hold your horses: A dynamic computational role for the subthalamic nucleus in decision making.
1272 *Neural Networks* 19 (8), 1120 – 1136, *neurobiology of Decision Making* *Neurobiology of Decision Making*.
- 1273 Frank, M. J., Seeberger, L. C., O’Reilly, R. C., 2004. By carrot or by stick: Cognitive reinforcement learning in parkin-
1274 sonism. *Science* 306 (5703), 1940–1943.
- 1275 Freeze, B. S., Kravitz, A. V., Hammack, N., Berke, J. D., Kreitzer, A. C., 2013. Control of basal ganglia output by direct
1276 and indirect pathway projection neurons. *Journal of Neuroscience* 33 (47), 18531–18539.
- 1277 Gillies, Willshaw, D., Li, Z., 03 2002. Subthalamic–pallidal interactions are critical in determining normal and abnor-

mal functioning of the basal ganglia. *Proceedings of the Royal Society of London. Series B: Biological Sciences* 269 (1491), 545.
 URL <http://rspb.royalsocietypublishing.org/content/269/1491/545.abstract>

Gillies, A. J., Willshaw, D. J., 1998. A massively connected subthalamic nucleus leads to the generation of widespread pulses. *Proceedings of the Royal Society of London B: Biological Sciences* 265 (1410), 2101–2109.
 URL <http://rspb.royalsocietypublishing.org/content/265/1410/2101>

Glajch, K. E., Kelder, D. A., Hegeman, D. J., Cui, Q., Xenias, H. S., Augustine, E. C., Hernández, V. M., Verma, N., Huang, T. Y., Luo, M., Justice, N. J., Chan, C. S., 2016. Npas1+ pallidal neurons target striatal projection neurons. *Journal of Neuroscience* 36 (20), 5472–5488.
 URL <http://www.jneurosci.org/content/36/20/5472>

Grace, A. A., Floresco, S. B., Goto, Y., Lodge, D. J., 2007. Regulation of firing of dopaminergic neurons and control of goal-directed behaviors. *Trends in Neurosciences* 30 (5), 220 – 227, fifty years of dopamine research.

Grillner, S., 07 2003. The motor infrastructure: from ion channels to neuronal networks. *Nature Reviews Neuroscience* 4, 573 EP –.
 URL <http://dx.doi.org/10.1038/nrn1137>

Grillner, S., Ekeberg, Ö., Manira, A. E., Lansner, A., Parker, D., Tegnér, J., Wallén, P., 1998. Intrinsic function of a neuronal network — a vertebrate central pattern generator|published on the world wide web on 8 april 1998.1. *Brain Research Reviews* 26 (2), 184 – 197.
 URL <http://www.sciencedirect.com/science/article/pii/S0165017398000022>

Grillner, S., Heggren, J., Ménard, A., Saitoh, K., Wikström, M. A., 2005. Mechanisms for selection of basic motor programs – roles for the striatum and pallidum. *Trends in Neurosciences* 28 (7), 364 – 370.
 URL <http://www.sciencedirect.com/science/article/pii/S0166223605001293>

Grillner, S., Robertson, B., 2016. The basal ganglia over 500 million years. *Current Biology* 26 (20), R1088 – R1100.

Gurney, Humphries, M., Wood, R., J.Prescott, T., P.Redgrave, 2004. Testing computational hypotheses of brain systems function: a case study with the basal ganglia. *Network: Computation in Neural Systems* 15 (4), 263–290.

Gurney, Prescott, T., Redgrave, P., 1998. *The Basal Ganglia viewed as an Action Selection Device*. Springer London, London.

Gurney, Prescott, T. J., Redgrave, P., May 2001a. A computational model of action selection in the basal ganglia. i. a new functional anatomy. *Biological Cybernetics* 84 (6), 401–410.

Gurney, Prescott, T. J., Redgrave, P., May 2001b. A computational model of action selection in the basal ganglia. ii. analysis and simulation of behaviour. *Biological Cybernetics* 84 (6), 411–423.

Gurney, K. N., Humphries, M. D., Redgrave, P., 01 2015. A new framework for cortico-striatal plasticity: Behavioural theory meets in vitro data at the reinforcement-action interface. *PLOS Biology* 13 (1), 1–25.

Hegeman, D. J., Hong, E. S., Hernández, V. M., Chan, C. S., 2016. The external globus pallidus: progress and perspectives. *European Journal of Neuroscience* 43 (10), 1239–1265.

Hernández, V. M., Hegeman, D. J., Cui, Q., Kelder, D. A., Fiske, M. P., Glajch, K. E., Pitt, J. E., Huang, T. Y., Justice, N. J., Chan, C. S., 08 2015. Parvalbumin⁺ neurons and npas1⁺ neurons are distinct neuron classes in the mouse external globus pallidus. *The Journal of Neuroscience* 35 (34), 11830.

Hikosaka, O., Takikawa, Y., Kawagoe, R., 2000. Role of the basal ganglia in the control of purposive saccadic eye movements. *Physiological Reviews* 80 (3), 953–978.

Humphries, M., Gurney, K., 2002. The role of intra-thalamic and thalamocortical circuits in action selection. *Network: Computation in Neural Systems* 13 (1), 131–156, pMID: 11873842.

Humphries, M., Khamassi, M., Gurney, K., 2012. Dopaminergic control of the exploration-exploitation trade-off via the basal ganglia. *Frontiers in Neuroscience* 6, 9.
 URL <https://www.frontiersin.org/article/10.3389/fnins.2012.00009>

Humphries, M., Lepora, N., Wood, R., Gurney, K., 2009a. Capturing dopaminergic modulation and bimodal membrane behaviour of striatal medium spiny neurons in accurate, reduced models. *Frontiers in Computational Neuroscience* 3, 26.

Humphries, M. D., Stewart, R. D., Gurney, K. N., 2006. A physiologically plausible model of action selection and oscillatory activity in the basal ganglia. *Journal of Neuroscience* 26 (50), 12921–12942.

Humphries, M. D., Wood, R., Gurney, K., 2009b. Dopamine-modulated dynamic cell assemblies generated by the {GABAergic} striatal microcircuit. *Neural Networks* 22 (8), 1174 – 1188, cortical Microcircuits.

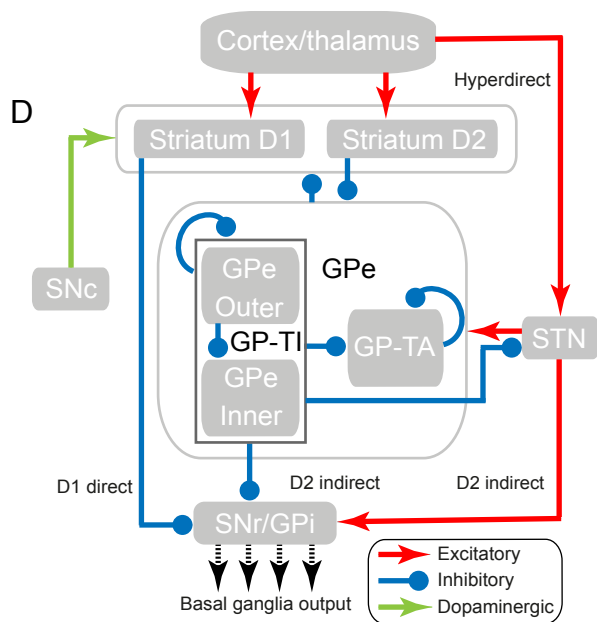
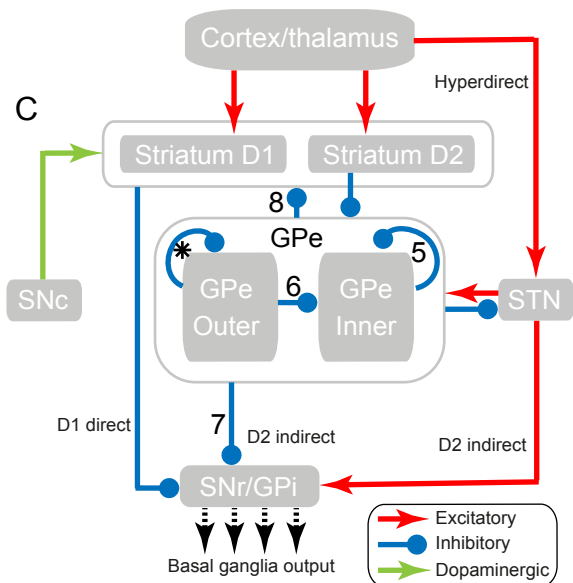
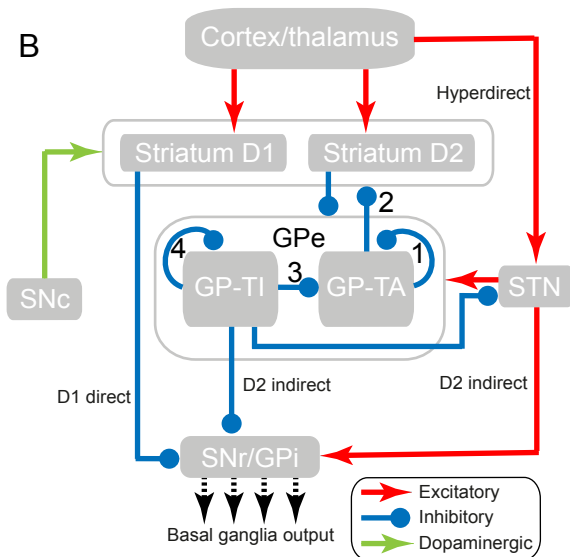
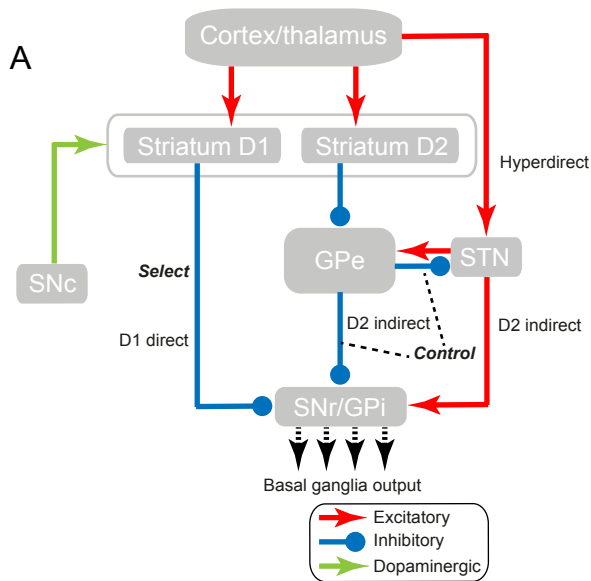
Hutchison, W. D., Dostrovsky, J. O., Walters, J. R., Courtemanche, R., Boraud, T., Goldberg, J., Brown, P., 2004. Neuronal oscillations in the basal ganglia and movement disorders: Evidence from whole animal and human recordings. *Journal of Neuroscience* 24 (42), 9240–9243.

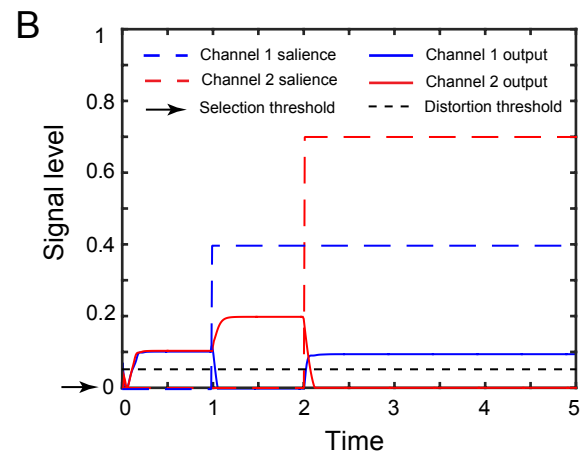
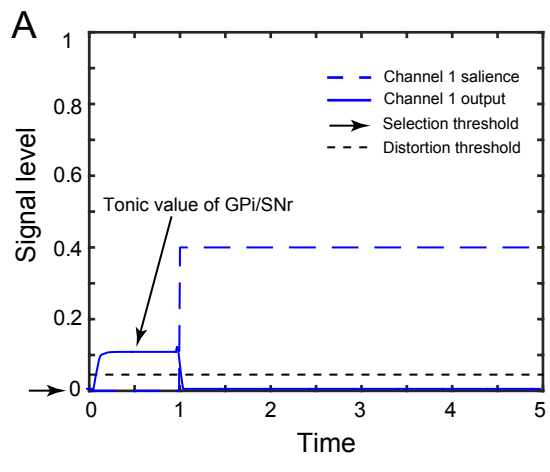
Jr, L. H., Zigmond, M., 1997. Influence of dopamine on gaba release in striatum: evidence for d1–d2 interactions and non-synaptic influences. *Neuroscience* 77 (2), 419 – 429.

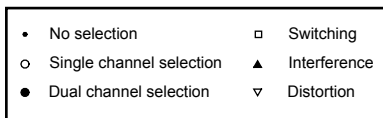
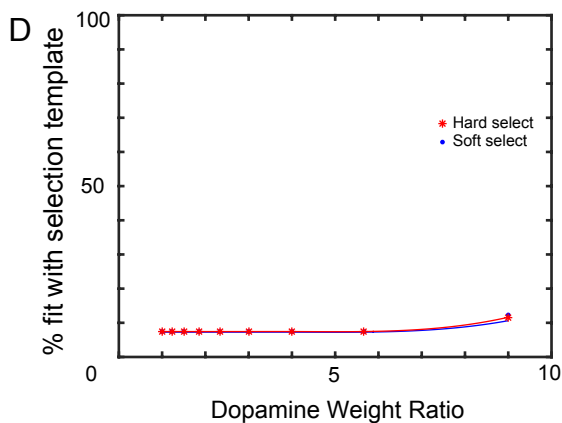
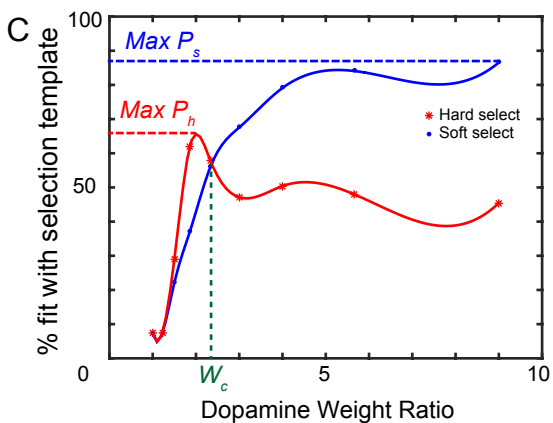
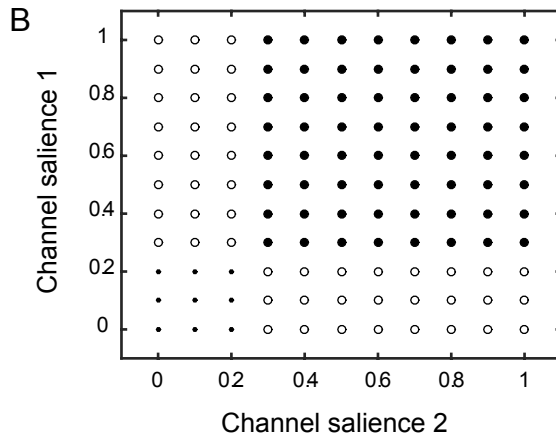
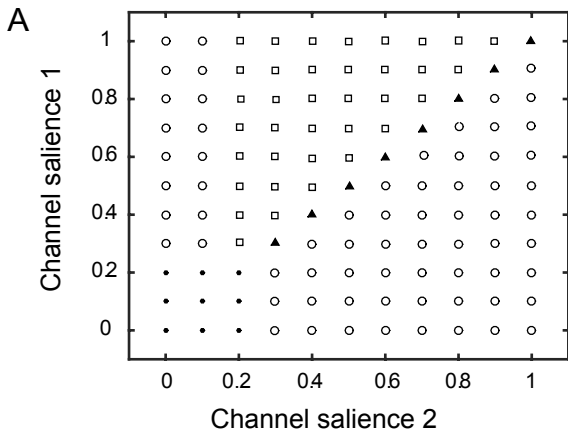
Kalva, S. K., Rengaswamy, M., Chakravarthy, V. S., Gupte, N., 2012. On the neural substrates for exploratory dynamics in basal ganglia: A model. *Neural Networks* 32, 65–73.

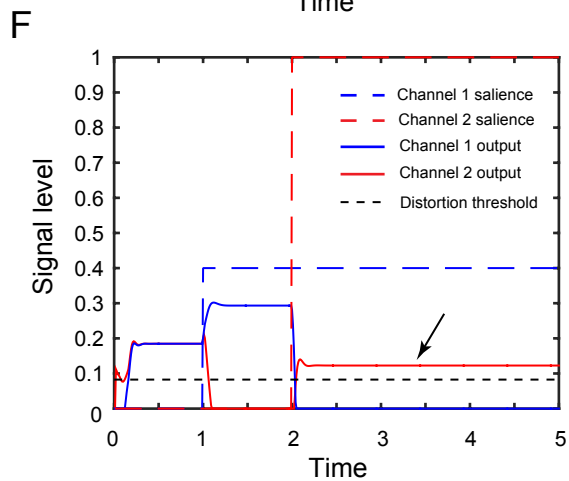
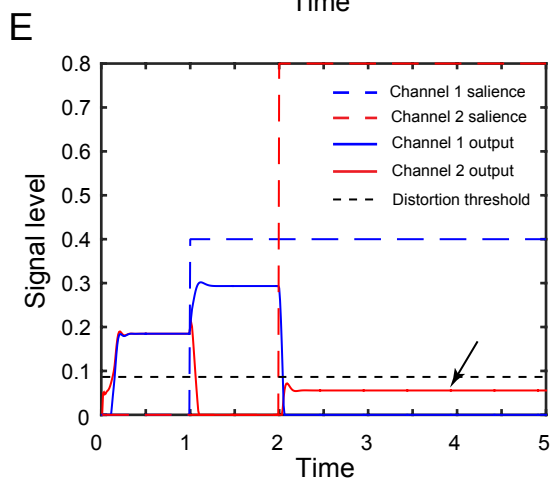
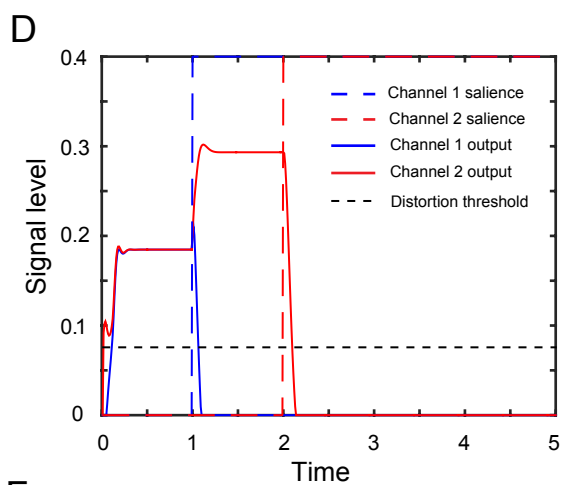
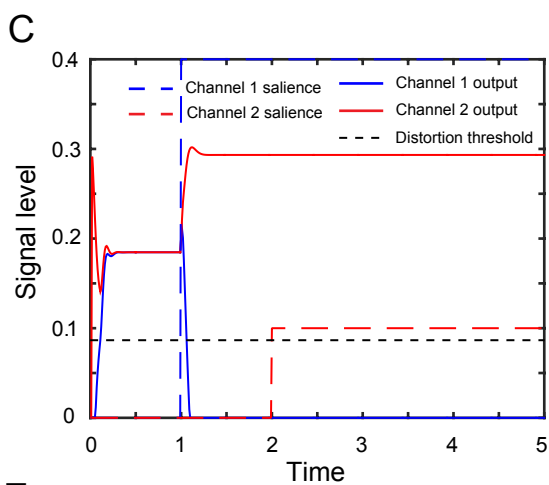
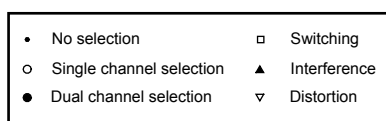
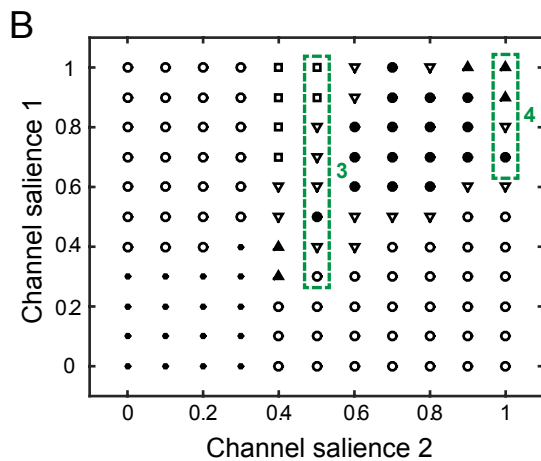
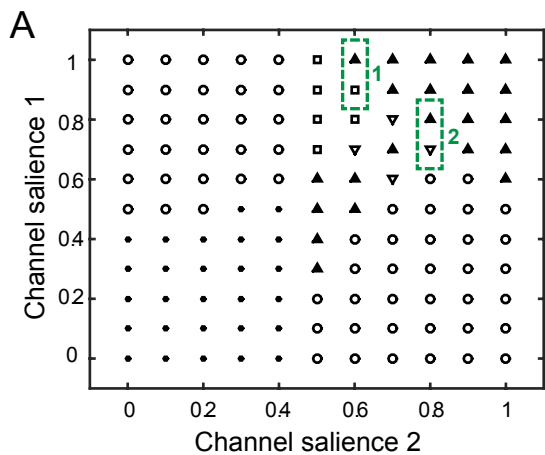
- 1337 URL <http://www.sciencedirect.com/science/article/pii/S0893608012000603>
- 1338 Kamali Sarvestani, I., Lindahl, M., Hellgren Kotaleski, J., Ekeberg, Ö., 2011. The arbitration-extension hypothesis: a
1339 hierarchical interpretation of the functional organization of the basal ganglia. *Frontiers in Systems Neuroscience* 5,
1340 13.
- 1341 Kasanetz, F., Riquelme, L. A., O'Donnell, P., Murer, M. G., 2006. Turning off cortical ensembles stops striatal up states
1342 and elicits phase perturbations in cortical and striatal slow oscillations in rat in vivo. *The Journal of Physiology*
1343 577 (1), 97–113.
- 1344 URL <http://dx.doi.org/10.1113/jphysiol.2006.113050>
- 1345 Kim, H. F., Hikosaka, O., 2015. Parallel basal ganglia circuits for voluntary and automatic behaviour to reach rewards.
1346 *Brain* 138 (7), 1776–1800.
- 1347 URL <http://dx.doi.org/10.1093/brain/awv134>
- 1348 Kravitz, A. V., Freeze, B. S., Parker, P. R. L., Kay, K., Thwin, M. T., Deisseroth, K., Kreitzer, A. C., 07 2010. Regulation
1349 of parkinsonian motor behaviours by optogenetic control of basal ganglia circuitry. *Nature* 466 (7306), 622–626.
- 1350 Lindahl, M., Hellgren Kotaleski, J., 2016. Untangling basal ganglia network dynamics and function: Role of dopamine
1351 depletion and inhibition investigated in a spiking network model. *eNeuro* 3 (6).
- 1352 Lindahl, M., Kamali Sarvestani, I., Ekeberg, Ö., Kotaleski, J., 2013. Signal enhancement in the output stage of the basal
1353 ganglia by synaptic short-term plasticity in the direct, indirect, and hyperdirect pathways. *Frontiers in Computational*
1354 *Neuroscience* 7, 76.
- 1355 Mallet, N., Micklem, B. R., Henny, P., Brown, M. T., Williams, C., Bolam, J. P., Nakamura, K. C., Magill, P. J., 2012.
1356 Dichotomous organization of the external globus pallidus. *Neuron* 74 (6), 1075 – 1086.
- 1357 Mallet, N., Schmidt, R., Leventhal, D., Chen, F., Amer, N., Boraud, T., Berke, J. D., 2016. Arky pallidal cells send a stop
1358 signal to striatum. *Neuron* 89 (2), 308 – 316.
- 1359 Mandali, A., Rengaswamy, M., Chakravarthy, V. S., Moustafa, A. A., 2015. A spiking basal ganglia model of synchrony,
1360 exploration and decision making. *Frontiers in Neuroscience* 9, 191.
- 1361 URL <https://www.frontiersin.org/article/10.3389/fnins.2015.00191>
- 1362 Mastro, K. J., Bouchard, R. S., Holt, H. A. K., Gittis, A. H., 2014. Transgenic mouse lines subdivide external segment of
1363 the globus pallidus (gpe) neurons and reveal distinct gpe output pathways. *Journal of Neuroscience* 34 (6), 2087–2099.
- 1364 Mink, J. W., 1996. The basal ganglia: Focused selection and inhibition of competing motor programs. *Progress in*
1365 *Neurobiology* 50 (4), 381 – 425.
- 1366 Moolchand, P., Jones, S. R., Frank, M. J., 2017. Towards a computational account of theta band (4-8 hz) power modulation
1367 in the subthalamic nucleus under response conflict. No. 336.10. Society for Neuroscience Abstract.
- 1368 Nevado-Holgado, A. J., Mallet, N., Magill, P. J., Bogacz, R., 2014. Effective connectivity of the subthalamic nucleus–
1369 globus pallidus network during parkinsonian oscillations. *The Journal of Physiology* 592 (7), 1429–1455.
- 1370 URL <http://dx.doi.org/10.1113/jphysiol.2013.259721>
- 1371 Okun, M. S., Vitek, J. L., 2004. Lesion therapy for parkinson's disease and other movement disorders: Update and
1372 controversies. *Movement Disorders* 19 (4), 375–389.
- 1373 URL <http://dx.doi.org/10.1002/mds.20037>
- 1374 Plamen, G., Olivier, D., Thomas, W., 2018/06/15 2006. Oscillations in the basal ganglia under normal conditions and in
1375 movement disorders. *Movement Disorders* 21 (10), 1566–1577.
- 1376 URL <https://doi.org/10.1002/mds.21033>
- 1377 Planert, H., Berger, T. K., Silberberg, G., 03 2013. Membrane properties of striatal direct and indirect pathway neurons
1378 in mouse and rat slices and their modulation by dopamine. *PLOS ONE* 8 (3), 1–14.
- 1379 URL <https://doi.org/10.1371/journal.pone.0057054>
- 1380 Prescott, T. J., Gurney, K., Redgrave, P., 2002. The basal ganglia: The handbook of brain theory and neural networks,
1381 2nd Edition. MIT Press, Cambridge.
- 1382 Prescott, T. J., Montes González, F. M., Gurney, K., Humphries, M. D., Redgrave, P., 2006. A robot model of the basal
1383 ganglia: Behavior and intrinsic processing. *Neural Networks* 19 (1), 31–61.
- 1384 URL <http://www.sciencedirect.com/science/article/pii/S0893608005001589>
- 1385 Redgrave, P., Gurney, K., 12 2006. The short-latency dopamine signal: a role in discovering novel actions? *Nat Rev*
1386 *Neurosci* 7 (12), 967–975.
- 1387 Redgrave, P., Prescott, T., Gurney, K., 1999. The basal ganglia: a vertebrate solution to the selection problem? *Neuro-*
1388 *science* 89 (4), 1009 – 1023.
- 1389 Rivlin-Etzion, M., Marmor, O., Heimer, G., Raz, A., Nini, A., Bergman, H., 2006. Basal ganglia oscillations and patho-
1390 physiology of movement disorders. *Current Opinion in Neurobiology* 16 (6), 629 – 637, motor systems / *Neurobiology*
1391 *of behaviour*.
- 1392 Roessner, V., Plessen, K. J., Rothenberger, A., Ludolph, A. G., Rizzo, R., Skov, L., Strand, G., Stern, J. S., Termine, C.,
1393 Hoekstra, P. J., 2011. European clinical guidelines for tourette syndrome and other tic disorders. part ii: pharmaco-
1394 logical treatment. *European Child & Adolescent Psychiatry* 20 (4), 173–196.
- 1395 URL <https://doi.org/10.1007/s00787-011-0163-7>

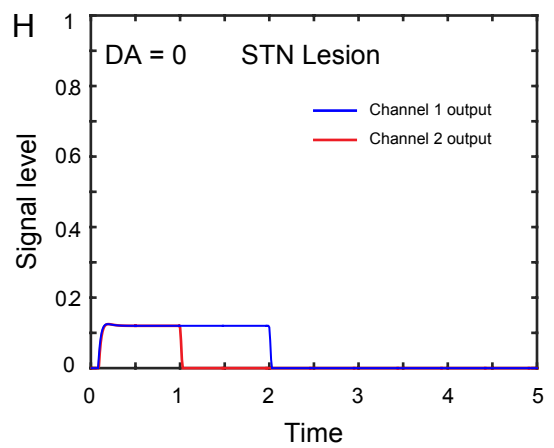
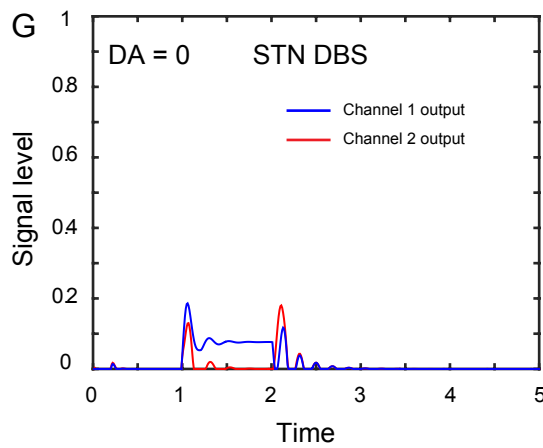
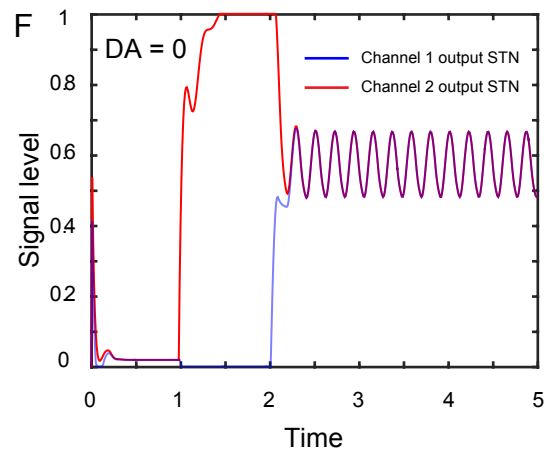
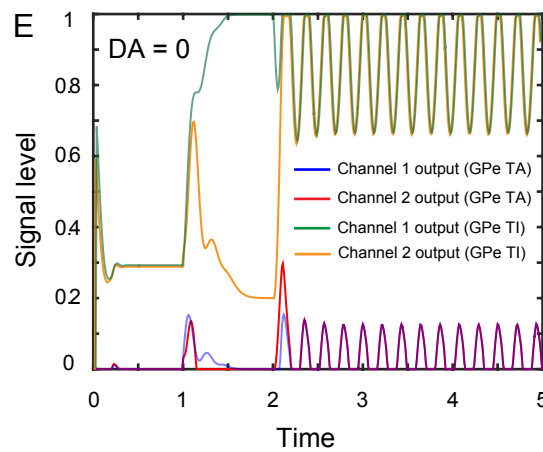
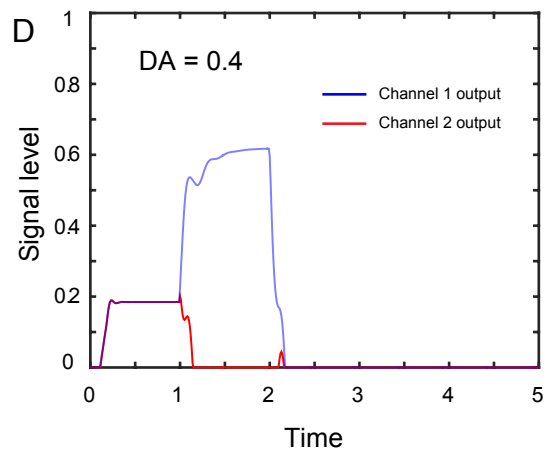
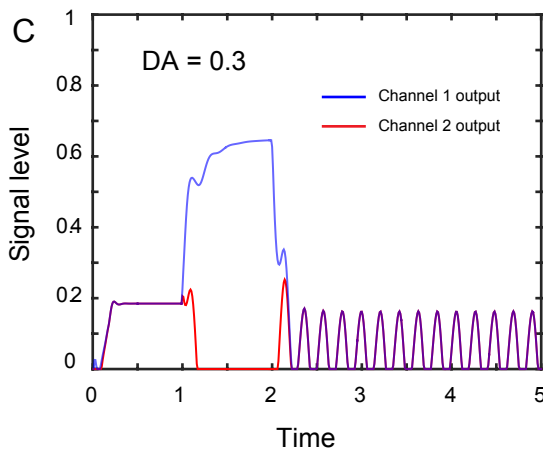
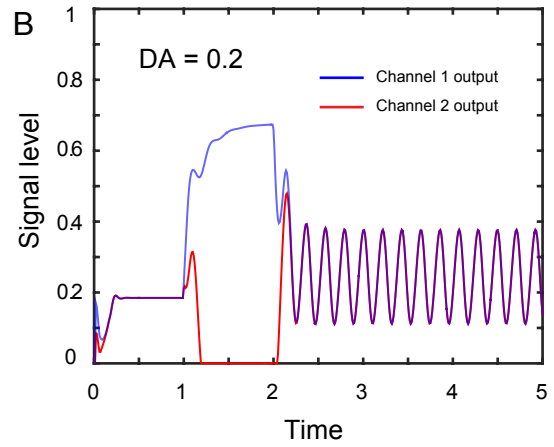
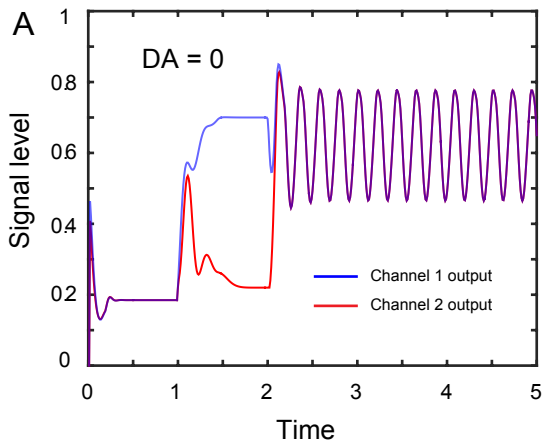
- 1396 Sadek, A. R., Magill, P. J., Bolam, J. P., 2007. A single-cell analysis of intrinsic connectivity in the rat globus pallidus.
1397 *Journal of Neuroscience* 27 (24), 6352–6362.
- 1398 Saunders, A., Huang, K. W., Sabatini, B. L., 02 2016. Globus pallidus externus neurons expressing parvalbumin inter-
1399 connect the subthalamic nucleus and striatal interneurons. *PLOS ONE* 11 (2), 1–20.
1400 URL <https://doi.org/10.1371/journal.pone.0149798>
- 1401 Schroll, H., Hamker, F., 2013. Computational models of basal-ganglia pathway functions: focus on functional neuro-
1402 anatomy. *Frontiers in Systems Neuroscience* 7, 122.
- 1403 Schroll, H., Vitay, J., Hamker, F. H., 2012. Working memory and response selection: A computational account of
1404 interactions among cortico-basalganglio-thalamic loops. *Neural Networks* 26 (Supplement C), 59 – 74.
- 1405 Schultz, W., 1998. Predictive reward signal of dopamine neurons. *Journal of Neurophysiology* 80 (1), 1–27.
- 1406 Shine, J. M., Handojoseno, A. M. A., Nguyen, T. N., Tran, Y., Naismith, S. L., Nguyen, H., Lewis, S. J. G., 2014.
1407 Abnormal patterns of theta frequency oscillations during the temporal evolution of freezing of gait in parkinson’s
1408 disease. *Clinical Neurophysiology* 125 (3), 569–576.
1409 URL <http://www.sciencedirect.com/science/article/pii/S1388245713010420>
- 1410 Shine, J. M., Matar, E., Ward, P. B., Bolitho, S. J., Gilat, M., Pearson, M., Naismith, S. L., Lewis, S. J. G., 04 2013.
1411 Exploring the cortical and subcortical functional magnetic resonance imaging changes associated with freezing in
1412 parkinson’s disease. *Brain* 136 (4), 1204–1215.
1413 URL <http://dx.doi.org/10.1093/brain/awt049>
- 1414 Stephenson-Jones, M., Samuelsson, E., Ericsson, J., Robertson, B., Grillner, S., 2011. Evolutionary conservation of the
1415 basal ganglia as a common vertebrate mechanism for action selection. *Current Biology* 21 (13), 1081 – 1091.
1416 URL <http://www.sciencedirect.com/science/article/pii/S0960982211005288>
- 1417 Stewart, T., Bekolay, T., Elias Smith, C., 2012. Learning to select actions with spiking neurons in the basal ganglia.
1418 *Frontiers in Neuroscience* 6, 2.
- 1419 Szydłowski, S. N., Pollak Dorocic, I., Planert, H., Carlén, M., Meletis, K., Silberberg, G., 2013. Target selectivity of
1420 feedforward inhibition by striatal fast-spiking interneurons. *Journal of Neuroscience* 33 (4), 1678–1683.
1421 URL <http://www.jneurosci.org/content/33/4/1678>
- 1422 Tachibana, Y., Iwamuro, H., Kita, H., Takada, M., Nambu, A., 2018/08/25 2011. Subthalamo-pallidal interactions un-
1423 derlying parkinsonian neuronal oscillations in the primate basal ganglia. *European Journal of Neuroscience* 34 (9),
1424 1470–1484.
1425 URL <https://doi.org/10.1111/j.1460-9568.2011.07865.x>
- 1426 van Albada, S., Robinson, P., 2009. Mean-field modeling of the basal ganglia-thalamocortical system. i: Firing rates in
1427 healthy and parkinsonian states. *Journal of Theoretical Biology* 257 (4), 642 – 663.
- 1428 Wahlstrom, D., Collins, P., White, T., Luciana, M., 2010. Developmental changes in dopamine neurotransmission in
1429 adolescence: Behavioral implications and issues in assessment. *Brain and Cognition* 72 (1), 146–159.
1430 URL <http://www.sciencedirect.com/science/article/pii/S027826260900205X>
- 1431 Weinberger, M., Dostrovsky, J. O., 03 2011. A basis for the pathological oscillations in basal ganglia: the crucial role of
1432 dopamine. *Neuroreport* 22 (4), 151–156.
1433 URL <http://www.ncbi.nlm.nih.gov/pmc/articles/PMC3076312/>
- 1434 Wilson, C. J., Groves, P. M., 1981. Spontaneous firing patterns of identified spiny neurons in the rat neostriatum. *Brain*
1435 *Research* 220 (1), 67 – 80.
1436 URL <http://www.sciencedirect.com/science/article/pii/0006899381902110>
- 1437 Wylie, S., van den Wildenberg, W., Ridderinkhof, K., Bashore, T., Powell, V., Manning, C., Wooten, G., 2009. The effect
1438 of parkinson’s disease on interference control during action selection. *Neuropsychologia* 47 (1), 145 – 157.
- 1439 Yoon, D. Y., Gause, C. D., Leckman, J. F., Singer, H. S., 2007. Frontal dopaminergic abnormality in tourette syndrome:
1440 A postmortem analysis. *Journal of the Neurological Sciences* 255 (1), 50–56.
1441 URL <http://www.sciencedirect.com/science/article/pii/S0022510X07000949>
- 1442 Zhang, J., Russo, G. S., Mewes, K., Rye, D. B., Vitek, J. L., 2006. Lesions in monkey globus pallidus externus exacerbate
1443 parkinsonian symptoms. *Experimental Neurology* 199 (2), 446 – 453.
1444 URL <http://www.sciencedirect.com/science/article/pii/S0014488606000136>

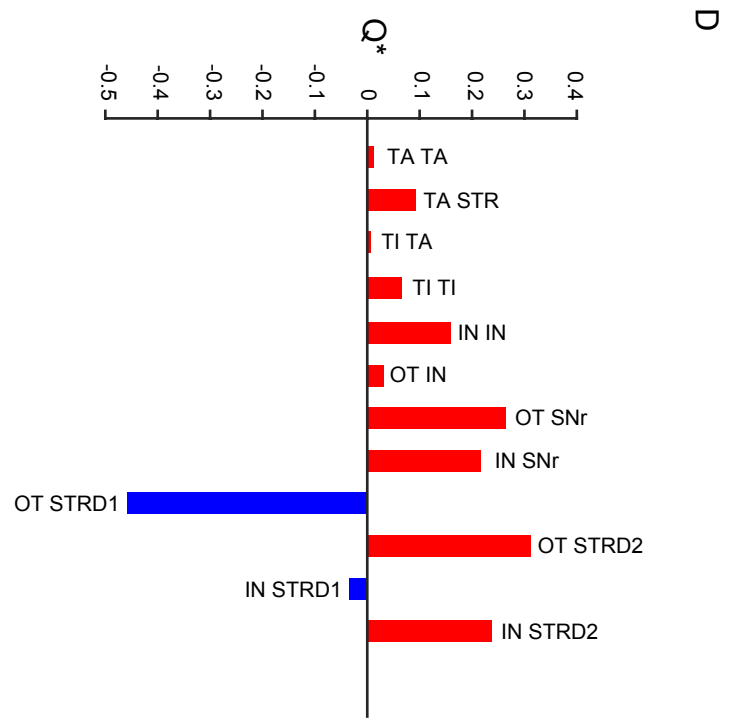
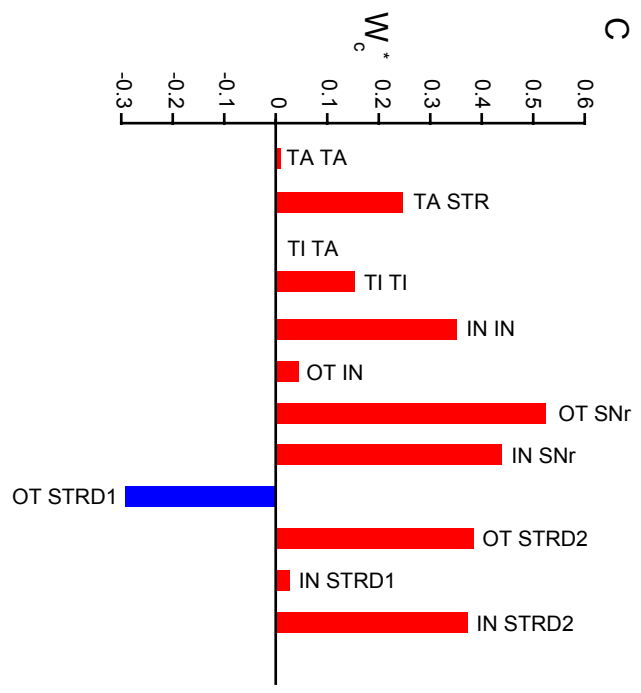
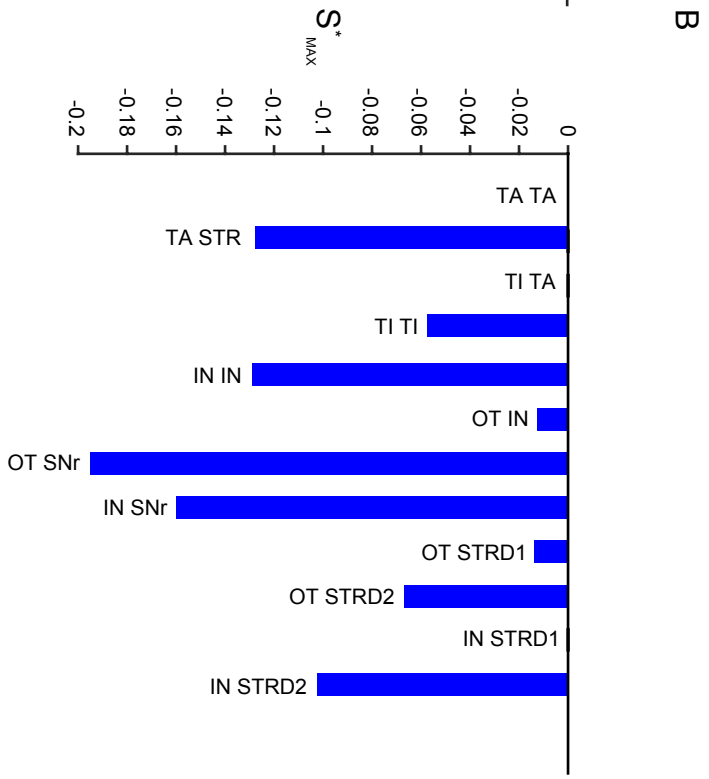
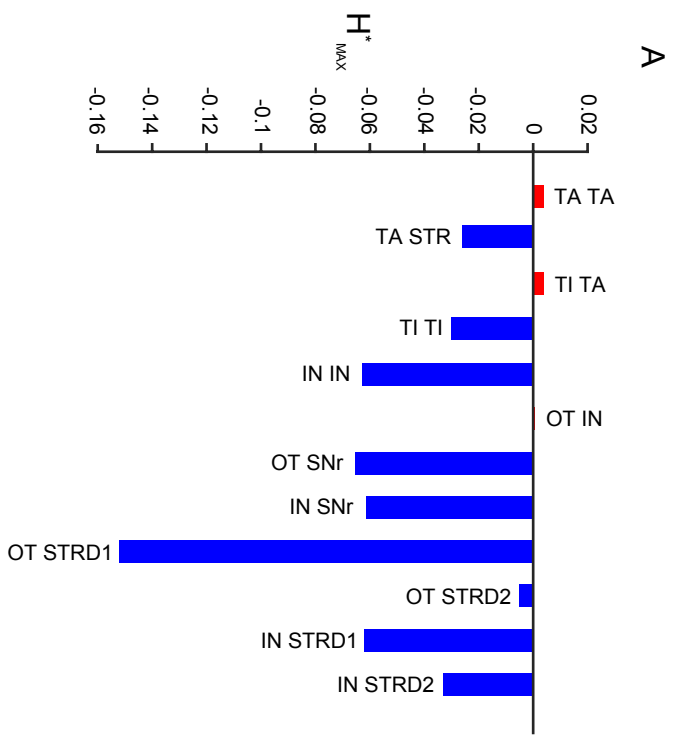


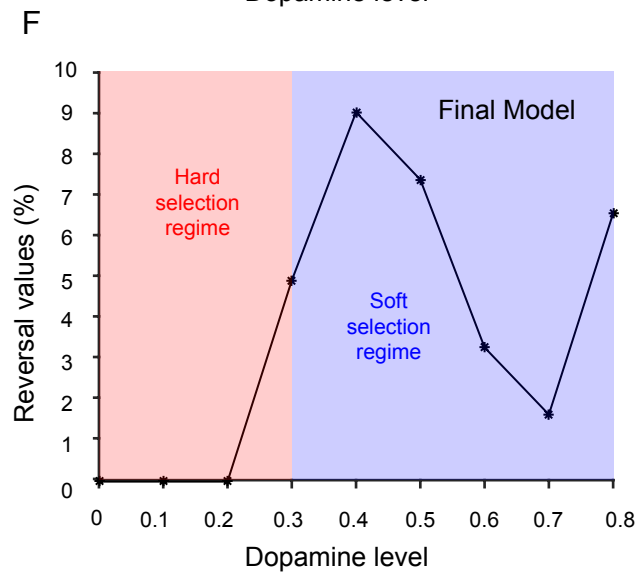
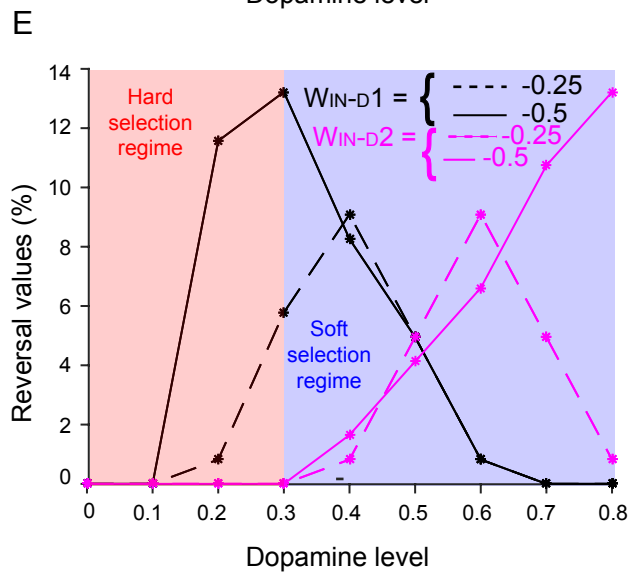
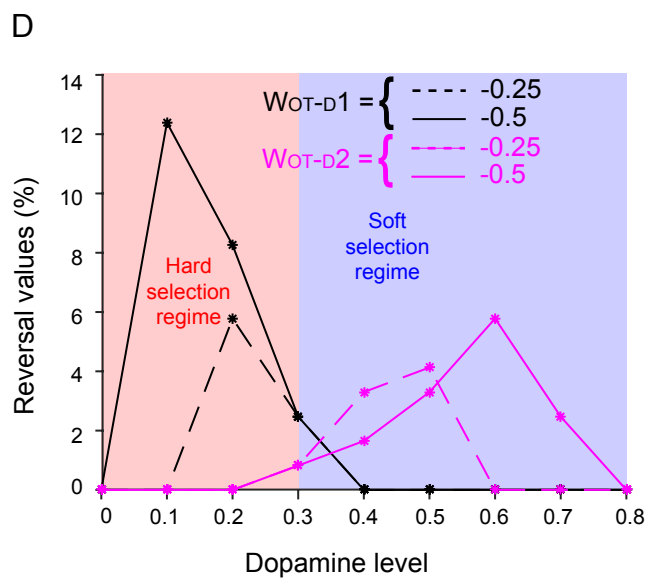
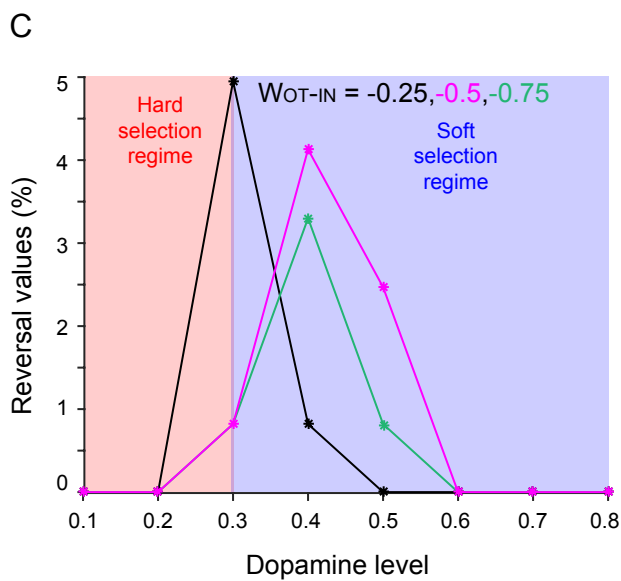
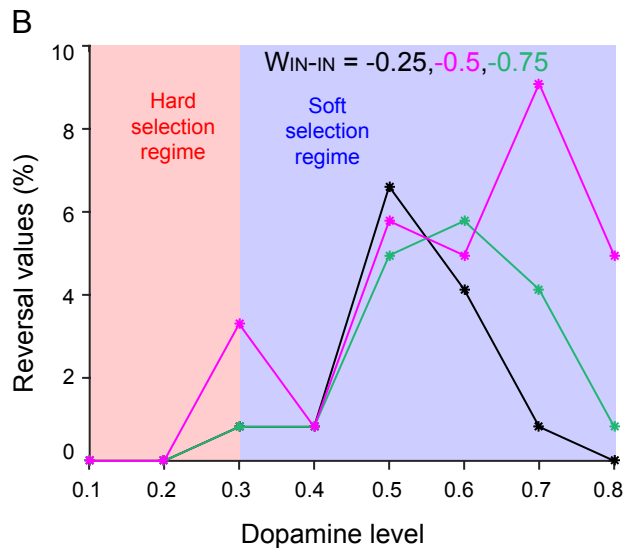
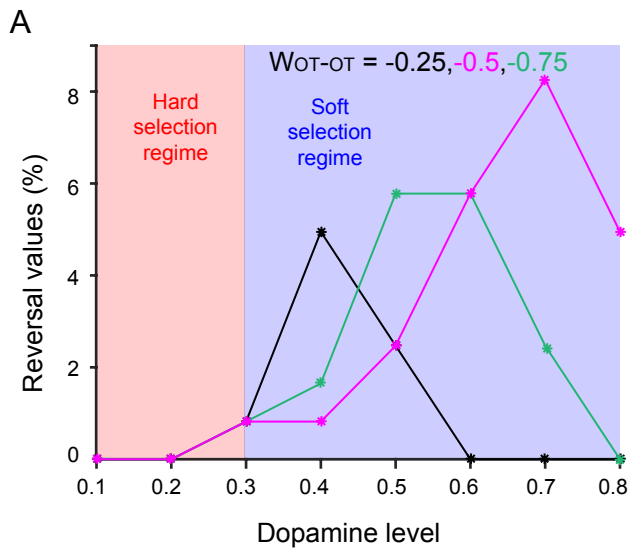


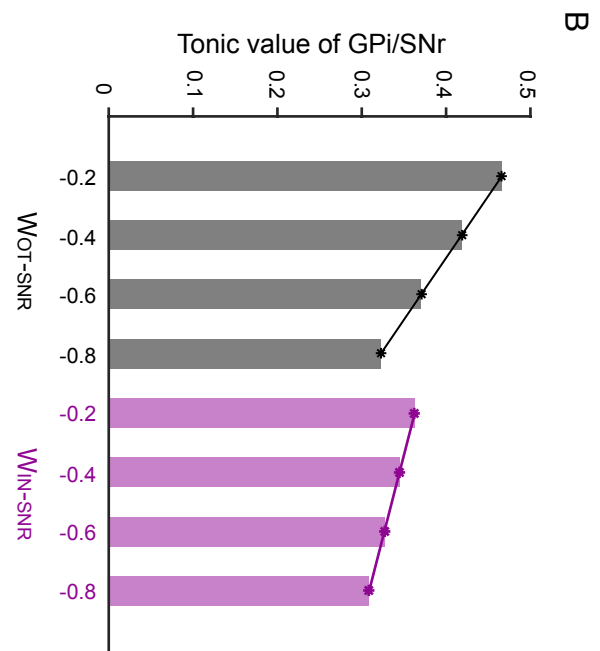
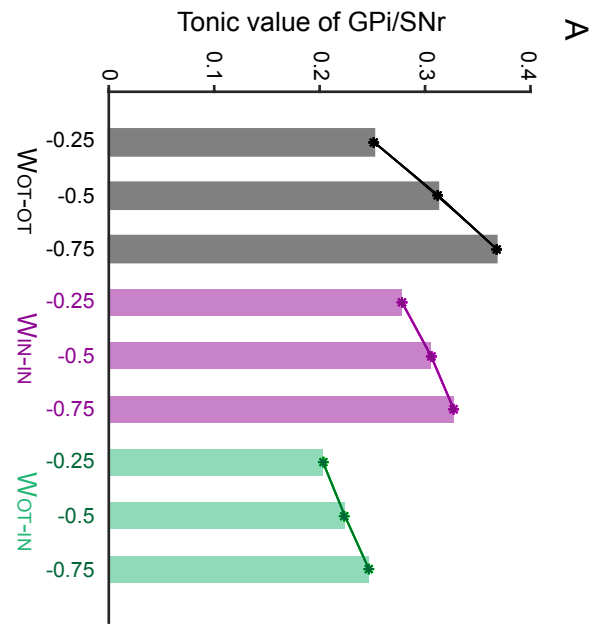


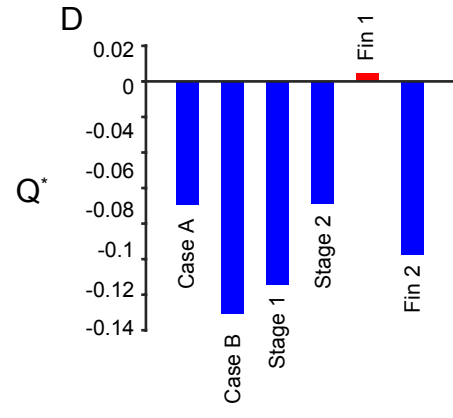
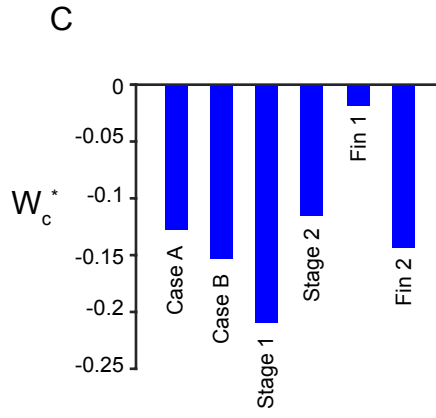
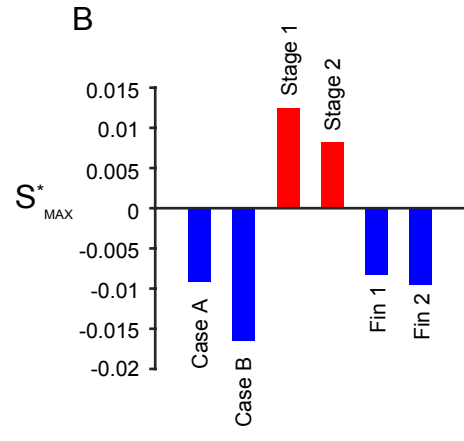
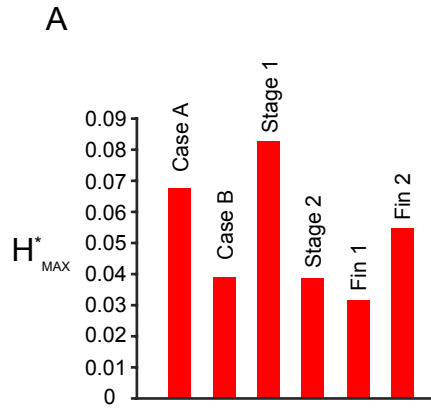


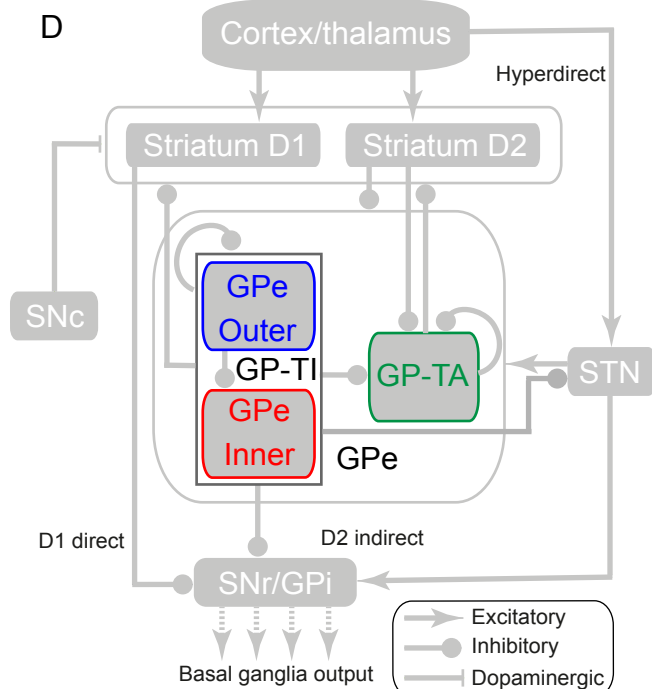
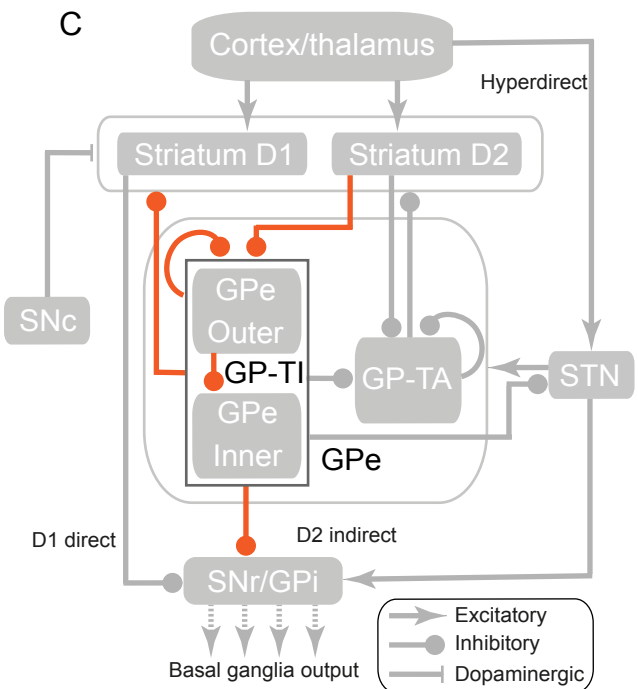
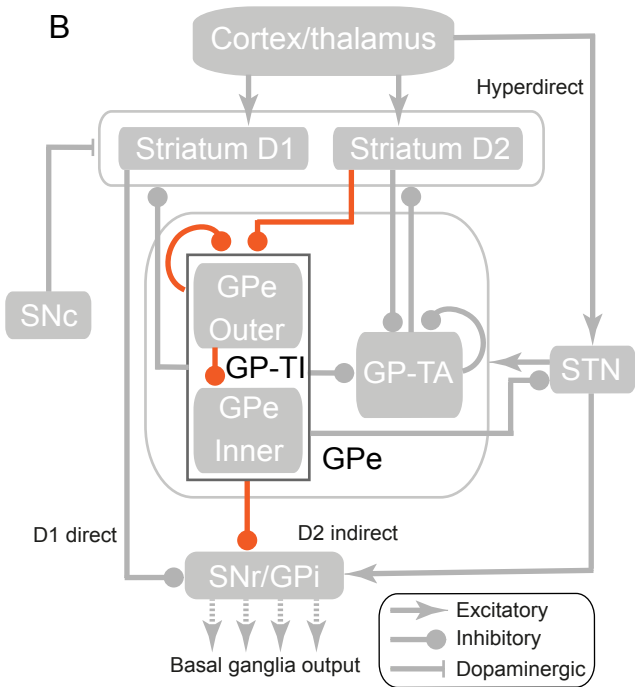
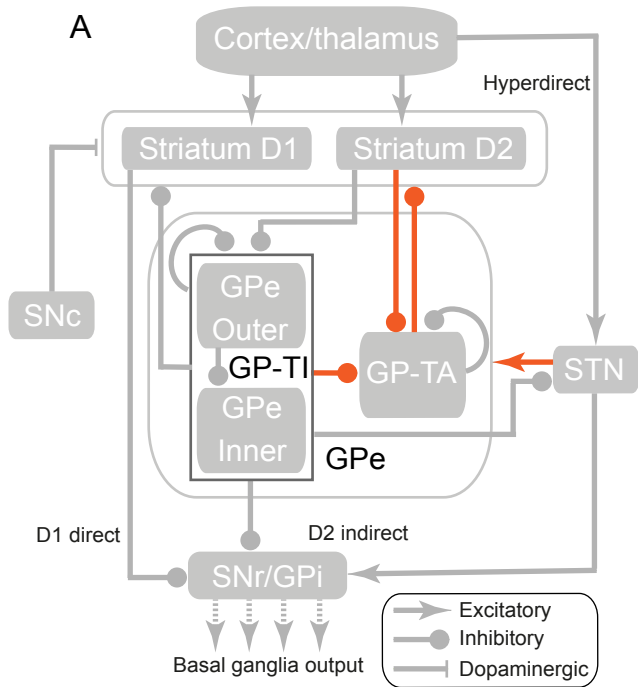


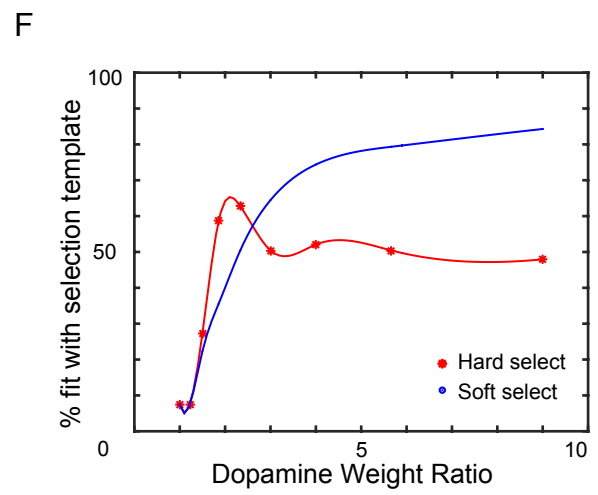
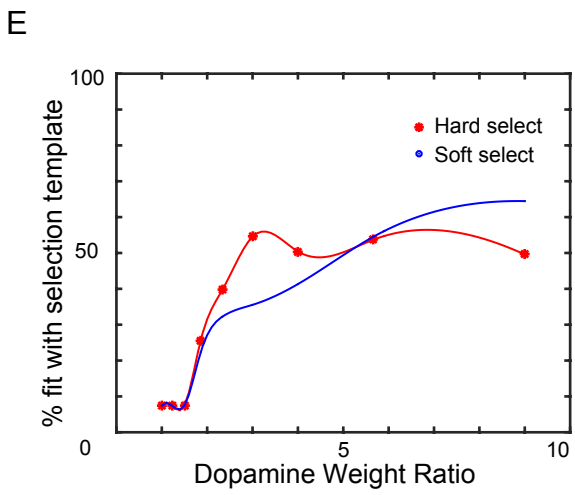
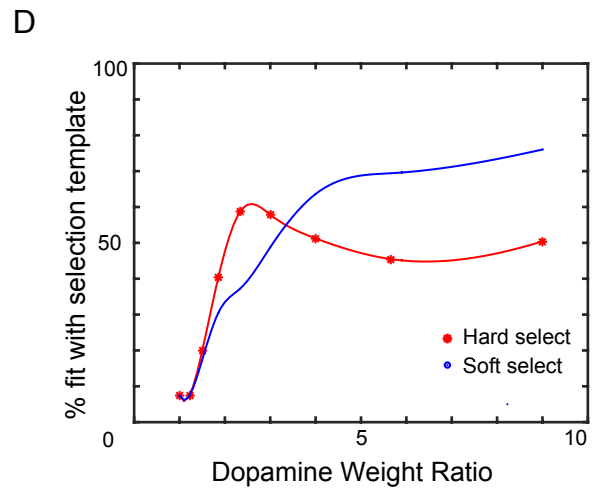
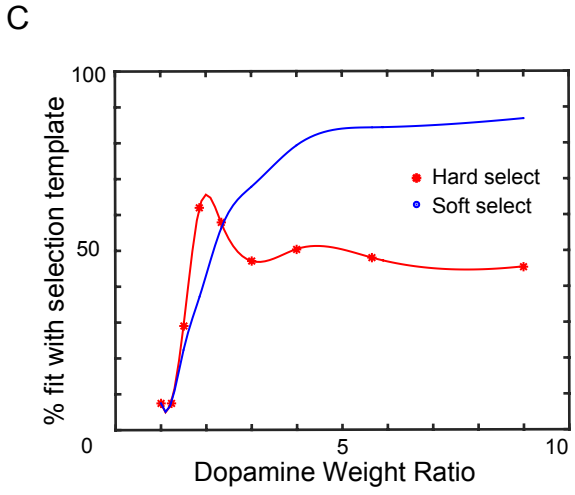
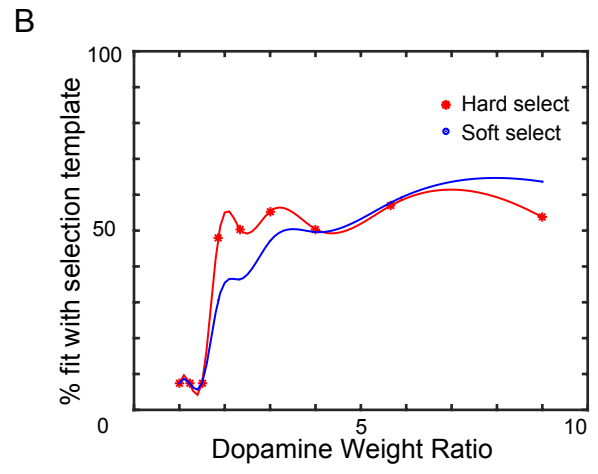
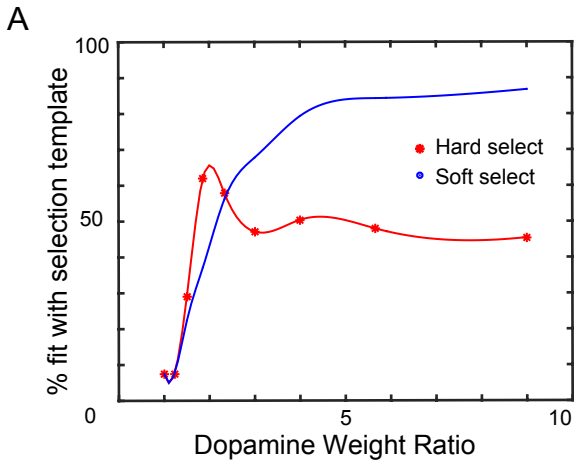


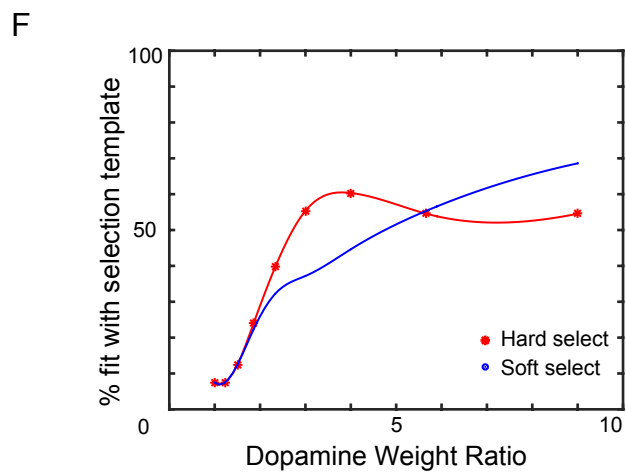
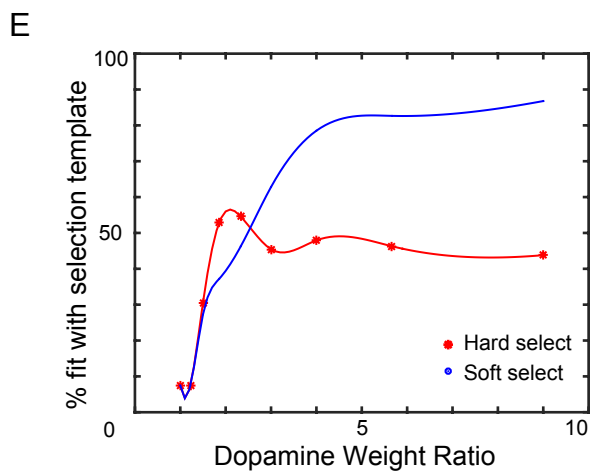
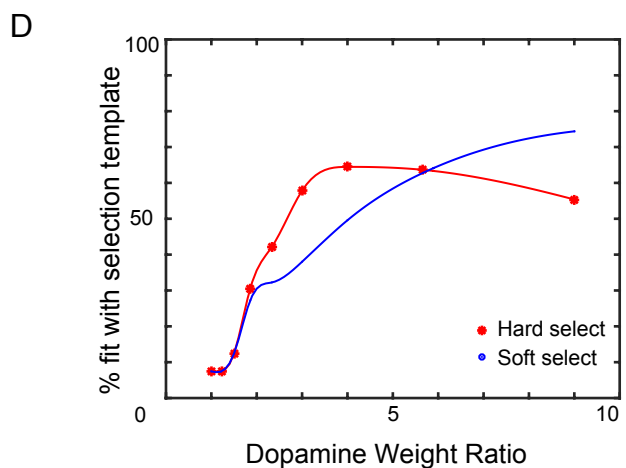
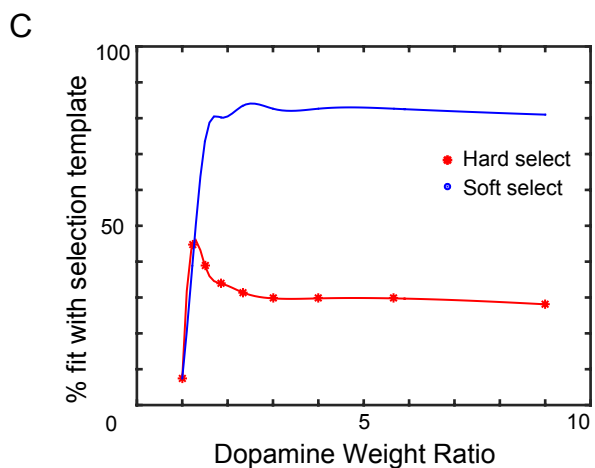
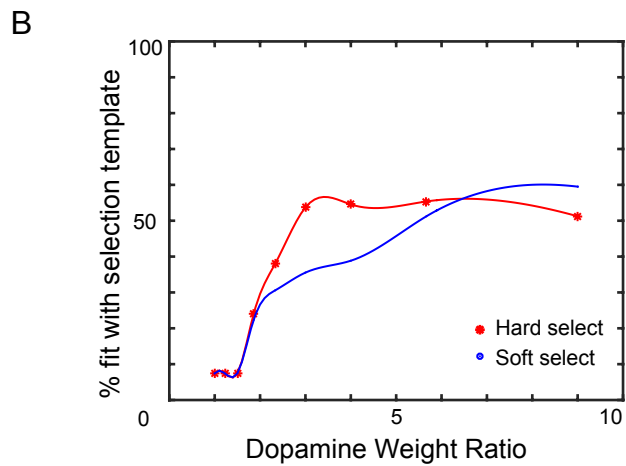
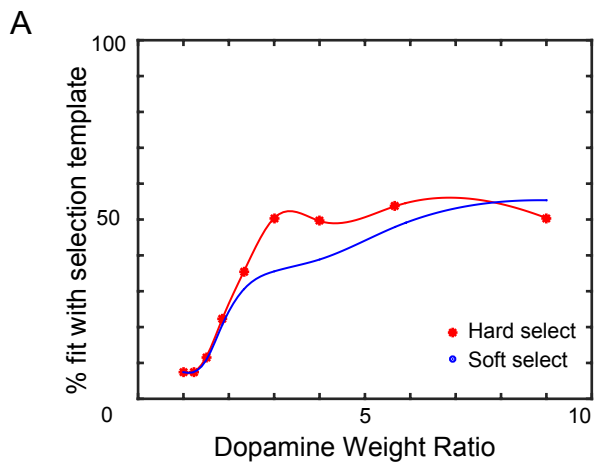


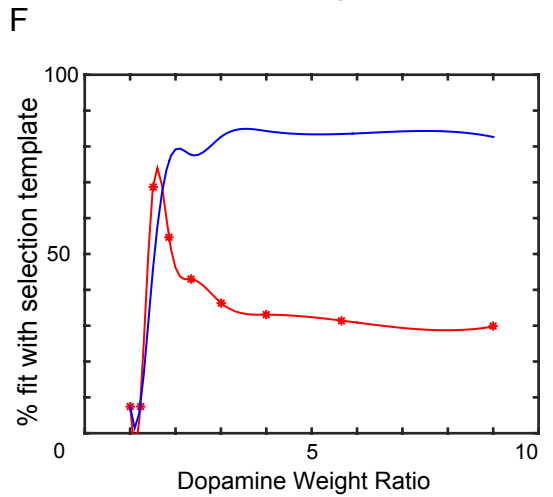
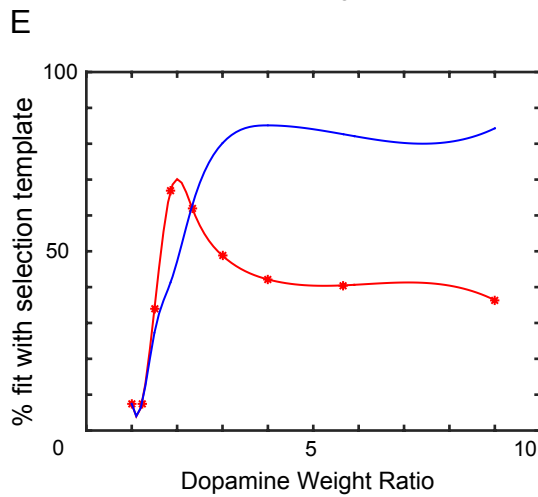
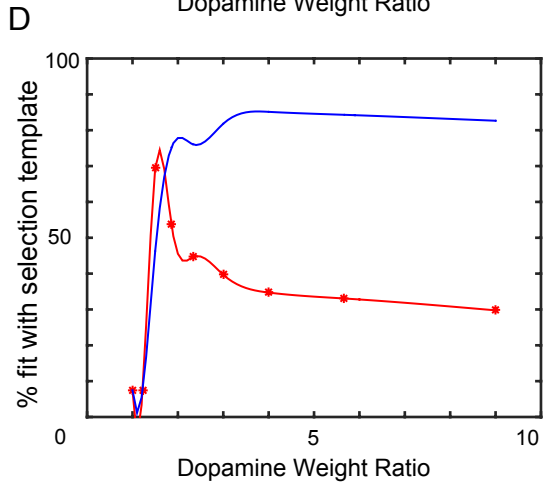
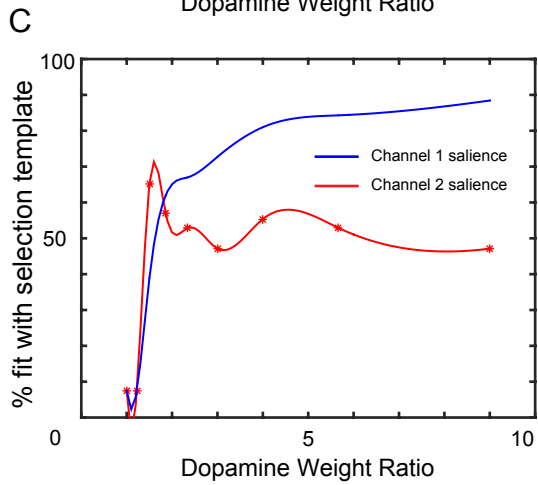
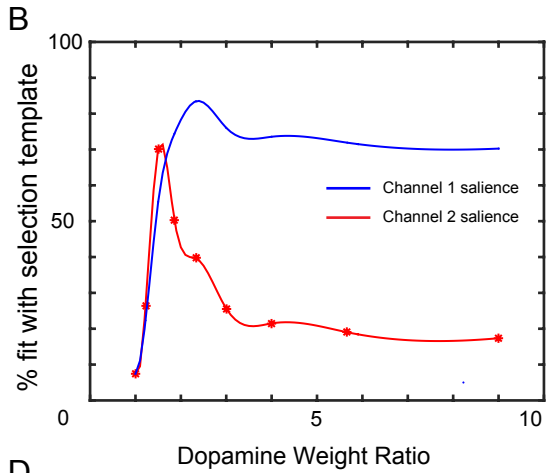
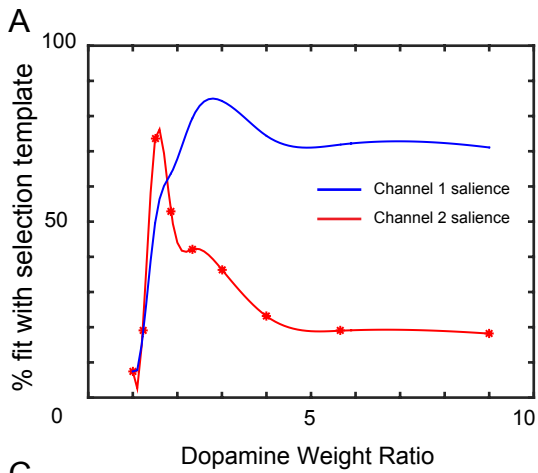


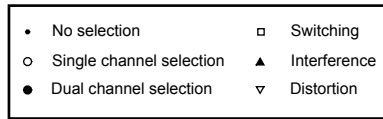
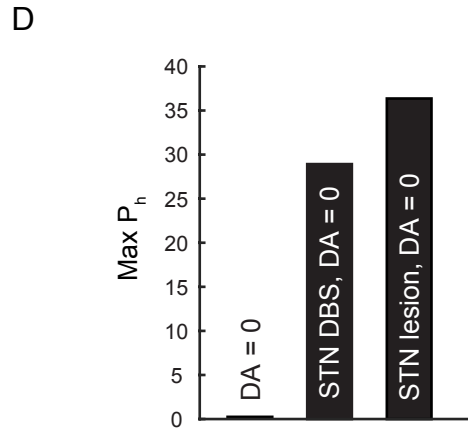
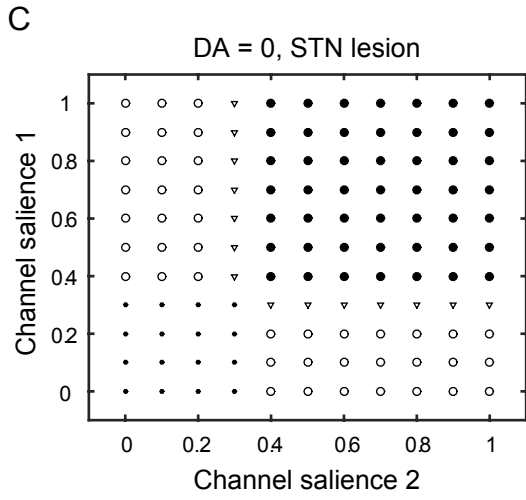
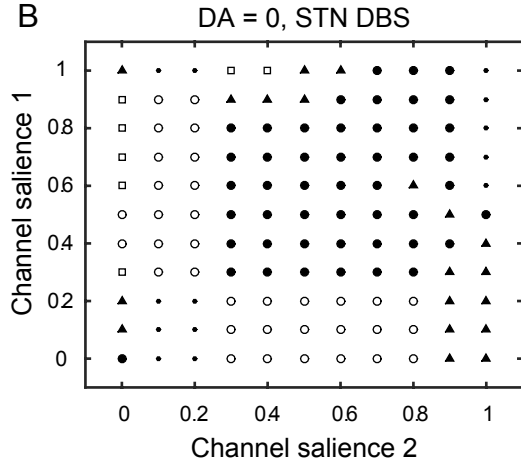
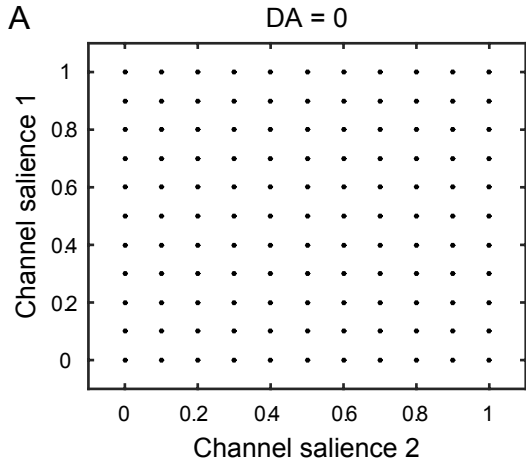












Appendix S1

Detailed modelling formalism of the various subnuclei

The activation and output equations and modelling details of all the subpopulations in various subnuclei of the basal ganglia are described here.

Striatum

Striatum D1 Let the input salience on the i^{th} channel be c , and the dopamine level for ‘Selection’/D1 pathway be λ_s . The other inputs to the striatum D1 are the inhibitory input from the GPe TA neurons, and the back projections from the GPe outer and GPe inner neurons. Let the output of GPe TA neurons be y_i^{ta} , and since its diffuse, input will be $Y_-^{ta} = \sum_j^N y_j^{ta}$, where N is the total number of channels. Let output of GPe outer neurons be y_i^{ot} , and that of GPe inner neurons be y_i^{in} . The total activation function will be,

$$\tilde{a}_i^s = c_i(1 + \lambda_s)w_i^{str} - Y_-^{ta}w_{ta-d1}^- + y_i^{ot}w_{ot-d1}^+ + y_i^{in}w_{in-d1}^+ \quad (1)$$

where, w_{ta-d1}^- is the synaptic weight of the GPe TA to STRD1 pathway, w_{ot-d1}^+ and w_{in-d1}^+ are the synaptic weights of back projections from GPe outer and GPe inner neurons respectively. The output relation will be,

$$y_i^s = m(\tilde{a}_i^s - \epsilon_{str})H(\tilde{a}_i^s - \epsilon_{str}) \quad (2)$$

where ϵ_{str} is the output threshold.

Striatum D2 Let the input salience on the i^{th} channel be c , and the dopamine level for ‘Control’/D2 pathway be λ_c . The other inputs to the striatum D2

are the diffuse inhibitory input from the GPe TA neurons, and the back projections from the GPe outer and GPe inner neurons. Considering the inputs already defined in previous section, the total activation function will be,

$$\tilde{a}_i^c = c_i(1 - \lambda_c)w_i^{str} - Y_-^{ta}w_{ta-d2}^- + y_i^{ot}w_{ot-d2}^+ + y_i^{in}w_{in-d2}^+ \quad (3)$$

where, w_{ta-d2}^- is the synaptic weight of the GPe TA to STRD2 pathway, w_{ot-d2}^+ and w_{in-d2}^+ are the synaptic weights of back projections from GPe outer and GPe inner neurons respectively. The output relation will be,

$$y_i^c = m(\tilde{a}_i^c - \epsilon_{str})H(\tilde{a}_i^c - \epsilon_{str}) \quad (4)$$

where ϵ_{str} is the output threshold.

STN

Let synaptic weight of the input from the cortex to the STN be w_i^{stn} , the synaptic weights of GPe outer to STN and GPe inner to STN pathways be w_{ot-stn}^- and w_{in-stn}^- respectively. The activation function is,

$$\tilde{a}_i^{stn} = c_iw_i^{stn} - y_i^{ot}w_{ot-stn}^- - y_i^{in}w_{in-stn}^- \quad (5)$$

The output relation will be,

$$y_i^{stn} = m(\tilde{a}_i^{stn} - \epsilon_{stn})H(\tilde{a}_i^{stn} - \epsilon_{stn}) \quad (6)$$

where ϵ_{stn} is the output threshold.

GPe

This section forms the focus of this study, wherein we have modelled different neural populations and their afferent and efferent pathways. We will look at each subpopulation in turn.

GPe outer (part of GPe TI) GPe outer neurons receive diffuse input from the STN, so every GPe outer unit gets an excitatory input $Y_+^{stn} = \sum_j^N y_j^{stn}$, input from the striatum D2 y_i^c , and intrinsic local collaterals providing an inhibition of $Y_-^{ot} = \sum_{j \neq i} w_{ot-ot}^- y_j^{ot}$, where w_{ot-ot}^- is the local collateral weight. If w_{stn-ot}^+ and w_{d2-ot}^- are the synaptic weights of STN to GPe outer and STRD2 to GPe outer pathways respectively, then the activation function becomes,

$$\tilde{a}_i^{ot} = Y_+^{stn} w_{stn-ot}^+ - y_i^c w_{d2-ot}^- - Y_-^{ot} \quad (7)$$

The output relation will be,

$$y_i^{ot} = m(\tilde{a}_i^{ot} - \epsilon_{ot}) H(\tilde{a}_i^{ot} - \epsilon_{ot}) \quad (8)$$

where ϵ_{ot} is the output threshold.

GPe inner (part of GPe TI) GPe inner neurons receive diffuse input from the STN, so every GPe inner unit gets an excitatory input $Y_+^{stn} = \sum_j^N y_j^{stn}$, input from the striatum D2 y_i^c , and intrinsic local collaterals providing an inhibition of $Y_-^{in} = \sum_{j \neq i} w_{in-in}^- y_j^{in}$, where w_{in-in}^- is the local collateral weight. Further, they also receive processed input from the GP-outer neurons, y_i^{ot} , which is inhibitory. If w_{stn-in}^+ , w_{d2-in}^- and w_{ot-in}^- are the synaptic weights of STN to GPe inner, STRD2 to GPe inner and the GPe outer to GPe inner

pathways respectively, then the activation function becomes,

$$\tilde{a}_i^{in} = Y_+^{stn} w_{stn-in}^+ - y_i^c w_{d2-in}^- - y_i^{ot} w_{ot-in}^- - Y_-^{in} \quad (9)$$

The output relation will be,

$$y_i^{in} = m(\tilde{a}_i^{in} - \epsilon_{in}) H(\tilde{a}_i^{in} - \epsilon_{in}) \quad (10)$$

where ϵ_{in} is the output threshold.

GPe TA GPe TA neurons receive diffuse excitatory input from the STN, $Y_+^{stn} = \sum_j^N y_j^{stn}$, input from STRD2 y_i^c , local different population collaterals from GPe outer and GPe inner neurons which are inhibitory, y_i^{ot} and y_i^{in} respectively, and local intrinsic collaterals from neighbouring TA neurons, $Y_-^{ta} = \sum_{j \neq i} w_{ta-ta}^- y_j^{ta}$. If w_{d2-ta}^- , w_{stn-ta}^+ , w_{ot-ta}^- and w_{in-ta}^- are the synaptic weights of STRD2 to GPe TA, STN to GPe TA, GPe outer to GPe TA and GPe inner to GPe TA pathways respectively, then the activation function is,

$$\tilde{a}_i^{ta} = Y_+^{stn} w_{stn-ta}^+ - y_i^c w_{d2-ta}^- - y_i^{ot} w_{ot-ta}^- - y_i^{in} w_{in-ta}^- - Y_-^{ta} \quad (11)$$

The output relation will be,

$$y_i^{ta} = m(\tilde{a}_i^{ta} - \epsilon_{ta}) H(\tilde{a}_i^{ta} - \epsilon_{ta}) \quad (12)$$

where ϵ_{ta} is the output threshold.

GPi/SNr

The output nucleus receives inhibitory input from the STRD1 y_i^s , diffuse excitatory input from STN $Y_+^{stn} = \sum_j^N y_j^{stn}$, inhibitory inputs from the GPe outer and GPe inner neuron populations y_i^{ot} and y_i^{in} respectively. If $w_{stn-snr}^+$, w_{d1-snr}^- , w_{ot-snr}^- and w_{in-snr}^- are the synaptic weights of STN to SNr, STRD1 to SNr, GPe outer to SNr and GPe inner to SNr respectively, then the activation function becomes,

$$\tilde{a}_i^{snr} = Y_+^{stn} w_{stn-snr}^+ - y_i^s w_{d1-snr}^- - y_i^{ot} w_{ot-snr}^- - y_i^{in} w_{in-snr}^- \quad (13)$$

The output relation will be,

$$y_i^{snr} = m(\tilde{a}_i^{snr} - \epsilon_{snr})H(\tilde{a}_i^{snr} - \epsilon_{snr}) \quad (14)$$

where ϵ_{snr} is the output threshold.

Appendix S2

All the models and the weights used in them are given below for reference. If the value says ‘Varied’, then these were the weights which were varied in that particular model. If the value is 0, then either the path didn’t exist or had been ‘lesioned’ in the model. If two or more weights have ‘varied/0’, then it means that while testing one, it was varied while the others were set to 0. This has been provided owing to the large number of models and weights associated with them.

GP TI - GP TI Control Model

$w_i^{str} = 1$	$w_{stn-in}^+ = 0$	$w_{ot-stn}^- = -0.8$	$w_{ot-ot}^- = Varied$
$w_{d2-ot}^- = -1$	$w_{stn-ta}^+ = 0$	$w_{ot-snr}^- = -0.4$	$w_{in-in}^- = 0$
$w_{d2-in}^- = 0$	$w_{stn-snr}^+ = 0.9$	$w_{in-stn}^- = 0$	$w_{ot-in}^- = 0$
$w_{d2-ta}^- = 0$	$w_{ot-d2}^- = 0$	$w_{in-snr}^- = 0$	$w_{ot-ta}^- = 0$
$w_{d1-snr}^- = -1$	$w_{ot-d1}^- = 0$	$w_{ta-d2}^- = 0$	$w_{in-ta}^- = 0$
$w_i^{stn} = 1$	$w_{in-d2}^- = 0$	$w_{ta-d1}^- = 0$	
$w_{stn-ot}^+ = 0.8$	$w_{in-d1}^- = 0$	$w_{ta-ta}^- = 0$	

GP TA - GP TA Control Model

$w_i^{str} = 1$	$w_{stn-in}^+ = 0$	$w_{ot-stn}^- = -0.8$	$w_{ot-ot}^- = 0$
$w_{d2-ot}^- = -1$	$w_{stn-ta}^+ = 0.8$	$w_{ot-snr}^- = -0.4$	$w_{in-in}^- = 0$
$w_{d2-in}^- = 0$	$w_{stn-snr}^+ = 0.9$	$w_{in-stn}^- = 0$	$w_{ot-in}^- = 0$
$w_{d2-ta}^- = -1$	$w_{ot-d2}^- = 0$	$w_{in-snr}^- = 0$	$w_{ot-ta}^- = -1$
$w_{d1-snr}^- = -1$	$w_{ot-d1}^- = 0$	$w_{ta-d2}^- = -1$	$w_{in-ta}^- = 0$
$w_i^{stn} = 1$	$w_{in-d2}^- = 0$	$w_{ta-d1}^- = -1$	
$w_{stn-ot}^+ = 0.8$	$w_{in-d1}^- = 0$	$w_{ta-ta}^- = varied$	

GP TI GP TA Control Model

$w_i^{str} = 1$	$w_{stn-in}^+ = 0$	$w_{ot-stn}^- = -0.8$	$w_{ot-ot}^- = 0$
$w_{d2-ot}^- = -1$	$w_{stn-ta}^+ = 0.8$	$w_{ot-snr}^- = -0.4$	$w_{in-in}^- = 0$
$w_{d2-in}^- = 0$	$w_{stn-snr}^+ = 0.9$	$w_{in-stn}^- = 0$	$w_{ot-in}^- = 0$
$w_{d2-ta}^- = -1$	$w_{ot-d2}^- = 0$	$w_{in-snr}^- = 0$	$w_{ot-ta}^- = varied$
$w_{d1-snr}^- = -1$	$w_{ot-d1}^- = 0$	$w_{ta-d2}^- = -1$	$w_{in-ta}^- = 0$
$w_i^{stn} = 1$	$w_{in-d2}^- = 0$	$w_{ta-d1}^- = -1$	
$w_{stn-ot}^+ = 0.8$	$w_{in-d1}^- = 0$	$w_{ta-ta}^- = 0$	

GP TI and GP TA Combined Model - I

$w_i^{str} = 1$	$w_{stn-in}^+ = 0$	$w_{ot-stn}^- = -0.8$	$w_{ot-ot}^- = varied$
$w_{d2-ot}^- = -1$	$w_{stn-ta}^+ = 0.8$	$w_{ot-snr}^- = -0.4$	$w_{in-in}^- = 0$
$w_{d2-in}^- = 0$	$w_{stn-snr}^+ = 0.9$	$w_{in-stn}^- = 0$	$w_{ot-in}^- = 0$
$w_{d2-ta}^- = -1$	$w_{ot-d2}^- = 0$	$w_{in-snr}^- = 0$	$w_{ot-ta}^- = varied$
$w_{d1-snr}^- = -1$	$w_{ot-d1}^- = 0$	$w_{ta-d2}^- = -1$	$w_{in-ta}^- = 0$
$w_i^{stn} = 1$	$w_{in-d2}^- = 0$	$w_{ta-d1}^- = -1$	
$w_{stn-ot}^+ = 0.8$	$w_{in-d1}^- = 0$	$w_{ta-ta}^- = varied$	

GP TA - STR Control Model

$w_i^{str} = 1$	$w_{stn-in}^+ = 0$	$w_{ot-stn}^- = -0.8$	$w_{ot-ot}^- = 0$
$w_{d2-ot}^- = -1$	$w_{stn-ta}^+ = 0.8$	$w_{ot-snr}^- = -0.4$	$w_{in-in}^- = 0$
$w_{d2-in}^- = 0$	$w_{stn-snr}^+ = 0.9$	$w_{in-stn}^- = 0$	$w_{ot-in}^- = 0$
$w_{d2-ta}^- = -1$	$w_{ot-d2}^- = 0$	$w_{in-snr}^- = 0$	$w_{ot-ta}^- = varied$
$w_{d1-snr}^- = -1$	$w_{ot-d1}^- = 0$	$w_{ta-d2}^- = varied$	$w_{in-ta}^- = 0$
$w_i^{stn} = 1$	$w_{in-d2}^- = 0$	$w_{ta-d1}^- = varied$	
$w_{stn-ot}^+ = 0.8$	$w_{in-d1}^- = 0$	$w_{ta-ta}^- = 0$	

GP Inner - GP Inner Control Model

$w_i^{str} = 1$	$w_{stn-in}^+ = 0.8$	$w_{ot-stn}^- = -0.8$	$w_{ot-ot}^- = -1$
$w_{d2-ot}^- = -1$	$w_{stn-ta}^+ = 0$	$w_{ot-snr}^- = 0$	$w_{in-in}^- = varied$
$w_{d2-in}^- = -1$	$w_{stn-snr}^+ = 0.9$	$w_{in-stn}^- = -0.8$	$w_{ot-in}^- = -1$
$w_{d2-ta}^- = 0$	$w_{ot-d2}^- = 0$	$w_{in-snr}^- = -0.4$	$w_{ot-ta}^- = 0$
$w_{d1-snr}^- = -1$	$w_{ot-d1}^- = 0$	$w_{ta-d2}^- = 0$	$w_{in-ta}^- = 0$
$w_i^{stn} = 1$	$w_{in-d2}^- = 0$	$w_{ta-d1}^- = 0$	
$w_{stn-ot}^+ = 0.8$	$w_{in-d1}^- = 0$	$w_{ta-ta}^- = 0$	

GP Outer - GP Inner Control Model

$w_i^{str} = 1$	$w_{stn-in}^+ = 0.8$	$w_{ot-stn}^- = -0.8$	$w_{ot-ot}^- = -1$
$w_{d2-ot}^- = -1$	$w_{stn-ta}^+ = 0$	$w_{ot-snr}^- = -0.4$	$w_{in-in}^- = -1$
$w_{d2-in}^- = -1$	$w_{stn-snr}^+ = 0.9$	$w_{in-stn}^- = -0.8$	$w_{ot-in}^- = varied$
$w_{d2-ta}^- = 0$	$w_{ot-d2}^- = 0$	$w_{in-snr}^- = -0.4$	$w_{ot-ta}^- = 0$
$w_{d1-snr}^- = -1$	$w_{ot-d1}^- = 0$	$w_{ta-d2}^- = 0$	$w_{in-ta}^- = 0$
$w_i^{stn} = 1$	$w_{in-d2}^- = 0$	$w_{ta-d1}^- = 0$	
$w_{stn-ot}^+ = 0.8$	$w_{in-d1}^- = 0$	$w_{ta-ta}^- = 0$	

GP Outer - SNr Control Model

$w_i^{str} = 1$	$w_{stn-in}^+ = 0$	$w_{ot-stn}^- = -0.8$	$w_{ot-ot}^- = -1$
$w_{d2-ot}^- = -1$	$w_{stn-ta}^+ = 0$	$w_{ot-snr}^- = varied$	$w_{in-in}^- = 0$
$w_{d2-in}^- = 0$	$w_{stn-snr}^+ = 0.9$	$w_{in-stn}^- = 0$	$w_{ot-in}^- = 0$
$w_{d2-ta}^- = 0$	$w_{ot-d2}^- = 0$	$w_{in-snr}^- = 0$	$w_{ot-ta}^- = 0$
$w_{d1-snr}^- = -1$	$w_{ot-d1}^- = 0$	$w_{ta-d2}^- = 0$	$w_{in-ta}^- = 0$
$w_i^{stn} = 1$	$w_{in-d2}^- = 0$	$w_{ta-d1}^- = 0$	
$w_{stn-ot}^+ = 0.8$	$w_{in-d1}^- = 0$	$w_{ta-ta}^- = 0$	

GP Inner - SNr Control Model

$w_i^{str} = 1$	$w_{stn-in}^+ = 0.8$	$w_{ot-stn}^- = -0.8$	$w_{ot-ot}^- = -1$
$w_{d2-ot}^- = -1$	$w_{stn-ta}^+ = 0$	$w_{ot-snr}^- = 0$	$w_{in-in}^- = -1$
$w_{d2-in}^- = -1$	$w_{stn-snr}^+ = 0.9$	$w_{in-stn}^- = -0.8$	$w_{ot-in}^- = -1$
$w_{d2-ta}^- = 0$	$w_{ot-d2}^- = 0$	$w_{in-snr}^- = varied$	$w_{ot-ta}^- = 0$
$w_{d1-snr}^- = -1$	$w_{ot-d1}^- = 0$	$w_{ta-d2}^- = 0$	$w_{in-ta}^- = 0$
$w_i^{stn} = 1$	$w_{in-d2}^- = 0$	$w_{ta-d1}^- = 0$	
$w_{stn-ot}^+ = 0.8$	$w_{in-d1}^- = 0$	$w_{ta-ta}^- = 0$	

GP Outer - STR Control Models

$w_i^{str} = 1$	$w_{stn-in}^+ = 0$	$w_{ot-stn}^- = -0.8$	$w_{ot-ot}^- = 0$
$w_{d2-ot}^- = -1$	$w_{stn-ta}^+ = 0$	$w_{ot-snr}^- = -0.4$	$w_{in-in}^- = 0$
$w_{d2-in}^- = 0$	$w_{stn-snr}^+ = 0.9$	$w_{in-stn}^- = 0$	$w_{ot-in}^- = 0$
$w_{d2-ta}^- = 0$	$w_{ot-d2}^- = varied/0$	$w_{in-snr}^- = 0$	$w_{ot-ta}^- = 0$
$w_{d1-snr}^- = -1$	$w_{ot-d1}^- = varied/0$	$w_{ta-d2}^- = 0$	$w_{in-ta}^- = 0$
$w_i^{stn} = 1$	$w_{in-d2}^- = 0$	$w_{ta-d1}^- = 0$	
$w_{stn-ot}^+ = 0.8$	$w_{in-d1}^- = 0$	$w_{ta-ta}^- = 0$	

GP Inner - STR Control Models

$w_i^{str} = 1$	$w_{stn-in}^+ = 0.8$	$w_{ot-stn}^- = 0$	$w_{ot-ot}^- = 0$
$w_{d2-ot}^- = -1$	$w_{stn-ta}^+ = 0$	$w_{ot-snr}^- = 0$	$w_{in-in}^- = 0$
$w_{d2-in}^- = -1$	$w_{stn-snr}^+ = 0.9$	$w_{in-stn}^- = -0.8$	$w_{ot-in}^- = varied$
$w_{d2-ta}^- = 0$	$w_{ot-d2}^- = 0$	$w_{in-snr}^- = -0.4$	$w_{ot-ta}^- = 0$
$w_{d1-snr}^- = -1$	$w_{ot-d1}^- = 0$	$w_{ta-d2}^- = 0$	$w_{in-ta}^- = 0$
$w_i^{stn} = 1$	$w_{in-d2}^- = varied/0$	$w_{ta-d1}^- = 0$	
$w_{stn-ot}^+ = 0.8$	$w_{in-d1}^- = varied/0$	$w_{ta-ta}^- = 0$	

GP Outer - GP Inner Combined Model:Case A

$w_i^{str} = 1$	$w_{stn-in}^+ = 0.8$	$w_{ot-stn}^- = -0.8$	$w_{ot-ot}^- = 0$
$w_{d2-ot}^- = -1$	$w_{stn-ta}^+ = 0$	$w_{ot-snr}^- = -0.4$	$w_{in-in}^- = 0$
$w_{d2-in}^- = -1$	$w_{stn-snr}^+ = 0.9$	$w_{in-stn}^- = -0.8$	$w_{ot-in}^- = varied$
$w_{d2-ta}^- = 0$	$w_{ot-d2}^- = varied$	$w_{in-snr}^- = -0.4$	$w_{ot-ta}^- = 0$
$w_{d1-snr}^- = -1$	$w_{ot-d1}^- = varied$	$w_{ta-d2}^- = 0$	$w_{in-ta}^- = 0$
$w_i^{stn} = 1$	$w_{in-d2}^- = varied$	$w_{ta-d1}^- = 0$	
$w_{stn-ot}^+ = 0.8$	$w_{in-d1}^- = varied$	$w_{ta-ta}^- = 0$	

GP Outer - GP Inner Combined Model:Case B

$w_i^{str} = 1$	$w_{stn-in}^+ = 0.8$	$w_{ot-stn}^- = -0.8$	$w_{ot-ot}^- = varied$
$w_{d2-ot}^- = -1$	$w_{stn-ta}^+ = 0$	$w_{ot-snr}^- = -0.4$	$w_{in-in}^- = varied$
$w_{d2-in}^- = -1$	$w_{stn-snr}^+ = 0.9$	$w_{in-stn}^- = -0.8$	$w_{ot-in}^- = varied$
$w_{d2-ta}^- = 0$	$w_{ot-d2}^- = 0.5$	$w_{in-snr}^- = -0.4$	$w_{ot-ta}^- = 0$
$w_{d1-snr}^- = -1$	$w_{ot-d1}^- = 0.5$	$w_{ta-d2}^- = 0$	$w_{in-ta}^- = 0$
$w_i^{stn} = 1$	$w_{in-d2}^- = 0.25$	$w_{ta-d1}^- = 0$	
$w_{stn-ot}^+ = 0.8$	$w_{in-d1}^- = 0.25$	$w_{ta-ta}^- = 0$	

Combined Models:Final Model

Though there were three stages, only the final model is presented, which included all the instantiations.

$w_i^{str} = 1$	$w_{stn-in}^+ = 0.8$	$w_{ot-stn}^- = -0.8$	$w_{ot-ot}^- = varied$
$w_{d2-ot}^- = -1$	$w_{stn-ta}^+ = 0.8$	$w_{ot-snr}^- = varied$	$w_{in-in}^- = varied$
$w_{d2-in}^- = -1$	$w_{stn-snr}^+ = 0.9$	$w_{in-stn}^- = -0.8$	$w_{ot-in}^- = varied$
$w_{d2-ta}^- = -1$	$w_{ot-d2}^- = 0.5$	$w_{in-snr}^- = varied$	$w_{ot-ta}^- = varied$
$w_{d1-snr}^- = -1$	$w_{ot-d1}^- = 0.5$	$w_{ta-d2}^- = varied$	$w_{in-ta}^- = varied$
$w_i^{stn} = 1$	$w_{in-d2}^- = 0.25$	$w_{ta-d1}^- = varied$	
$w_{stn-ot}^+ = 0.8$	$w_{in-d1}^- = 0.25$	$w_{ta-ta}^- = varied$	